Design and study of bioorganometallic artemisinins as antimicrobials.

By

Christoff Christiaan Albertyn

Supervisor: Dr Prinessa Chellan

Co-Supervisor: Prof. Erick Strauss

University of Stellenbosch

Faculty of Science

Department of Chemistry & Polymer Science

December 2021

DECLARATION

By submitting this thesis electronically, I declare that the entirety of the work contained therein is my own original work, that I am the sole author thereof (save to the extent explicitly otherwise stated), that reproduction and publication thereof by Stellenbosch University will not infringe any third-party rights and that I have not previously in its entirety or in part submitted it for obtaining any qualification.

Christoff Christiaan Albertyn December 2021

Abstract

Due to the rise in artemisinin resistant *Plasmodium falciparum* strains, the main focus of this study was to maintain and increase the efficacy of artemisinin to optimise the production of reactive oxygen species (ROS) released from artemisinin. To achieve this, the moieties, ruthenium *p*-cymene and ferrocene, known to increase electrochemical reactions, were used to derivatise the artemisinin structure for new possible drug candidates. Artemisinin was modified into a triazole (compounds **1-3**) and artesunate (compounds **4-6**) derivatives. Generally greater yields for the artesunate derivatives (45-63%) were obtained compared to the triazole derivatives (8-42%). Two new artemisinin ligands, compounds **1** and **4**, that can coordinate with a variety of organometallic moieties were successfully synthesised and characterised. Although optimisation to the synthesis of compound **1** is required (21% yield), likely due to the interaction of the copper (I) catalyst with the endoperoxide bridge, high purity could be achieved using easily accessible gravity column chromatography (98% pure). Moreover, two major stereo isomers of compound **1** could be isolated for future studies. Two new ferrocenyl compounds **3** and **6** were obtained and fully characterised. The synthesis and characterisation of a new ferrocene precursor, **intermediate 3**, was also obtained in high yield (86%) and purity (> 99%). Ruthenium complexes, compounds **2** and **5**, were much more challenging to obtain and purify ("± 40%" purity) compared to the ferrocenyl derivatives, compounds **3** (98% pure) and **6** (99% pure).

Solubility studies revealed that the triazole derivatives were generally less soluble (10-80 µM) in the biological buffer system (PBS and HEPES) compared to the artesunate derivatives (10-160 µM). *In vitro* biological studies showed the influence of the halogen ligand on ruthenium complexes **2** and **5** did indicate that the bulkier and more polar iodido-derivative (**2b**: 69.8 ± 0.58 nM Dd2) had a slightly higher activity against P. *falciparum* than its chlorido-counterparts (**2a**: 70.9 ± 2.6 nM Dd2). Furthermore, data suggested that the ferrocenyl derivatives were the most active against the *P. falciparum* parasite, with compound **6** with the highest activity of 3.0 ±0.49 nM against the chloroquine resistant strain (Dd2). Overall, the data indicated that the isolated organometallic groups do not have any significant activity but requires the artemisinin moiety to improve activity. The unexpected, but most satisfactory result, was the very low toxicity of the compounds synthesised.

The artemisinin derivatives tested against *Escherichia coli* and *Staphylococcus aureus* strains, unfortunately did not yield any promising biological data to prove that artemisinin could be effective as an antibacterial drug, due to solubility complications with most of the compounds (**1-3** and **6**). Furthermore, only compound **4** proved capable of decreasing bacterial growth of the *E. coli* and *S. aureus* at the maximal tested concentration, 500 µM, to 53.0 ± 2.3 % active growth and 70.8 ± 2.8 % active growth, respectively. However, compound **4** had much greater growth inhibition against the *E. coli* compared to the base artemisinin drug (93 ± 1.8 % active growth) and even the proposed active dihydroartemisinin species (77.7 ± 3.4% active growth).

The findings in this project are preliminary and further studies, directing towards artesunate derivatives and similar artesunate species, is needed. Therefore, these results could shift our understanding of which derivatisation is more likely to improve upon the pharmacological properties artemisinin lacks. Data further

suggested that the ferrocenyl species can be developed further along with similar sandwich type organometallic complexes.

Opsomming

Hierdie projek fokus op die verbetering van artemisinin om weerstandige stamme van *Plasmodium falciparum* te bestry. Die hoofdoel was om die vervaardiging van reaktiewe suurstof spesies (ROS) wat deur artemisinin geproduseer is, te vermeerder . Artemisinin kan verbeter word deur ruthenium *p*-cymene en ferrocene, wat elektrochemiese reaksies verbeter, aan die artemisinin struktuur te bind. Die organo-metaal verbindings was met verskeie triasool verbindings (verbindings **1-3**) óf deur artesunate verbindings (verbindings **4-6**) verbind met artemisinin. Die algehele opbrengs van die artesunate verbindings het tussen 45-63% gelê, hoër as die van die triasool verbindings wat tussen 8-42% gelê het. Die twee nuwe verbindings **1** en **4**, wat met verskeie organo-metaal verbindings kan bind, was albei suksesvol gesintetiseer en gekarakteriseer. Alhoewel die maksimale opbrengs vir verbinding **1** (21%) laag was, weens die redoks reaksie tussen die koper (I) katalis met die endo-peroksied brug, was ’n hoë graad van suiwerheid bereik (98%). Benewens die feit dat ’n hoë suiwerheid verkry was, is twee stereo-isomere geïdentifiseer wat vir toekomstige studies geïsoleer kan word. Verder was twee nuwe ferroseen-verbindings (**3** en **6)** suksesvol gesintetiseer en gekarakteriseer. “**Intermediate 3**”, ’n nuwe ferroseen-voorloper verbinding, was met hoë opbrengs (86%) gesintetiseer en het ‘n hoë suiwerheid bereik (>99%). Ruthenium-kompleks verbindings **2** en **5** was, na verskeie pogings om die verbindings te genereer, suksesvol gesintetiseer, maar onsuksesvol om ‘n hoë graad van suiwerheid te bereik (± 40% suiwer), wat laag is in vergelyking met die ferroseen-verbindings **3** (98% suiwer) en **6** (99% suiwer).

Die oplosbaarheid toetse het aangetoon dat die triasool-verbindings wel minder oplosbaar (10-80 µM) is in beide buffer sisteme (PBS en HEPES) as met die artesunate verbindings (10-160 µM). *In vitro* biologiese toetse teen die *P. falciparum* parasiet dui aan dat die ruthenium verbindings **2** en **5** meer aktiwiteit toon met die jodium-afstammeling (**2b**: 69.8 ± 0.58 nM Dd2) as met die chloried-afstammeling (**2a**: 70.9 ± 2.6 nM Dd2). Van die organo-metaal verbindings, toon ferroseen-verbindings hoofsaaklik die sterkste biologiese aktiwiteit teen *P. falciparum*. Verbinding **6** met ’n aktiwiteit van 3.0 ± 0.49 nM teen die chloroquine weerstandige stam (Dd2), is ‘n goeie voorbeeld hiervan. Verdere afleidings meen dat die organo-metaal verbindings op hulle eie min na geen aktiwiteit teen die malaria parasiet toon, maar toon wel verhoogde aktiwiteit nadat dit met die artemisinin verbinding geheg is. Die verbindings gesintetiseer tydens die projek toon baie lae toksisiteit teen gesonde menslike selle.

Weens swak oplosbaarheid in die biologiese buffer vir bakteriële toetse, het die meeste verbindings min na geen biologiese aktiwiteit teen *Escherichia coli* en *Staphylococcus aureus* stamme getoon. Van al die verbindings kon slegs verbindings **4** en **5a** getoets word, maar slegs **4** teen die hoogste getoetste konsentrasie (500 µM), toon die beste groei inhibisie teen *E. coli* (53.0 ± 2.3 % ooflewend) en *S. aureus* (70.8 ± 2.8 % oorlewend). Verbinding **4** het wel hoër aktiwiteit as artemisinin (93 ± 1.8 % oorlewend) en dihydroartemisinin teen *E. coli* (77.7 ± 3.4% oorlewend) getoon.

Hierdie projek is slegs ’n voorlopige studie om verskeie nuwe idees en verdere ondersoeke vir toekomstige projekte te skep. Die data van hierdie projek dui ondermeer aan dat artesunate-verbindings en onder meer,

ferroseen-verbindings, die beste keuses sou wees om verdere ondersoeke te loods ten einde aan artemisinin verbeterde farmaseutiese eienskappe te gee.

Acknowledgements

- Dr Prinessa Chellan, my supervisor, thank you for your continued guidance, training and support.
- Prof. Erick Strauss, my co-supervisor, thank you for your input and insight to help steer this project and the use of your laboratory to perform biological assays.
- Dr Deon Neveling, thank you for performing MIC assays against *Escherichia coli* and *Staphylococcus aureus*.
- Prof. Vicky Avery and your team at Griffith University for testing our samples against *Plasmodium falciparum* strains.
- Ms Elsa Malherbe and Dr Jaco Brand at the NMR unit for CAF for you training and continued advice operating the NMR equipment and software.
- Dr Marietjie Stander at the MS unit for CAF, thank you for providing and analysing our MS-ESI data.
- To the ICP-MS & XRF laboratory of CAF, thank you for performing EA.
- Prof. Selwyn Mapolie, thank you for providing access to use your laboratory equipment.
- Dr Katherine de Villiers thank you for the use of your laboratory and spectroscopic equipment used to perform solubility assays.
- To the members of group of medicinal and organic chemistry (GOMOC) and the members of the Inorganic chemistry group and in Stellenbosch University, thank you for your continued advice, guidance, support and use of laboratory space and equipment that helped realising this project.
- To Stellenbosch University and the NRF for funding and giving me the opportunity to grow in the field of study.
- To the dear technical staff of the De Beers building and inorganic building, Raymond Willemse, Maxwell Wakens, Debbie Isaacs, Peta Steyn, Shafiek Mohamed, Malcolm McLean thank you for your assistance.
- Thank you to all my family and friends who supported me during this project.

Abbreviations and Symbols

3D7	chloroquine sensitive *Plasmodium falciparum* strain
ACT	Artemisinin based combination therapy
ARS	Artesunate
ART	Artemisinin
ART-N_3	10-azidoartemisinin
ATR	Attenuated total reflection (for infrared spectroscopy)
BL21	Pathogenic *Escherichia coli* strain
cp	Cyclopentadienyl ring
d	Doublet (NMR assignment)
DIPEA	N,N-Diisopropylethylamine
DAPI	4’,6-Diamidino-2-phenylindole
DCM	Methylene chloride (dichloromethane)
Dd2	Chloroquine resistant *Plasmodium falciparum* strain
dH_2O	Distilled water
DHA	Dihydroartemisinin
DMSO	Dimethyl sulfoxide
EA	Elemental analysis
EC_{50}	Half-maximal effective concentration
EDC	N-(3-Dimethylaminopropyl)-N′-ethylcarbodiimide hydrochloride
EtOH	Ethanol
GSH	Glutathione
GSSG	Glutathione disulphide
HEK293	Human embryonic kidney mammalian cell line
HEPES	4-(2-Hydroxyethyl)-1-piperazineethane sulfonic acid
HOBt	1-Hydroxybenzotriazole hydrate
HPLC	High-performance liquid chromatography
IC_{50}	Half-maximal inhibitory concentration

IR	Infrared
J	Coupling constant
m	Multiplet (NMR assignment)
m/z	Mass to charge ratio
MeOH	Methanol
$MgSO_4$	Magnesium sulphate
MRSA	Methicillin-resistant *Staphylococcus aureus*
MS	Mass spectroscopy
N	Normality
NMR	Nuclear magnetic resonance spectroscopy
PBS	Phosphate buffered saline
p-cymene	1-Methyl-4-(propan-2-yl) benzene
RI	Resistance index
rt	Room temperature (ambient temperature)
s	Singlet (NMR assignment)
t	Triplet (NMR assignment)
t-AmOH	Tertiary-amyl alcohol
TLC	Thin layer chromatography
WHO	World health organisation
Xen36	methicillin resistant *Staphylococcus aureus* strain

Table of contents:

Chapter 1: Malaria & the application of bioorganometallic antiplasmodials

1.1. Introduction:

Infectious microorganisms are a high risk for millions of lives, albeit life threatening or not; with the battle against diseases resistant to treatments being a constant obstacle. Malaria, known as one of the world's most infectious diseases is especially deadly if left untreated.[1,2] The WHO reported that at the end of 2019, an estimated 229 million patients were infected with malaria.[1] It was estimated that globally 409 000 deaths were caused by malaria at the end of 2019. 95 % of these mortalities were from sub-Saharan Africa. Regions endemic to malaria are now facing rising drug-resistant *Plasmodium* strains.[3,4] *Plasmodium* is a protozoan parasite that infects its host's red blood cells and or hepatic cells (liver cells), that in turn will cause (possibly fatal) symptoms and damage to the host's body. [3] Of the known malaria caused by *Plasmodium* parasite species, *P. vivax* and especially *P. falciparum* are presented as the most dangerous species.[3] To combat against the resistant parasitic strains, novel chemotypes are researched or previously used antiplasmodial agents are derivatised to regain biological activity against the parasite. In recent years, the inclusion of metal moieties in the parent antimicrobial agent architecture shows great potential to improve the biological activity to inhibit its targets. Studies into the mechanism of action and properties that enhance the biological activity of these metal complexes are ongoing[49] and it is clear that these drug types have great a potential for future investigations and drug design.

1.2. Understanding the infection:

1.2.1. The life cycle of Plasmodium falciparum:

To prevent infection or further damage to the host, researchers intercept and disrupt the parasite's life cycle[5,6] at key stages. These key stages include the exoerythrocytic cycle or liver stage, the erythrocytic cycle and, lastly, the sporogonic cycle. Briefly described in **Figure 1.1**, the *P. falciparum* life cycle[5] involves *P. falciparum* parasites in the female *Anopheles* mosquito's (vector) salivary glands, in the protist's sporozoite stage. Haploid sporozoites enter the bloodstream when the mosquito has a blood meal (**I**). The sporozoites are rapidly transported to the liver through the bloodstream, entering the (liver) hepatic cells (**II**). During this exoerythrocytic cycle, the sporozoites mature or develop into merozoites through schizogony, or multiple asexual fission (**II**). The schizont (infected hepatic cell) ruptures and release the merozoites back into the bloodstream, infecting erythrocytes by entering the cells (**II→III**). During this 47-hour incubation period (during the erythrocytic cycle), the infected erythrocyte develops into a trophozoite that produces schizonts, by asexual reproduction, which divides further and produces more merozoites (**III→IV**).

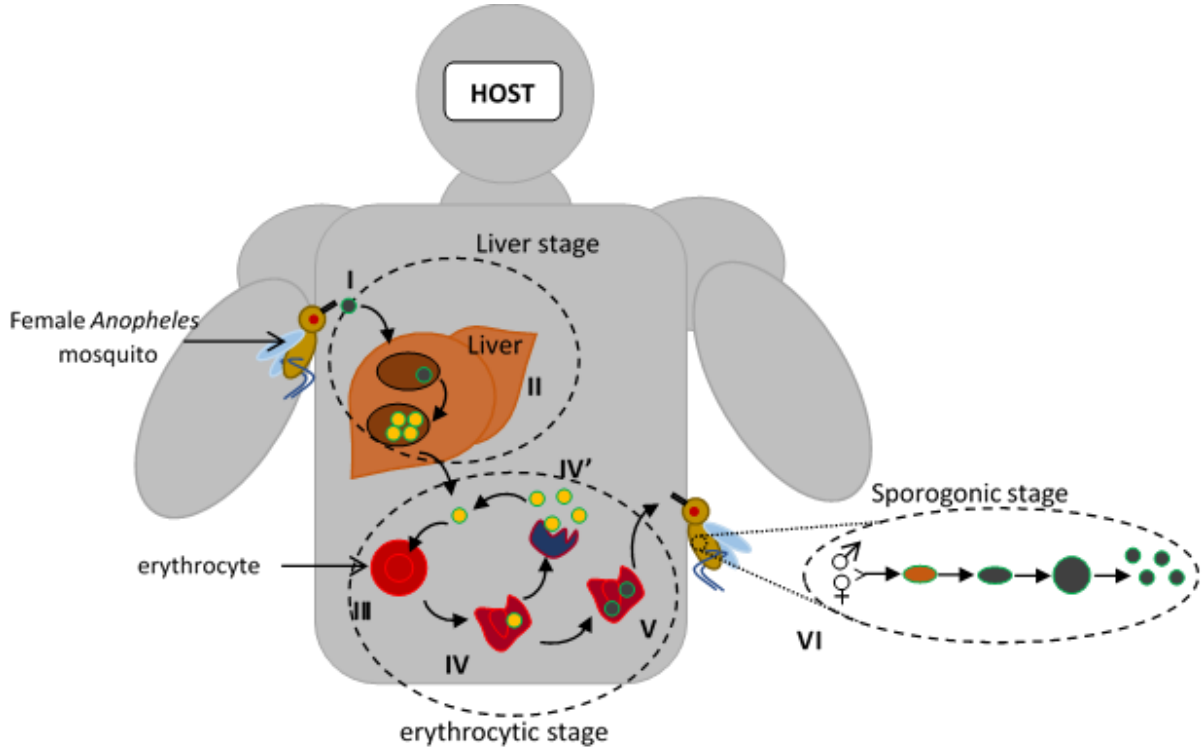

Figure 1.1. Simplified representation of the life cycle of *Plasmodium falciparum*.

Though most of the merozoites rupture out of the dead erythrocyte to infect other red blood cells (**IV→IV'**), occasionally some merozoites differentiate into sexual macrogametocytes (female) or microgametocytes (male) (**IV→V**). These sexual gametocytes do not rupture the infected erythrocyte and remain in the bloodstream (**V**). When another female *Anopheles* mosquito subsequently feeds on the infected host, the parasite proceeds to the sporogonic cycle during which the gametocytes in the mosquito's gut fuse (**V→VI**). The fused gametocytes develop into a zygote, becoming an elongated cell called an ookinete (**VI**). The ookinete travel and infects the gut wall, developing into an oocyst which undergoes meiosis, after which it ruptures to release haploid sporozoites that travel to the salivary glands of the mosquito (**VI**). These sporozoites

will infect new hosts in the next bloodmeal (**VI→I**). By understanding the life cycle and the biology of *P. falciparum*, one would be able to develop prevention methods, like antiplasmodial drugs.

1.2.2. How Plasmodium falciparum resists treatment

Recent studies reveal that resistance against artemisinin is starting to appear in malaria parasites originating from Cambodia.[1,7] Like chloroquine-resistant parasites, artemisinin-resistant parasites contained single nucleotide polymorphisms in the *pfcrt* and *pfmdr1* genes, which encodes *P. falciparum* chloroquine resistance transporter (PfCRT) and *P. falciparum* multidrug resistance protein-1 (PfMDR1), homologous to human P-glycoprotein.[7–9] As the PfCRT protein causes great efflux of chloroquine, PfMDR1 protein is an ATP-Binding Cassette (ABC) efflux transporter[8,9] that was first thought to resist transporting artemisinin into the cell,[8] which meant that the drug could not reach its target location in the digestive- or food vacuole. Recent research strongly suggests that the PfMDR1 protein and PfCRT protein can modulate the influx and or efflux of antiplasmodial agents;[9] rather than the mutant gene *Pfk13*, which encodes the PFK13 protein that is homologous to the human Keap1 protein.[10,11] The human Keap1 is a negative regulator protein that responds to cytotoxic signals, i.e. high oxidative environment, inducing the recruitment of an antioxidant response.[12–14] The mutant gene enables the haploid-stage parasite to become dormant more quickly and enables it to relieve the oxidative stress due to artemisinin damage.[11] Due to the *Pfk13* mutation, the parasite's genes encoding chaperones (proteins that fold proteins) at the UPR pathway is upregulated, therefore able to repair or metabolise damaged proteins.[11] Another mutation indicated a prolonged ring stage, that is known as the PfKelch13 mutation.[15] The prolonged ring stage parasite would increase the survivability of the parasite, due to the decreased availability of haem.[15] This is due to less haemoglobin digestion during the ring stage of the parasite, therefore does not activate the artemisinin. [15]

1.2.3. GSH homeostasis in Plasmodium falciparum as a drug-target:

Certain biological components in organisms have restricted genetic makeup that codes for the synthesis of the protein or structural molecules. By targeting the key biomolecules or processes, the virulent organism is hesitant to undergo genetic mutation, as the mutation could leave important proteins losing its function. Disrupting key processes in blood stage parasitic development of *P falciparum*, like DNA replication, transport of molecules and membrane synthesis will decrease levels of parasitaemia and lower the risk of fatal symptoms manifesting.[2,16] One such key process is the glutathione (GSH) homeostasis.[17] Glutathione homeostasis is important as GSH is involved in the antioxidant defence mechanism, seen in **Scheme 1.1**.[17]

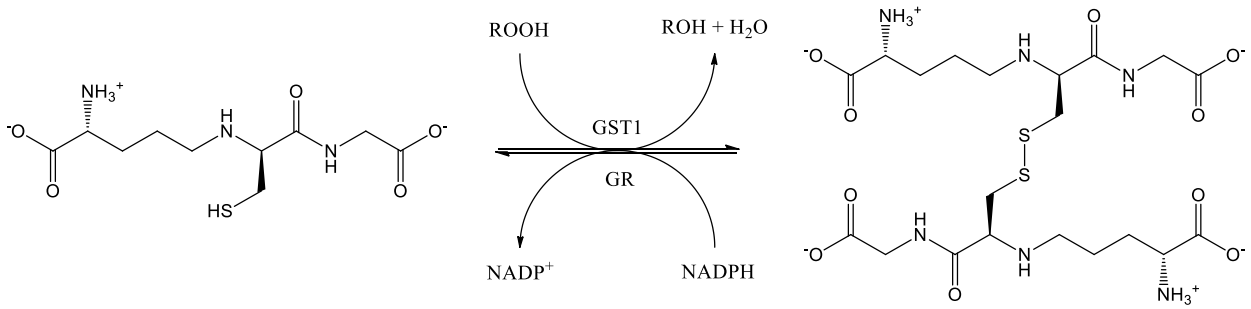

Scheme 1.1. Simplified glutathione redox reaction in *P. falciparum*. GST1: glutathione S-transferase 1; GR: Glutathione reductase.

The process involves the reaction of free GSH with another GSH to dimerise in a redox reaction.[17,18] The glutathione acts as a co-factor in glutathione-S-transferases and glyoxalases. [17,18] The glutathione disulphide (GSSG) is reduced back to GSH by glutathione reductase using NADPH, an important co-factor for the synthesis of ribose and or deoxyribose genetic nucleoside biosynthesis.[17–19] It was shown that the *P. falciparum* parasite is able to synthesise the GSH *de novo* from glutamate, cysteine and glycine amino acids.[17] Studies indicated that the GSH homeostasis is also a defence measure for possible haem by-products (from haem digestion), which is highly redox active, that would leave the digestive vacuole to be detoxified by GSH.[17]

1.3. Antiplasmodial agents:

1.3.1. Chloroquine:

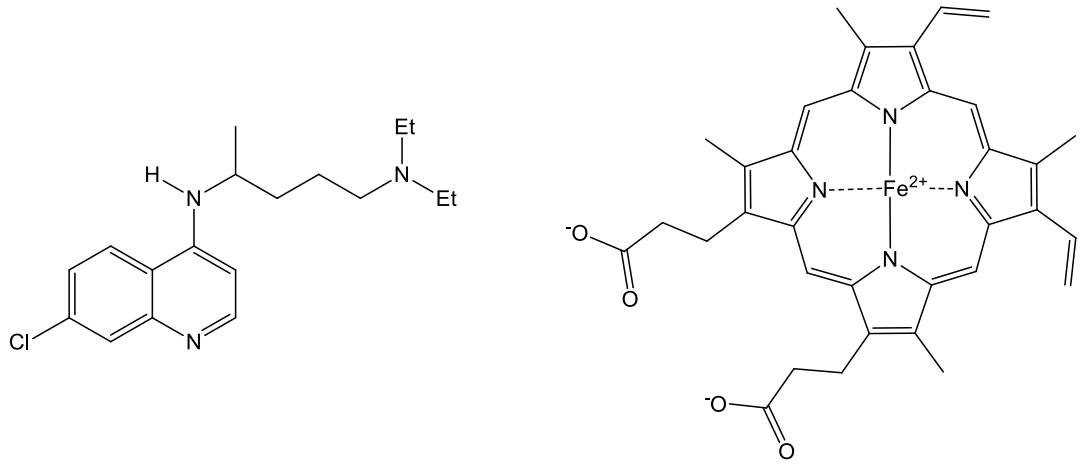

Figure 1.2. Chemical structure of chloroquine (left) and haem (right).

One of the early drugs developed to fight the malaria parasite is chloroquine (**Figure 1.2**), a fast-acting antimalarial drug; reported to be most effective during the erythrocytic cycle (targeting trophozoites, schizonts and gametocytes present).[20] Although chloroquine is not presently effective against malaria as less uncomplicated malaria strains and species are surviving,[2,4,21] chloroquine (the half maximal effective concentration (EC_{50}) = 49 nM and the half maximal inhibitory concentration (IC_{50}) = 137 nM against resistant malaria strains W2 and Dd2, respectively[2,22]) has similar mechanisms of action in both strains which causes toxicity as the drug accumulates in the acidic food vacuoles of the trophozoites, due to its basic nature.[20,23] Furthermore, quinoline-compounds are protonated at acidic pH's, rendering quinoline-compounds less lipophilic and less likely to be expelled from the parasite cytosol.[20] The less lipophilic nature of the protonated quinoline compound has a positive effect, by increasing the concentration of the drug present in the digestive vacuole that leads to less haemeglobin degradation. The consequence of quinoline accumulation in the digestive vacuole results in an inhibitory effect on the trophozoites' haem polymerase enzyme, which polymerises haem into a non-toxic crystalline structure called hemozoin.[2,20,23,24] Haem (as seen in **Figure 1.2**) is a Fe(II) containing group that is surrounded by a porphyrin structure and acts as a co-factor for haemoglobin, an oxygen carrier in human erythrocytes.[19] Haem can induce a pro-inflammatory response assisting ROS generation.[2]

1.3.2. Artemisinin and other peroxide-based drugs:

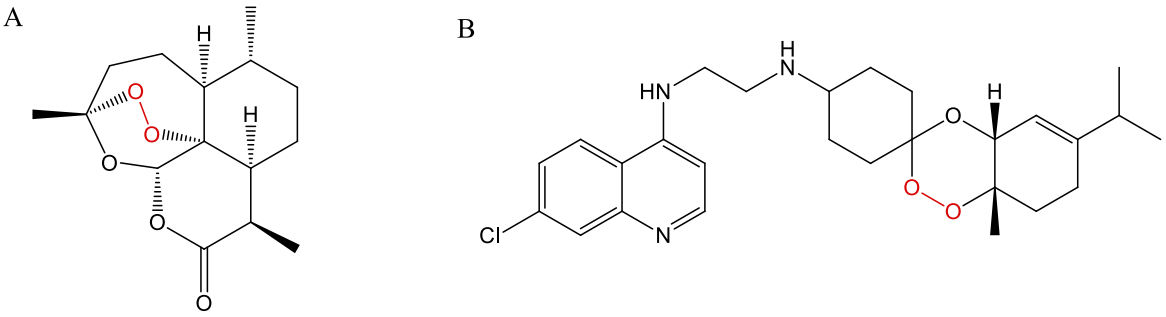

Figure 1.3. Structures of peroxide containing compounds: (A) artemisinin (ART) and (B) Trioxaquine DU1301.

To combat resistant malaria strains, artemisinin (extractable from the wormwood, *Artemisia annua*[7]) and its derivatives are used in conjunction with drugs such as chloroquine and other quinoline based drugs.[25] Artemisinin (**Figure 1.3A**) has a characteristic sesquiterpene trioxane lactone structure, with the endo-peroxide bridge as the pharmacophore. Further development and research of artemisinin revealed to show biological activity against some cancer cell lines. C. Reiter *et al.*[26] reported that although dihydroartemisinin (Figure 1.3A: IC_{50} = 0.48 µM) has less activity than the anti-cancer drug, doxorubicin (Figure 1.3C: IC_{50} = 0.009 µM), against the CCRF-CEM leukaemia cell line, dihydroartemisinin and an organometallic derivative of dihydroartemisinin (**Figure 1.4B**) has much more activity against the multidrug resistant leukaemia cell line, CEM/ADR5000. The artemisinin combination therapy (ACT) usually couples the fast acting artemisinin, which targets the blood-stage of the parasite,[27] with slower acting lumefantrine and piperaquine[2,4,7] which replaced previous first line drugs like chloroquine and sulfadoxine-pyrimethamine.[2,7] Also, like chloroquine, artemisinin concentrates in the food/digestive vacuole of the malarial parasite.[28] Artemisinin's mechanism of action was hypothesised to produce toxic levels of oxygen radicals by cleaving the peroxide bond through interacting with the parasite's haem and haem containing proteins (**Scheme 1.2**).[2,9] Artemisinin and derivatives are also suggested to be able to alkylate proteins,[11] rendering the proteins unable to catalyse reactions effectively.

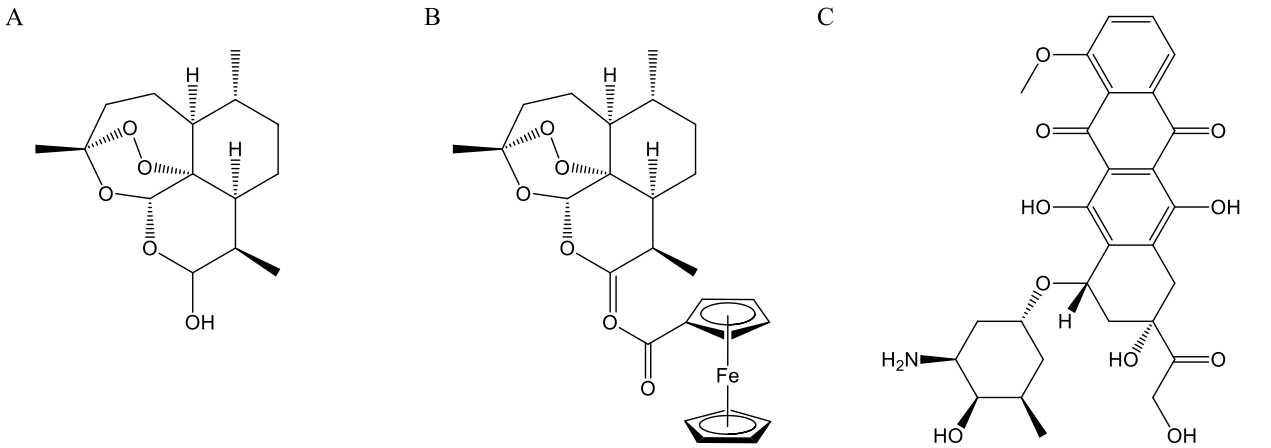

IC_{50} = 0.48 µM (CCRF-CEM) IC_{50} = 0.13 µM (CCRF-CEM) IC_{50} = 0.009 µM (CCRF-CEM)
IC_{50} = 0.68 µM (CEM/ADR5000) IC_{50} = 0.53 µM (CEM/ADR5000) IC_{50} = 23.27 µM (CEM/ADR5000)

Figure 1.4. Chemical structures of artemisinin derivatives with anti-cancer activity as reported.[26]

Despite the great biological activity of artemisinin, it is not yet possible to mass produce artemisinin thus research into synthesis of simplified trioxanes has also been investigated. As seen in **Figure 1.3B**, alternative peroxide compounds were investigated. 1,2,4-trioxane structures were identified and further derived into possible artemisinin-alternatives.[29] Trioxaquine **DU1301** was developed due to the rise in resistance of chloroquine and other quinoline-type antiplasmodial agents, with the addition of another pharmacophore, the peroxide bridge, increasing the activity against chloroquine resistant strains.[30]

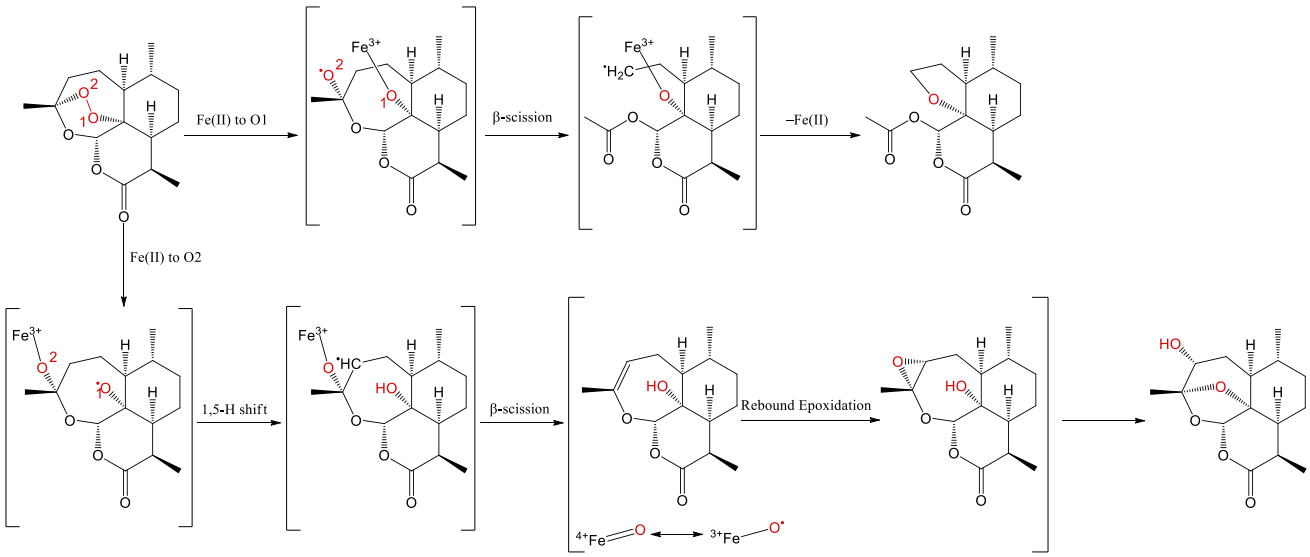

Scheme 1.2. Proposed artemisinin activation in the presence ferrous iron. Artemisinin activation leads to the production of ROS radicals.

Artemisinin's activity is limited to the plasmodium parasite's metabolism of haemoglobin, which mostly is active during the blood-stage of the parasite's life cycle. The mechanism or the activation of artemisinin's oxidative potential of exterminating the parasite was debated between many researchers, to which a core proposed scheme was accepted using ferrous iron seen in **Scheme 1.**2. [31–36] Where the ferrous iron would bind to either O1 or O2 of the endoperoxide bridge from artemisinin, through a Fe^{2+}-dependent Fenton process to eventually produce carbon centred radicals.[34]

A later research model was proposed to generate the radicals, using ferrous haem – which can perform an electron transfer to induce the scission of the peroxide bridge.[34] This "open-peroxide" model, proposed by Haynes *et al.*, proposed that the bio-activation of artemisinin is facilitated by first complexing with the haem, which could act as a Lewis acid, being in the food vacuole, leading to the dissociation of the oxygen-iron "free" radical.[32]

1.3.3. Recent antiplasmodial drug discoveries:

Different approaches to modify previously used antiplasmodial drugs have been investigated. One of these studies involves synthesis of molecules with two drug moieties as seen in **Figure 1.5** for artemisinin. These compounds showed an improvement in biological activities than in artemisinin when comparing chloroquine sensitive and resistant *P. falciparum* strains.[37,38]

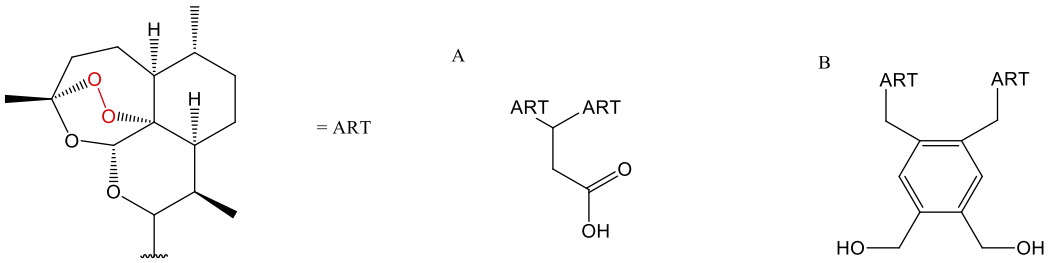

Figure 1.5. Examples of multiple artemisinin moieties in one structure.[37,38]

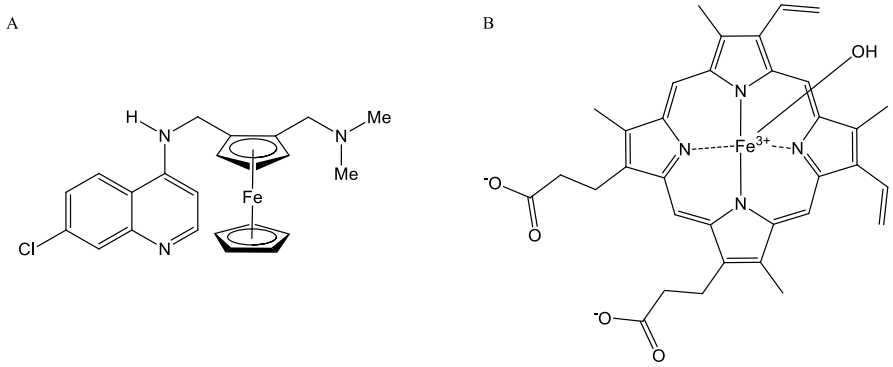

Figure 1.6. A: ferroquine **B**: Hematin monomer.

Later drug discoveries led to the synthesis of ferroquine (**Figure 1.**6**A**), currently in clinical trials,[2] an organometallic drug where ferrocene was incorporated into a chloroquine like structure. It has similar mechanisms of action as chloroquine,[22] is able to accumulate in the food/digestive vacuoles of the malaria resistant strain carrying the PfCRT (*P. falciparum* chloroquine resistant transporter) and inhibits the chloroquine resistant transporter, thereby exerting a second mode of action.[2] Comparing chloroquine with ferroquine, their EC_{50} values of 49 nM and of 6.6 nM, respectively against the chloroquine-resistant strain W2[2] provided evidence that the addition of an organometallic group could increase efficacy of antiplasmodial drugs. Since then, there has been other examples of increased biological activity with the incorporation of transition metals such as zinc and gold into an organic framework, seen in **Figure 1.7**. Ferroquine's less basic nature and structural differences owed to the shorter intramolecular hydrogen bond length between the anilino of the chloroquine moiety and tertiary nitrogen of ferroquine, was speculated to be the reason for unfavourable binding to the PfCRT protein.[22]

A

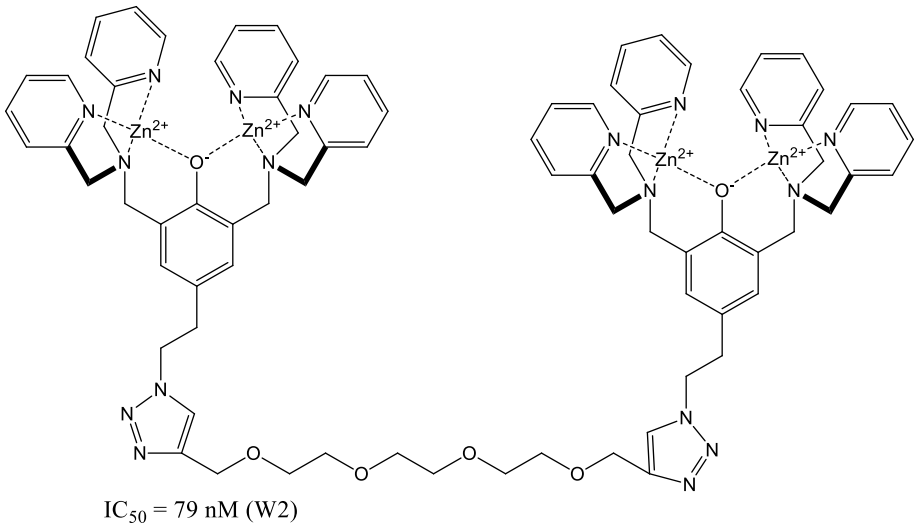

IC_{50} = 79 nM (W2)

B

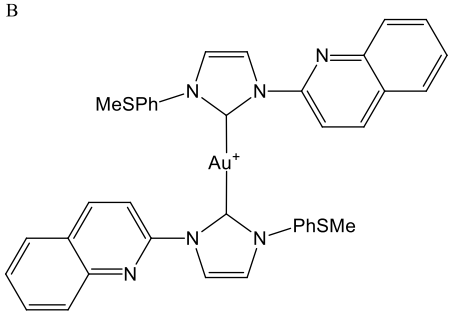

IC_{50} = 0.47 μM (FcM29)

Figure 1.7. Organometallic antiplasmodial structures as reported in **A**[39] and **B**.[40]

Ferroquine disrupts the redox potential in the parasite as it was proposed that the ferrocene groups on ferroquine increased the generation and release of hydroxyl radicals into the cytosol.[41] This build-up of radicals leads to oxidative stress in the parasite, as its antioxidant defences cannot compete with the concentration of ROS, leading to membrane disruptions (peroxidise lipids) and less efficient reinvasion or development in erythrocytes. [20,23,41,42] It is possible that the less efficient reinvasion is caused by damaged DNA sequences which are responsible for the production of the required proteins and enzymes for merozoite development and membrane formation.[43]

Since the discovery of ferroquine, researchers have studied the possibilities of using other transition metals in metallocenes coupled to a quinoline based scaffold. A ferroquine derivative, ruthenoquine was developed (**Figure 1.8A**). Compared to chloroquine (IC_{50} = 352.3 nM against the CQR K1 strain), ruthenoquine has a significantly higher activity (IC_{50} = 12.7 nM) which is similar to ferroquine (IC_{50} of 13.5 nM).[44]

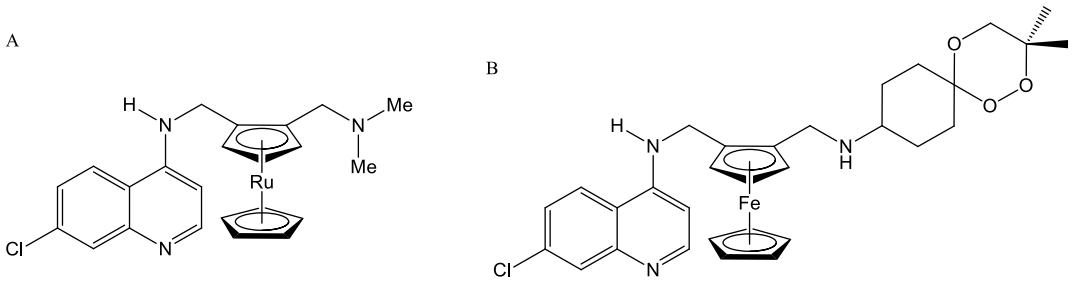

Figure 1.8. Structure of (**A**) ruthenoquine and **(B)** trioxaferroquine.

In addition to the efficacy of trioxanes, antiplasmodial drug candidates like trioxaferroquine, were also synthesised and studied (**Figure 1.8B**), reported to have an IC_{50} against the FcM29 strain (chloroquine resistant) of 17 nM compared to chloroquine and ferroquine, 735 nM and 7 nM respectively. The trioxaferroquine seen in **Figure 1.8B**, was also tested in mice with a dose of 10 mg/kg/day leading to barely detectable levels of parasitaemia within four days.[45] Incorporation of ferrocene into the artemisinin drug has also been reported (**Figure 1.9**).[46]

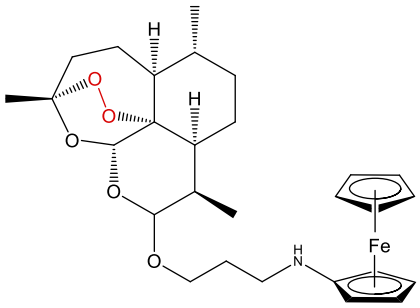

Figure 1.9. Artemisinin ferrocene hybrids.

The incorporation of the transition metals ruthenium, iridium and rhodium have been investigated. The physicochemical properties of these transition metals are very similar to iron and platinum. Due to the ability of these transition metals to coordinate with arene moieties, the expansion of drug candidates is a realisation. Examples of incorporation of ruthenium to produce ruthenocenyl complexes with antimalarial activity is seen below in **Figure 1.10**.[47,48]

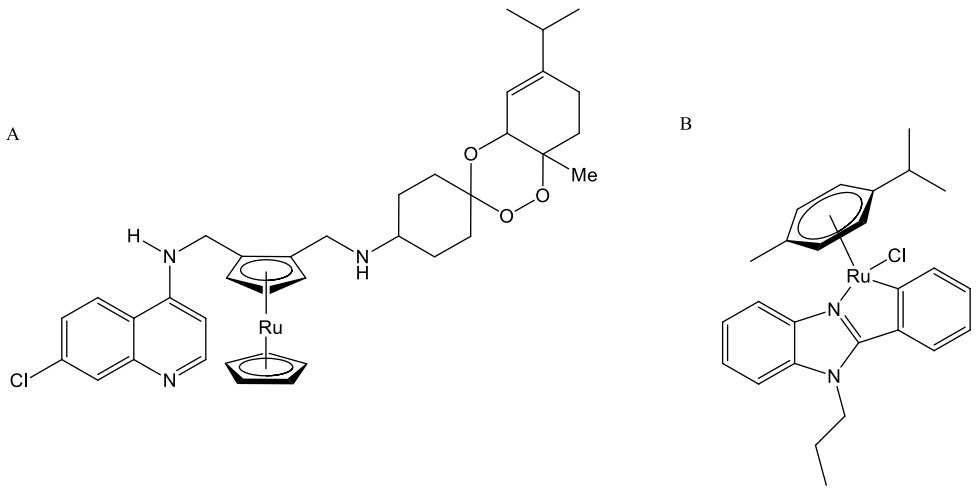

Figure 1.10. Ruthenium based antiplasmodial complexes.

Another example of improved antiplasmodial activity is a thiosemicarbazone derivative (**Figure 1.11**) with a ruthenium half-sandwich moiety, which has an IC_{50} value of 2.57 µM compared to its precursor (175.74 µM) on the NF54 parasite strain.[49]

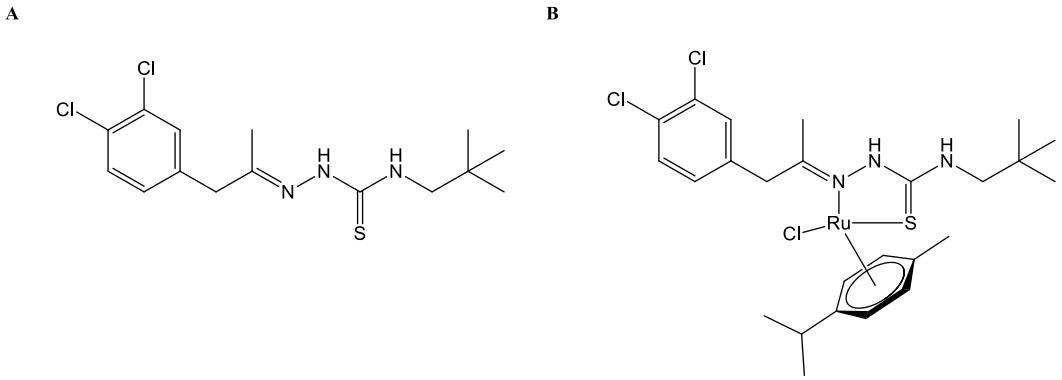

Figure 1.11. Ruthenium based antiplasmodial complex reported by M. Adams *et al*.[49]

Ferroquine has increased biological activity due to its ferrocenyl group, moreover the reduction of Fe(II) in the complex to Fe(III) inhibits the ability of the parasite to reinvade another erythrocyte through increased oxidative stress in the parasite.[41,50] Furthermore, co-factors present in the malaria parasite's enzymes (proteins) that contain nucleophilic groups such as GSH are susceptible to Michael addition reactions.[51] GSH is an important molecule in a defence mechanism against oxidative stress.[17]GSH binds to an intermediate that is formed from the reaction of the ferrocenyl and quinolyl groups of ferroquine..[17,51] The data collected from studying ferrocenyl derivatised artemisinins suggests that the physical proximity of the ferrocenyl group to the endoperoxide bridge effects the antiplasmodial activity by acting as a catalyst for redox reactions.[26] Ligand exchange of certain biologically relevant bonds such as Fe-S bonds, can result in irreversible binding to enzymatic active sites or association/coordination to molecules resulting in biological activity/stability being compromised.[50,52]

Many other metal complexes with Au(I) or Au(III), displayed great biological activity against the *Plasmodium* parasite.[53–55] It is still not fully elucidated as to how and why metal complexation to organic drugs improve the biological activity to the targeted organism, but that some form of synergism between the metal and drug exist.[54] Although organometallic complexes have a wide range of applications, from antiplasmodial to anti-cancer to anti-bacterial, the organometallics require adaptations to alleviate toxicity to patients.[50]

1.4. Artemisinin as anti-microbials:

Since the incorporation of artemisinin and its derivatives as anti-plasmodial agents, many researchers investigated the application of artemisinins for the treatment of cancer, bacterial infections and viral infections.[56–62] Most anti-bacterial drugs, such as the β-lactams (penicillins), targets the synthesis of the bacterial cell wall. Other antimicrobial agents target genetic material or proteins. [63] Due to rising drug resistant and extreme multidrug resistant bacterial strains, either further refinement of current antimicrobial agents are researched or new targets are investigated.[63–67] One such target of interest is increasing oxidative stress in the bacteria induced by the generation of ROS species.[65,66] Bacteria has a variety of anti-oxidant defence

mechanisms that employs either protein (enzyme) based reactions (superoxide dismutase) or utilisation of metabolites such as GSH or ketoacids (reducing ROS species forming non-toxic carboxylic acids).[66] Depending on the source of ROS, i.e. through metals (Fe, Zn, Ga and Al), endogenous sources (such as O_2 produced from aerobic metabolism) and xenobiotics (environmental pollutants), different ROS would be produced and different defence mechanisms used. The various ROS, such as $O_2^{\bullet-}$, causes damage to iron-sulphur containing enzymes or $^{\bullet}OH$ radicals causes DNA damage, oxidation of amino acids of proteins or lipid peroxidation.[65,66] Notably, the regulation of oxidative stress in bacteria would have a cascading effect of the availability of the crucial enzymatic co-factors, such as NADPH and NADH (electron sources) for their metabolism to produce energy (in the form of ATP).[65,66] The co-factors are used during the neutralisation of ROS. Thus, if therapeutic agents that enhance or generate ROS molecules, it would have a detrimental effect on cell proliferation and growth.

Research of artemisinin as a possible anti-bacterial included studies tested against *Mycobacterium tuberculosis* (that causes tuberculosis), *Escherichia coli* and *Staphylococcus aureus*.[68–71] Evaluation of these literature articles reveal that artemisinin in its current state requires increased bioavailability with either being assisted to properly mediate into the bacteria or chemical modification. This is most likely due to the low water solubility of artemisinin. In the study published by H. Cui *et al*.,[69] artemisinin was supported onto silica nanoparticles and a plasma treated silica nanoparticles that greatly increased the solubility of artemisinin. Incorporation of antimicrobial agents onto nanoparticles is becoming an increasingly popular study, since evidence points to increased antimicrobial solubility and biological activity and selevtivity.[72] Their results reported degradation of some artemisinin molecules during the preparation of the nanoparticles, however it still retained much biological activity. They obtained a minimum inhibitory concentration (MIC) of 3.6 mg/mL and a minimum bactericidal concentration (MBC) of 7.2 mg/mL against both *E. coli* and *S. aureus*, while no biological activity was observed when only pure unsupported artemisinin was tested. Moreover, the artemisinin dosed plasma treated nanoparticles was much more selective for bacterial cells, showing high cell viability (95.8% for 293T human embryonic kidney cell line). They reported > 99.9999% reduction in bacterial growth after 8 hours against both species of bacteria. Another research group encapsulated artemisinin in β-cyclodextrin (β-CD).[70] L. Lin *et al*. reported that the artemisinin β-CD compound (with a molar ratio 1:1; artemisinin: β-CD) cleared 99.94% of bacterial methicillin resistant *S. aureus* (MRSA) growth after 4 days with a dose of 20 mg/mL. In both these studies the authors reported that the artemisinin dosed compounds disrupted the cell membrane of the bacteria which disrupted the function of an important enzyme, namely ATPase. ATPase hydrolyse adenosine triphosphate (ATP) to adenosine diphosphate (ADP) to harness energy for the biological system during many metabolic reactions. Although the study of H. Cio *et al*.[69] indicated generation of hydroxyl radicals (ROS-generation), the activation of the endoperoxide bridge is not yet elucidated.

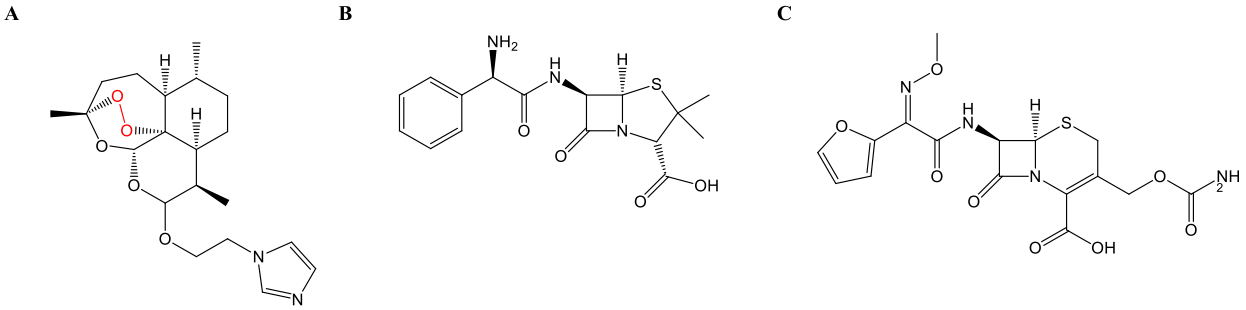

Figure 1.12. Artemisinin-amino derivatives tested for anti-bacterial activity reported by C. Wu *et al.*[71] **A**: Artemisinin-amino compound; **B**: ampicillin; **C**: Cefuroxime.

A study performed by C. Wu *et al.*[71] designed artemisinin derivatives with various amino- and thio-containing structures to specifically bind to the binding pocket of a membrane efflux pump protein of *E. coli*, namely AcrB – reported to confer antibiotic resistance. As with the previous studies of H. Cui *et al*. and L. Lin *et al*., some of the artemisinin-amino derivatives synthesised by C. Wu *et al*. also struggled with solubility. One particular artemisinin derivative stood out in this study (seen in **Figure 1.12A**). This compound was one of the only compounds that, with combination of ampicillin antibiotic, had displayed antimicrobial activity against the *E. coli* AG100A/pET28a-AcrB strain (drug resistant strain). The researched speculated that the artemisinin moiety, after binding, blocks the binding pocket of the efflux pump and therefore allows the accumulation of the antibiotic drug. Thus, the artemisinin-amino compound has a synergic effect with the anti-bacterial drug. Another study conducted by Y. S. Patel *et al*.[73] also reported a similar synergic effect of artemisinin with the anti-mycobacterial agent, rifampicin, against *Mycobacterium bovis* and *M. tuberculosis*. Similarly, artemisinin synergise with antiplasmodial agents. Alone, artemisinin had a high MIC value (100 µg/mL), however when it was administered with rifampicin (MIC in combination with artemisinin = 0.0075 µg/mL), significantly reduced to 25 µg/mL against *M. tuberculosis*. Within the article, they report that the presence of artemisinin does indeed elevate peroxide levels in the cell, producing ROS radicals. They suspect that due to the hydrophobic nature of artemisinin, it resides mostly in the lipid membrane of the cells, where it can peroxidise the membrane which would lead to the degradation of the membrane and eventual cell death.

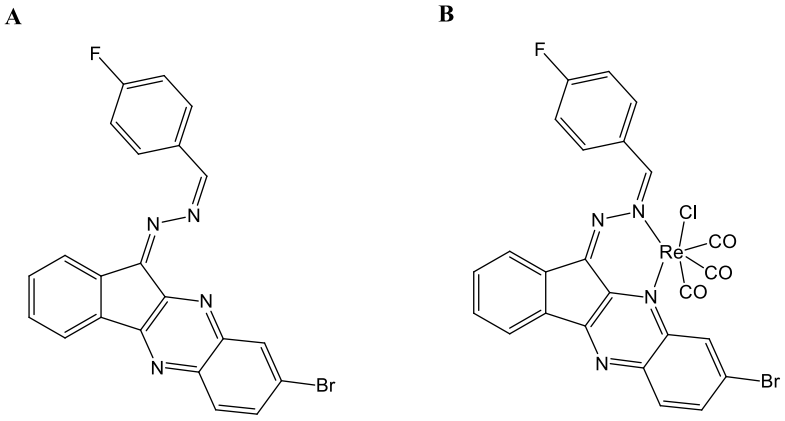

Figure 1.13. Antimicrobial structures synthesised by R. Varma *et al.*[74]

Examples of organometallic antibacterial agents are already being researched and show promising data for future studies. One such example, recently published by R. Varma *et al*.,[74] complexed rhenium to a quinoxaline base structure (seen in **Figure 1.13**) – quinoxaline is present in various antibacterial compounds. They reported

a significant increase in biological activity of the rhenium complexed scaffold (**Figure 1.13B** MIC against *S. aureus* = 82 µM), compared to its ligand (**Figure 1.13A** MIC against *S. aureus* = 265 µM). It would be interesting to study how future research would develop artemisinin as an antimicrobial that would include the incorporation of organometallic moieties to the artemisinin structure.

1.5. Aims and objectives:

1.5.1. Aim:

This project aims to improve the biological action of artemisinin primarily against the *P. falciparum* parasite by synthesising derivatives which contain organometallic groups. By addition of the organometallic moieties to the artemisinin scaffold, we hypothesise that it would improve the *in vitro* biological activity against *P. falciparum* and develop candidates for further study. We will also screen the compounds for anti-bacterial activity. The rise of anti-microbial resistance (AMR) is becoming a pressing concern and new anti-microbial candidates need to be found.

1.5.2. Objectives:

1.5.2.1. Synthesis and characterisation:

Two sets of compounds classified as (***1***) artemisinin triazole derivatives and (***2***) artesunate derivatives were synthesised. Both groups have either a ferrocenyl moiety or a ruthenium *p*-cymene moiety (**Figure 1.14**).

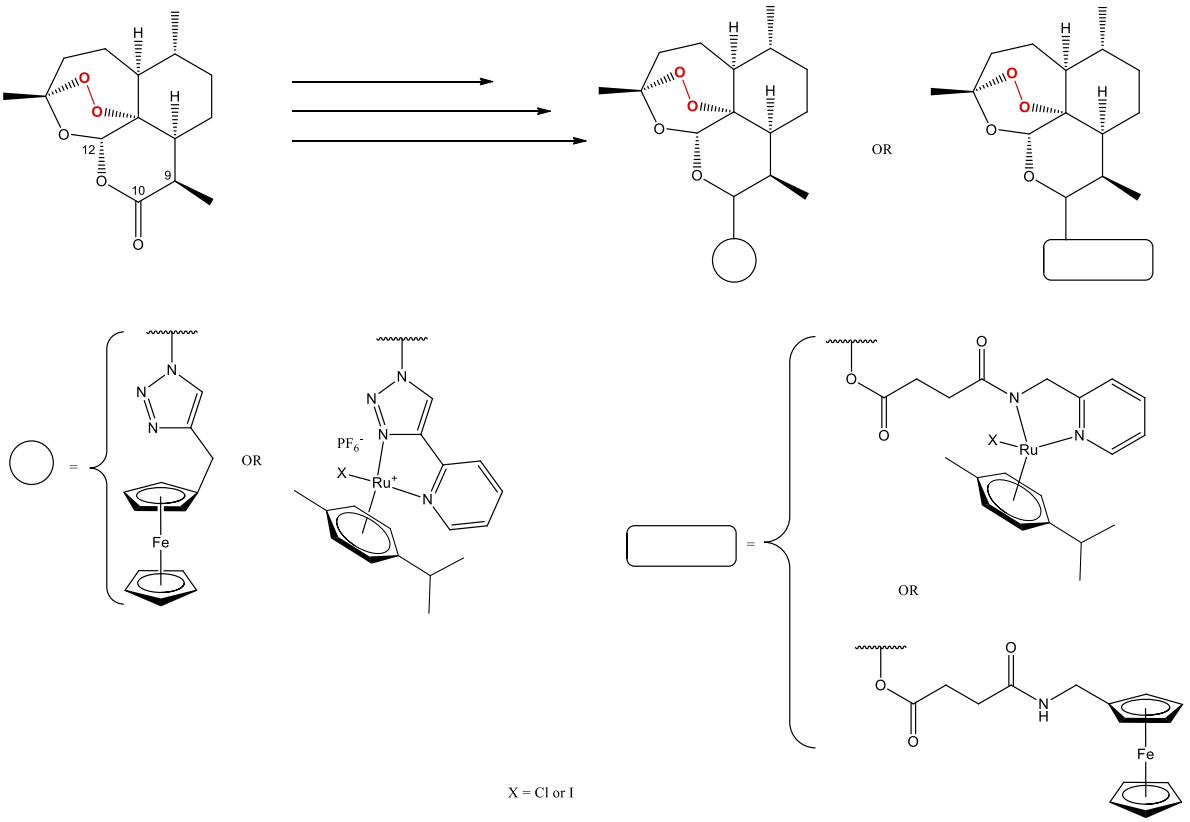

Figure 1.14. General depiction of the organometallic artemisinin derivatives that were prepared. The endoperoxide bridge is highlighted in red – which is the primary suspected pharmacophore.

Utilising simple and quick chemical reactions, we aimed to obtain our desired products in high yields after standard purification procedures. All new drug candidates were characterised with ^{1}H-NMR, ^{13}C{^{1}H}-NMR, infra-red (IR) spectroscopy and mass spectrometry to elucidate chemical structures. High performance liquid chromatography (HPLC) was performed to analyse the purity of the compounds prior to biological study.

We linked our organometallic moieties through either an amide-ester or a triazole group, in order to compare how it effects the biological efficacies against the *P. falciparum* parasites. It is well known that triazoles are chemically quite stable – not easily degraded in physiological conditions – whereas the ester bond of artesunate is easily hydrolysed in the human body. This is why artesunate type derivatives (hydrolysable acetyl C-10 derivatives) are highly biological active but are also short lived – low pharmacokinetic properties.[75] With the addition of an ionic metallacycle, a ruthenium (II) *para*-cymene moiety, we also try to improve the pharmacokinetic properties. For a comparison between the azide and amide-ester ruthenium complexes, we coordinated the ligand to the metal in a *N,N*-configuration. Literature shows that it is possible to isolate the *N,N*-configuration instead of the *N,O*-configuration for a picolinamide ruthenium *p*-cymene complex by the addition of electron withdrawing groups.[76,77] By using different linkers with a similar organometallic group, comparisons between their biological activities and physico-chemical properties, such as solubility, can be made. The final compounds were compared to their organometallic precursors and artemisinin in order to observe whether the organometallic incorporation will increase their respective biological activity and solubility.

1.5.2.2. Biological studies:

Turbidimetric assay

All drug candidates and precursors were tested for their solubility in the appropriate buffers; phosphate buffered saline (PBS) and HEPES used in anti-plasmodial assays.

Biological tests:

All drug candidates and their respective precursors were tested against 3D7 (wildtype) and Dd2 (chloroquine resistant) *P. falciparum* strains.

Cytotoxicity studies were carried out on a HEK cell line.

Minimum inhibition concentration (MIC) against the bacteria strains of *Staphylococcus aureus*, namely: Xen36 (wild type) strain and JE21 (methicillin resistant *S. aureus*) strain were also determined to probe the application to other microorganisms of our synthesised drug candidates.

1.6. Conclusion

With ACT becoming less reliable due to artemisinin resistant strains, the search for other chemotypes or the "recycling" of previously used antiplasmodial agents is a prime area of research. "Recycled" antiplasmodial agents refer to the derivatisation of the ineffective antimicrobial drug to regain biological activity. The recycled antimicrobial agents may also include the application against cancer or viral infections.

Increasing studies suggest that parent antiplasmodial drug complexed with metal moieties, like ferrocenyl groups and ruthenium-containing arene complexes were able to increase efficacy and inhibit antioxidant production, respectively.[26,50,78–81] Due to a metal's chemical properties, especially its bonding capabilities, increased structural diversity of organometallic complexes can exist compared to organic compounds.[50] Increased structural variability is accompanied by the metal and its ligands to rotate the positioning of its ligands as the stability of the isomers could differ slightly.[50] This is why second and third-row transition metals like Ru, Os, Ir, Rh are used in their stable oxidation state to constrain the ability for many structural isomers to form.[49,50,78–81] Excellent stability is presented in Ruthenium complexes (most with Ru(II)) that are resilient to degradation of biological molecules like glutathione.[50] This instigated the incorporation of ruthenium half-sandwich compounds into antiplasmodial agents to increase the biological activity of the drug.[49,50,78,80]

1.7. References:

1 WHO, *World Malaria report 2020: 20 years of global progress and challenges*, World Health Organization, 2020.

2 M. A. Biamonte, J. Wanner and K. G. Le Roch, *Bioorganic Med. Chem. Lett.*, 2013, 23, 2829–2843.

3 WHO, *Antimicrobial resistance: global report on surveillance.*, 2014.

4 World Health Organization, *Guidelines for the treatment of malaria*, 2015.

5 J. M. Willey, L. M. Sherwood and C. J. Woolverton, *Prescott's Microbiology, Eighth Edition*, McGraw Hill, Eight., 2010, vol. 11.

6 L. Florens, M. P. Washburn, J. D. Raine, R. M. Anthony, M. Grainger, J. D. Haynes, J. K. Moch, N. Muster, J. B. Sacci, D. L. Tabb, A. A. Witney, D. Wolters, Y. Wu, M. J. Gardner, A. A. Holder, R. E. Sinden, J. R. Yates and D. J. Carucci, *Nature*, 2002, **419**, 520–526.

7 A. M. Dondorp, S. Yeung, L. White, C. Nguon, N. P. J. Day, D. Socheat and L. Von Seidlein, *Nat. Rev. Microbiol.*, 2010, 8, 272–280.

8 P. E. Ferreira, G. Holmgren, M. I. Veiga, P. Uhlén, A. Kaneko and J. P. Gil, *PLoS One*, , DOI:10.1371/journal.pone.0023875.

9 R. T. Eastman, P. Khine, R. Huang, C. J. Thomas and X. Z. Su, *Sci. Rep.*, , DOI:10.1038/srep25379.

10 J. Gibbons, K. A. Button-Simons, S. R. Adapa, S. Li, M. Pietsch, M. Zhang, X. Liao, J. H. Adams, M. T. Ferdig and R. H. Y. Jiang, *BMC Genomics*, , DOI:10.1186/s12864-018-5207-7.

11 L. Paloque, A. P. Ramadani, O. Mercereau-Puijalon, J. Augereau and F. Benoit-Vical, *Malar. J.*, 2016, **15**, 149.

12 A. N. Mohon, M. S. Alam, A. G. Bayih, A. Folefoc, D. Shahinas, R. Haque and D. R. Pillai, *Malar. J.*, , DOI:10.1186/1475-2875-13-431.

13 A. K. Macleod, M. Mcmahon, S. M. Plummer, L. G. Higgins, T. M. Penning, K. Igarashi and J. D.

Hayes, *Carcinogenesis*, 2009, **30**, 1571–1580.

14 K. Itoh, N. Wakabayashi, Y. Katoh, T. Ishii, K. Igarashi, J. D. Engel and M. Yamamoto, *Genes Dev.*, 1999, **13**, 76–86.

15 J. Wang, C.-J. Zhang, W. N. Chia, C. C. Y. Loh, Z. Li, Y. M. Lee, Y. He, L.-X. Yuan, T. K. Lim, M. Liu, C. X. Liew, Y. Q. Lee, J. Zhang, N. Lu, C. T. Lim, Z.-C. Hua, B. Liu, H.-M. Shen, K. S. W. Tan and Q. Lin, *Nat. Commun.*, 2015, **6**, 10111.

16 A. S. Bhagavathula, A. A. Elnour and A. Shehab, *Infect. Dis. Poverty*, 2016, 5.

17 S. Müller, *Molecules*, 2015, 20, 10511–10534.

18 F. Mohring, M. Rahbari, B. Zechmann, S. Rahlfs, J. M. Przyborski, A. J. Meyer and K. Becker, *Free Radic. Biol. Med.*, 2017, **104**, 104–117.

19 J. D. Horton, H.R., Moran, L.A., Scrimgeour, K.G., Perry, M.D., and Rawn, L. A. Moran, H. R. Horton, K. G. Scrimgeour, M. Perry and J. D. Horton, H.R., Moran, L.A., Scrimgeour, K.G., Perry, M.D., and Rawn, *Principles of Biochemistry*, Pearson Prentice Hall, 2006.

20 A. F. G. Slater, *Chloroquine: Mechanism of drug action and resistance in plasmodium falciparum*, 1993, vol. 57.

21 P. D. Roepe, *Biochemistry*, 2011, **50**, 163–171.

22 C. Biot, D. Taramelli, I. Forfar-Bares, L. A. Maciejewski, M. Boyce, G. Nowogrocki, J. S. Brocard, N. Basilico, P. Olliaro and T. J. Egan, *Mol. Pharm.*, 2005, **2**, 185–193.

23 J. A. Read, K. W. Wilkinson, R. Tranter, R. B. Sessions and R. L. Brady, *J. Biol. Chem.* , 1999, **274**, 10213–10218.

24 A. Leed, K. DuBay, L. M. B. Ursos, D. Sears, A. C. De Dios and P. D. Roepe, *Biochemistry*, 2002, **41**, 10245–10255.

25 W. H. O. WHO, *WHO*, 2016, 186.

26 C. Reiter, T. Fröhlich, M. Zeino, M. Marschall, H. Bahsi, M. Leidenberger, O. Friedrich, B. Kappes, F. Hampel, T. Efferth and S. B. Tsogoeva, *Eur. J. Med. Chem.*, 2015, **97**, 164–172.

27 L. Tilley, J. Straimer, N. F. Gnädig, S. A. Ralph and D. A. Fidock, *Trends Parasitol.*, 2016, 32, 682–696.

28 A. V. Pandey, B. L. Tekwani, R. L. Singh and V. S. Chauhan, *Artemisinin, an endoperoxide antimalarial, disrupts the hemoglobin catabolism and heme detoxification systems in malarial parasite*, 1999, vol. 274.

29 B. Meunier and A. Robert, *Acc. Chem. Res.*, 2010, **43**, 1444–1451.

30 F. Benoit-Vical, J. Lelièvre, A. Berry, C. Deymier, O. Dechy-Cabaret, J. Cazelles, C. Loup, A. Robert, J. F. Magnaval and B. Meunier, *Antimicrob. Agents Chemother.*, 2007, **51**, 1463–1472.

31 P. Olliaro, *Mode of action and mechanisms of resistance for antimalarial drugs*, 2001, vol. 89.

32 R. K. Haynes and S. Krishna, *Microbes Infect.*, 2004, 6, 1339–1346.

33 S. R. Meshnick, *Artemisinin: Mechanisms of action, resistance and toxicity*, 2002, vol. 32.

34 P. M. O'Neill, V. E. Barton and S. A. Ward, *Molecules*, 2010, **15**, 1705–1721.

35 M. Asano and H. Iwahashi, *Eur. J. Med. Chem.*, 2017, **127**, 740–747.

36 A. Robert, F. Benoit-Vical and B. Meunier, in *Coordination Chemistry Reviews*, 2005, vol. 249, pp. 1927–1936.

37 C. Reiter, A. Çapcı Karagöz, T. Fröhlich, V. Klein, M. Zeino, K. Viertel, J. Held, B. Mordmüller, S. Emirdağ Öztürk, H. Anıl, T. Efferth and S. B. Tsogoeva, *Eur. J. Med. Chem.*, 2014, **75**, 403–412.

38 G. H. Posner, A. J. McRiner, I. H. Paik, S. Sur, K. Borstnik, S. Xie, T. A. Shapiro, A. Alagbala and B. Foster, *J. Med. Chem.*, 2004, **47**, 1299–1301.

39 D. R. Rice, M. de Lourdes Betancourt Mendiola, C. Murillo-Solano, L. A. Checkley, M. T. Ferdig, J. C. Pizarro and B. D. Smith, *Bioorganic Med. Chem.*, 2017, **25**, 2754–2760.

40 C. Hemmert, A. P. Ramadani, L. Boselli, Á. Fernández Álvarez, L. Paloque, J. M. Augereau, H. Gornitzka and F. Benoit-Vical, *Bioorganic Med. Chem.*, 2016, **24**, 3075–3082.

41 F. Dubar, C. Slomianny, J. Khalife, D. Dive, H. Kalamou, Y. Guérardel, P. Grellier and C. Biot, *Angew. Chemie - Int. Ed.*, 2013, **52**, 7690–7693.

42 K. Becker, L. Tilley, J. L. Vennerstrom, D. Roberts, S. Rogerson and H. Ginsburg, *Int. J. Parasitol.*, 2004, **34**, 163–189.

43 S. Kumar, M. Guha, V. Choubey, P. Maity and U. Bandyopadhyay, *Life Sci.*, 2007, 80, 813–828.

44 M. A. L. Blackie, P. Beagley, S. L. Croft, H. Kendrick, J. R. Moss and K. Chibale, *Bioorg. Med. Chem.*, 2007, **15**, 6510–6516.

45 W. A. Wani, E. Jameel, U. Baig, S. Mumtazuddin and L. T. Hun, *Eur. J. Med. Chem.*, 2015, 101, 534–551.

46 L. Delhaes, C. Biot, L. Berry, L. A. Maciejewski, D. Camus, J. S. Brocard and D. Dive, *Bioorganic Med. Chem.*, 2000, **8**, 2739–2745.

47 A. Martínez, C. Deregnaucourt, V. Sinou, C. Latour, D. Roy, J. Schrével and R. A. Sánchez-Delgado, *Med. Chem. Res.*, 2017, **26**, 473–483.

48 L. Rylands, A. Welsh, K. Maepa, T. Stringer, D. Taylor, K. Chibale and G. S. Smith, *Eur. J. Med. Chem.*, 2019, **161**, 11–21.

49 M. Adams, C. De Kock, P. J. Smith, K. M. Land, N. Liu, M. Hopper, A. Hsiao, A. R. Burgoyne, T. Stringer, M. Meyer, L. Wiesner, K. Chibale and G. S. Smith, *Dalt. Trans.*, 2015, **44**, 2456–2468.

50 G. Gasser and N. Metzler-Nolte, *Curr. Opin. Chem. Biol.*, 2012, 16, 84–91.

51 N. Chavain and C. Biot, *Curr. Med. Chem.*, 2010, **17**, 2729–2745.

52 S. P. Fricker, R. M. Mosi, B. R. Cameron, I. Baird, Y. Zhu, V. Anastassov, J. Cox, P. S. Doyle, E. Hansell, G. Lau, J. Langille, M. Olsen, L. Qin, R. Skerlj, R. S. Y. Wong, Z. Santucci and J. H. McKerrow, *J. Inorg. Biochem.*, 2008, **102**, 1839–1845.

53 C. Gabbiani, L. Messori, M. A. Cinellu, A. Casini, P. Mura, A. R. Sannella, C. Severini, G. Majori, A. R. Bilia and F. F. Vincieri, *J. Inorg. Biochem.*, 2009, **103**, 310–312.

54 M. Navarro, *Coord. Chem. Rev.*, 2009, 253, 1619–1626.

55 C. Hemmert, A. Fabié, A. Fabre, F. Benoit-Vical and H. Gornitzka, *Eur. J. Med. Chem.*, 2013, **60**, 64–75.

56 J. Yang, Y. He, Y. Li, X. Zhang, Y. K. Wong, S. Shen, T. Zhong, J. Zhang, Q. Liu and J. Wang, *Pharmacol. Ther.*, 2020, **216**, 107697.

57 Z. Li, Q. Li, J. Wu, M. Wang and J. Yu, *Molecules*, 2016, 21.

58 C.-J. Zhang, J. Wang, J. Zhang, Y. M. Lee, G. Feng, T. K. Lim, H.-M. Shen, Q. Lin and B. Liu, *Angew. Chemie*, 2016, **128**, 13974–13978.

59 T. Efferth, *Semin. Cancer Biol.*, 2017, 46, 65–83.

60 Y.-F. Dai, W.-W. Zhou, J. Meng, X.-L. Du, Y.-P. Sui, L. Dai, P.-Q. Wang, H.-R. Huo and F. Sui, *Med. Chem. Res.*, 2017, **26**, 867–880.

61 T. Efferth, M. R. Romero, A. Rita Bilia, A. Galal Osman, M. ElSohly, M. Wink, R. Bauer, I. Khan, M. Camilla Bergonzi and J. J.G. Marin, *World J. Tradit. Chinese Med.*, 2016, **2**, 1–23.

62 W. E. Ho, H. Y. Peh, T. K. Chan and W. S. F. Wong, *Pharmacol. Ther.*, 2014, 142, 126–139.

63 E. D. Brown and G. D. Wright, *Nature*, 2016, **529**, 336–343.

64 M. I. Konaklieva, *SLAS Discov.*, 2019, 24, 419–439.

65 A. T. Dharmaraja, *J. Med. Chem.*, 2017, **60**, 3221–3240.

66 J. Lemire, A. Alhasawi, V. P. Appanna, S. Tharmalingam and V. D. Appanna, *J. Appl. Microbiol.*, 2017, **123**, 798–809.

67 S. S. Boswihi and E. E. Udo, *Curr. Med. Res. Pract.*, 2018, **8**, 18–24.

68 W. Choi, *J. Clin. Med.*, 2017, **6**, 30.

69 H. Cui, X. Chen, M. Bai, D. Han, L. Lin and M. Dong, *ACS Appl. Mater. Interfaces*, 2019, **11**, 47299–47310.

70 L. Lin, X. Mao, Y. Sun and H. Cui, *Microb. Pathog.*, 2018, **118**, 66–73.

71 C. Wu, J. Liu, X. Pan, W. Xian, B. Li, W. Peng, J. Wang, D. Yang and H. Zhou, *Molecules*, 2013, **18**, 6866–6882.

72 L. Wang, C. Hu and L. Shao, *Int. J. Nanomedicine*, 2017, 12, 1227–1249.

73 Y. S. Patel, N. Mistry and S. Mehra, *Tuberculosis*, 2019, **115**, 146–153.

74 R. R. Varma, J. G. Pandya, F. U. Vaidya, C. Pathak, R. A. Dabhi, M. P. Dhaduk, B. S. Bhatt and M. N. Patel, *J. Mol. Struct.*, 2021, **1240**, 130529.

75 M. A. Van Agtmael, T. A. Eggelte and C. J. Van Boxtel, *Artemisinin drugs in the treatment of malaria: From medicinal herb to registered medication*, 1999, vol. 20.

76 S. H. van Rijt, A. J. Hebden, T. Amaresekera, R. J. Deeth, G. J. Clarkson, S. Parsons, P. C. McGowan and P. J. Sadler, *J. Med. Chem.*, 2009, **52**, 7753–7764.

77 A. Ashraf, M. Hanif, M. Kubanik, T. Söhnel, S. M. F. Jamieson, A. Bhattacharyya and C. G. Hartinger, *J. Organomet. Chem.*, 2017, **839**, 31–37.

78 P. Chellan, K. M. Land, A. Shokar, A. Au, S. H. An, D. Taylor, P. J. Smith, T. Riedel, P. J. Dyson, K. Chibale and G. S. Smith, *Dalt. Trans.*, 2014, **43**, 513–526.

79 E. Ekengard, L. Glans, I. Cassells, T. Fogeron, P. Govender, T. Stringer, P. Chellan, G. C. Lisensky, W. H. Hersh, I. Doverbratt, S. Lidin, C. de Kock, P. J. Smith, G. S. Smith and E. Nordlander, *Dalt. Trans*, 2015, 19314–19329.

80 N. B. de Souza, A. C. C. Aguiar, A. C. de Oliveira, S. Top, P. Pigeon, G. Jaouen, M. O. F. Goulart and A. U. Krettli, *Mem. Inst. Oswaldo Cruz*, 2015, **110**, 981–988.

81 P. Chellan, K. M. Land, A. Shokar, A. Au, S. H. An, D. Taylor, P. J. Smith, K. Chibale and G. S. Smith, *Organometallics*, 2013, **32**, 4793–4804.

Chapter 2: Synthesis of new organo-ruthenium and ferrocenyl artemisinin derivatives

2.1. Introduction:

Artemisinin (ART), a complex sesquiterpene lactone (**Figure 2.1**), does not possess as many sites that can be easily derivatised when compared to quinoline based compounds such as chloroquine and its many derivatives (**Figure 2.1**).[1,2] The introduction of organometallic moieties to the artemisinin scaffold has great potential to increase the biological efficacy of artemisinin against resistant plasmodium strains by increasing the structural diversity of artemisinin with the use of hypervalent transition metals or variation of ancillary ligands. In this way, solubility, physiological stability and biological activity of the compound can be improved.[3]

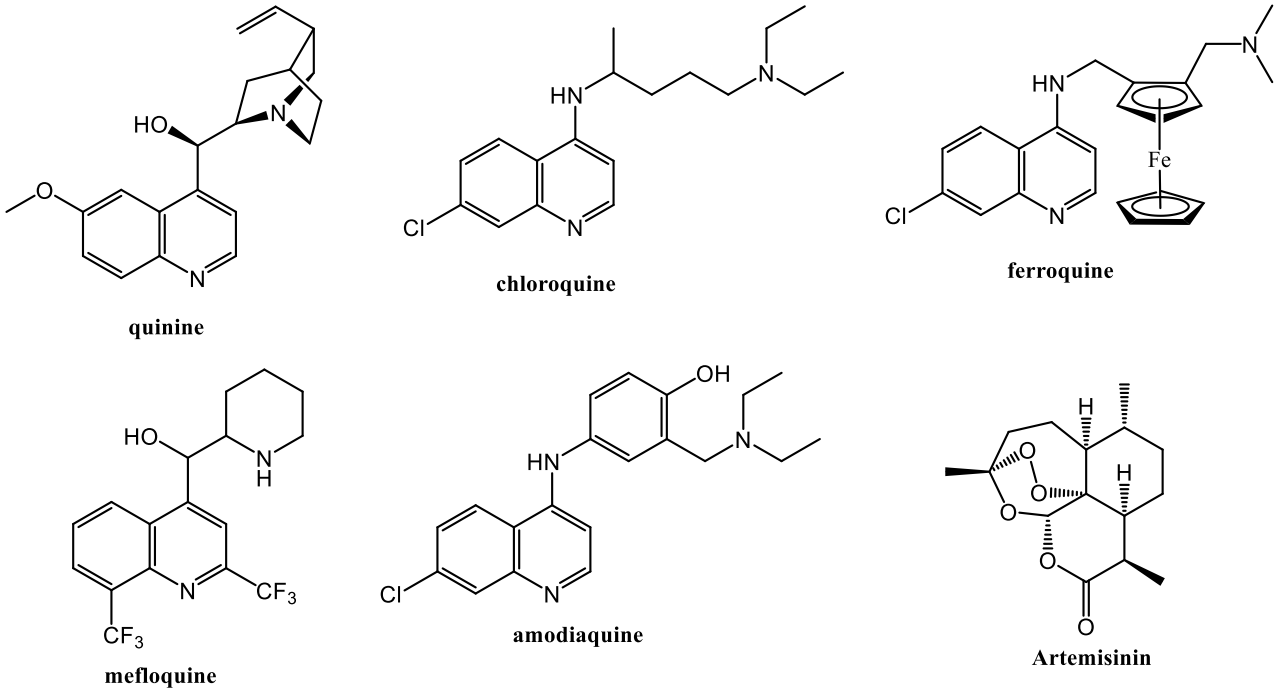

Figure 2.1. Structures of chloroquine and some of its derivatives and artemisinin.[1,2]

Even though ART has great activity against the *Plasmodium* parasite and displays promising pharmacodynamic properties, it lacks in pharmacokinetic properties, as it struggles with solubility and bioavailability.[4–7] Thus, there is a surge in research to develop artemisinin derivatives with improved pharmacokinetic properties, while maintaining or enhancing biological activities. Literature has shown that ART is easily derivatised at the 10th position (**Figure 2.2**) with various ethers, esters and alkyl derivatives.[8] Using more rigorous reaction methods, it is also possible to functionalise ART at the 11th position, producing tertiary lactam rings (**Figure 2.2**).[9–11] Derivatisation at position 9 can also be achieved but through extensive synthetic routes.[12–15]

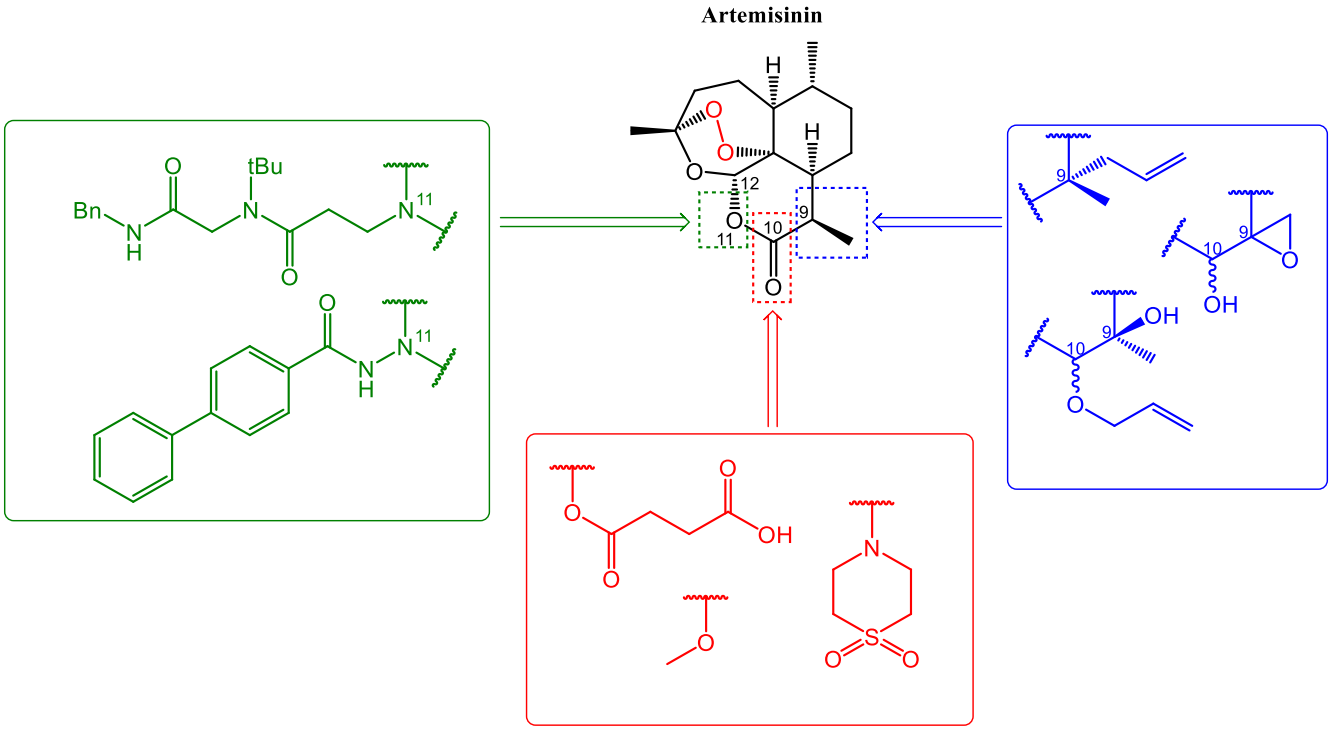

Figure 2.2. General schematic representation of reported derivatisations of artemisinin at positions 9, 10 and 11.[8–15]

Increasing evidence has indicated that non-acetal C-10 derivatives of ART have greater activity against the malarial parasite, compared to its acetal analogues which is hydrolysable.[15,16] We therefore designed our series of compounds to incorporate a very stable linker such as a triazole or an amide ester. – which has robust methods that were extensively researched and optimised for non-peroxide containing compounds[17] In this chapter the derivatisation of ART at the carbonyl group in position 10 to synthesise a small series of triazole (non-acetyl) and ester linked (acetyl) organometallic complexes is discussed. Examples of C-10 artemisinin triazoles, ester and amide-ester like artemisinin derivatives (**Figure 2.3**) have been reported.[11,18–21]

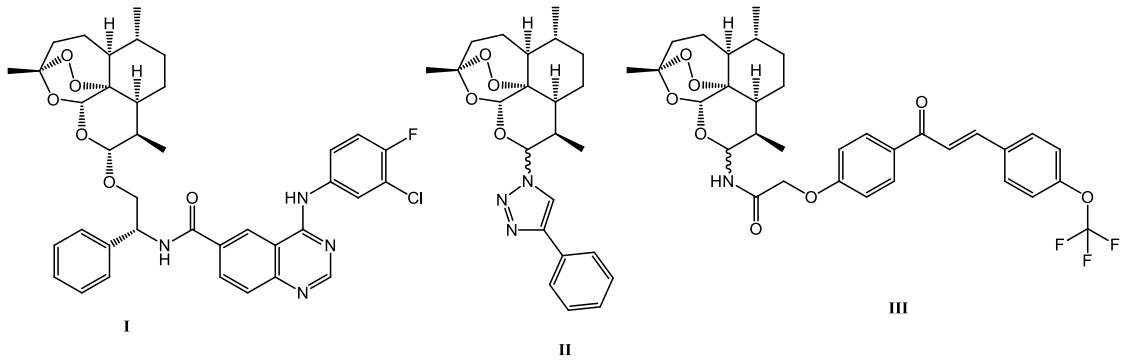

Figure 2.3. Reported artemisinin C-10 derivatives with promising biological activity.[19–21]

Multiple studies from several groups revealed that artemisinin derivatives have improved selectivity and potency towards diseases when hybridised or modified with other pharmacophores.[7,11,18–22] Compound **I** (**Figure 2.3**)[20] is a hybrid molecule of artemisinin with a 4-(arylamino)quinazoline, the pharmacophore of Gefitinib. It is a 10α isomer and showed excellent selectivity towards a colorectal cell-line compared to a skin melanoma cell-line. Moreover, it displayed comparably similar if not better activity than the clinically used Gefitinib during *in vitro* and *in vivo* studies at sub-micromolar levels. The researchers realised that certain linkers, chiral rigidity and its stereochemistry around the C-10 are important to biological activity. The

importance of stereochemistry around C-10 becomes apparent when reviewing biological data of compound **II**,[19] where the 10β isomer is less active than its 10α counterparts. Contrary to the latter results, amide compound **III**,[21] displayed IC_{50} against HT-29 cell-line (human colon cancer) respectively, as 0.36 μM (10β) and 0.39 μM (10α). Clearly there is a delicate balance between chain length from C-10 and the linker.

2.2. Results and discussion:

2.2.1. Triazole linked ART compound (1-3)

2.2.1.1. Synthesis

Complexes **2** and **3** were prepared as shown in **Scheme 2.1**, which required the artemisinyl-azido **intermediate 2** (**ART-N_3**). First, artemisinin (**ART**) was reduced with sodium borohydride stirred in cold methanol to produce compound **dihydroartemisinin** (**DHA**) in quantitative yields using a reproducible literature method.[23]

DHA was then subjected to a nucleophilic substitution reaction with chlorotrimethyl silane followed by substitution with an azide in a one pot reaction using a potassium iodide catalyst, affording **intermediate 2** as a colourless-yellow oil in 90% yield after purification with chromatography. The well-known copper(I)-catalysed alkyne-azide cycloaddition (CuAAC) reaction, also called "click-chemistry",[24] was applied to synthesise our ligand **1** and complex **3**.

Triazolisation is thermodynamically favoured,[24] however ligand **1** and complex **3** continued to be challenging to synthesise. **Intermediate 2** was reacted with the appropriate terminal alkyne (2-ethynyl pyridine or **intermediate 3**) with catalytic amounts of copper (I) iodide and the monodentate amino ligand, DIPEA, in acetonitrile, with the addition of sodium ascorbate. After purification with silica chromatography, both ligand **1** and complex **3** were obtained in low yields. Throughout our studies we obtained low yields performing modified click-reactions, ultimately suspecting oxidation of the copper (I) catalyst that reacted with the endo-peroxide bridge, hence the addition of sodium ascorbate. Since we desire the 1,4-triazole regioisomer, we investigated various copper(I) or copper(II) catalysts and reaction conditions however all the reactions yielded similar results.[24–28]

The ferrocenyl **intermediate 3** was synthesised in a one-pot reaction of propargyl amine with ferrocene carboxaldehyde followed by reduction of the imino-bond. **Intermediate 3** was obtained as an orange-red crystalline solid in 86% yield after purification with silica column chromatography. It was also noted that ferrocene methyl alcohol was produced as a minor by-product (from unreacted aldehyde).

Complexes **2a** and **2b** was synthesised by the addition of the appropriate ruthenium dimer to ligand **1** in a methanol/dichloromethane solution (for **2a**) and only dichloromethane solution (for **2b**) followed by the addition of the PF_6^- counterion after coordination of the metal moiety to the ligand. Purification was carried out via recrystallisation from a solution of toluene/hexane for complex **2a** and trituration with diethyl ether for complex **2b**. Thin layer chromatography indicated that the iodido-complex, **2b**, had a slower reaction rate

compared to **2a** which displayed full complexation of the ligand to the metal centre within one hour whereas **2b** had unreacted dimer present.

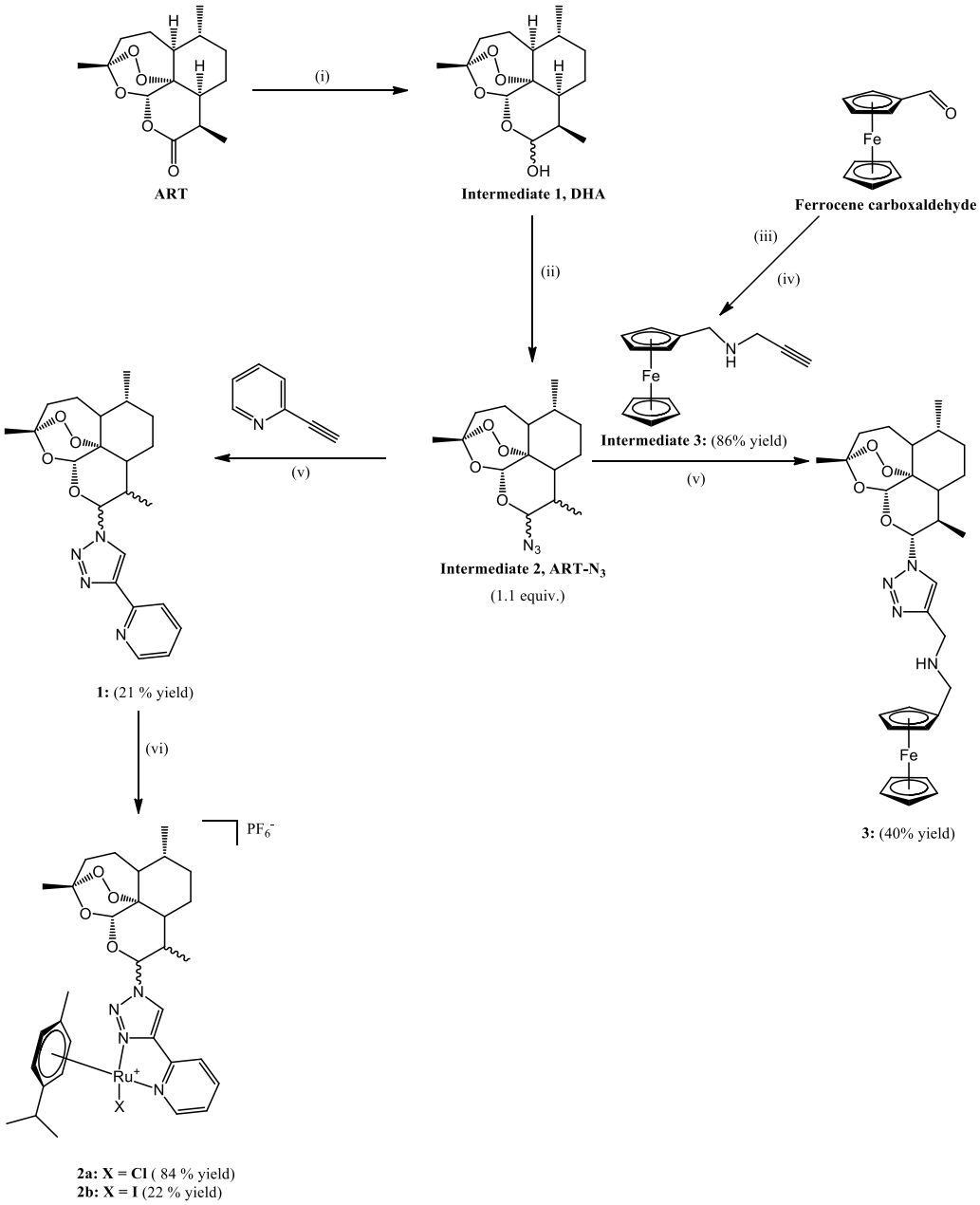

Scheme 2.1. Synthetic route to the artemisinyl-triazole complexes 2-3. Reaction conditions: (i) $NaBH_4$ (3.5 equiv.), MeOH, 1 h, *ca*. 0 °C; (ii) TMSCl (1.5 equiv.), NaN_3 (4.5 equiv.), KI (0.25 equiv.), DCM, 3 h 30 min, 0 °C – rt.; (iii) Propargyl amine (1.2 equiv.), MeOH, 24 h, rt.; (iv) $NaBH_4$ (2.0 equiv.), MeOH, 1 h, *ca*. 0 °C (v) appropriate alkyne (1.0 equiv.), CuI (0.05 equiv.), DIPEA (0.10 equiv.), sodium ascorbate (0.20 equiv.), MeCN/H_2O (1:1), 18 h, 0 °C – rt.; (vi) 2a: [Ru(*p*-cymene)Cl_2]$_2$ (0.5 equiv.), MeOH/DCM (2:1), 2 h, rt.; NH_4PF_6 (2 equiv.), MeOH/DCM (2:1), 50 min, rt.; 2b: [Ru(*p*-cymene)I_2]$_2$ (0.5 equiv.), DCM, 1 h 30 min, rt.; NH_4PF_6 (2 equiv.), MeOH/DCM (2:1), 1 h, rt.

2.2.1.2. Characterisation

The reduction of artemisinin to **DHA** (**intermediate 1**) was first confirmed by using ATR-IR spectroscopy, which clearly indicated the absence of the strong carbonyl-stretch absorption band that is observed for **ART** at 1733 cm^{-1} and the appearance of a very strong absorption band at 3377 cm^{-1} corresponding to the hydroxyl group.

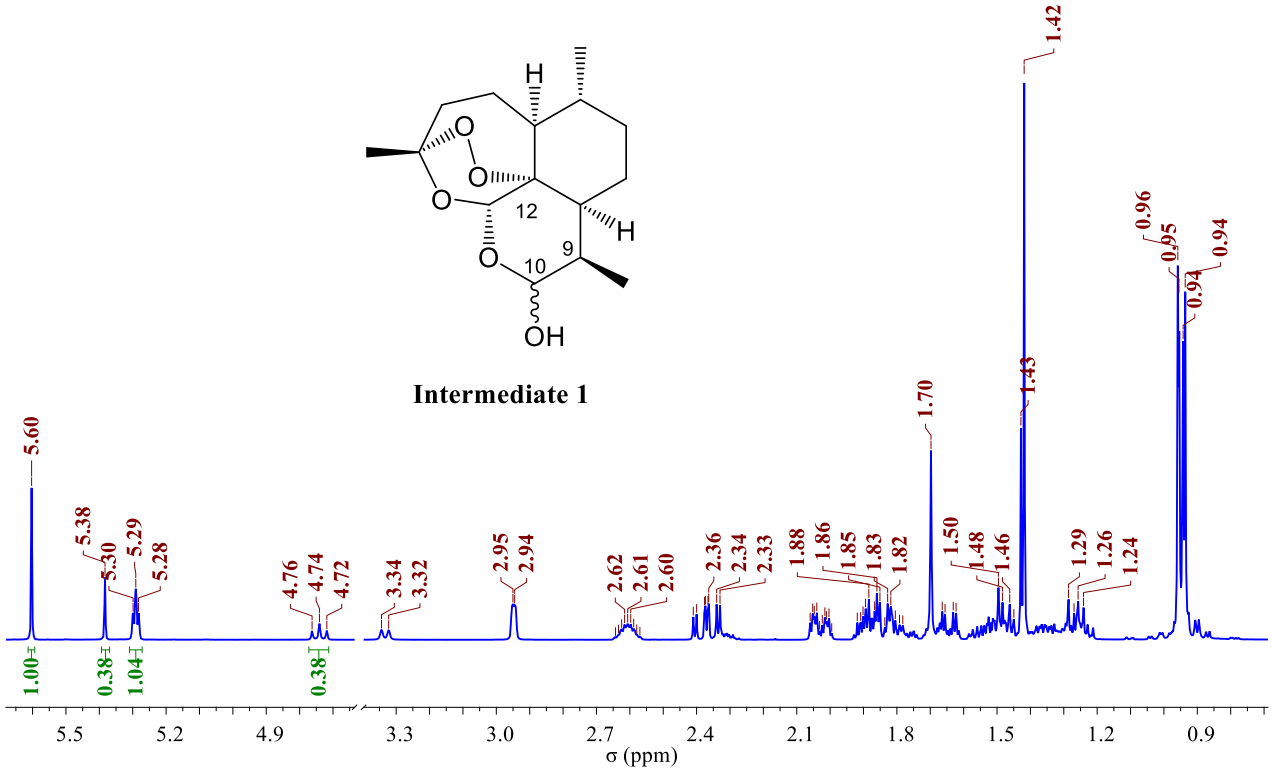

Figure 2.4. The ^{1}H-NMR ($CDCl_3$) spectrum of **DHA (Intermediate 1).**

The ^{1}H-NMR spectrum of **DHA** (**Figure 2.4**) was compared to literature results and similarly displayed the presence of both α-**DHA**- and β-**DHA**-epimers. It is known that **DHA** epimerises at position 10 in solution depending on the polarity of the solvent (**Figure 2.5**).[29] Characteristic proton resonances were identified in the region between 5.60 ppm and 4.60 ppm and assigned to protons H-12 and H-10. A correlation between the position of H-10 and the *J*-coupling constant to H-9 has been noted in the literature. [15,29–31]

According to previous studies, a gauche relationship exists between the proton H-10 and its neighbouring proton which is related to an antiperiplanar arrangement of protons like in a chair pyranose ring (**Figure 2.5**).[29] Due to the latter relationship, the lower ^{3}J-coupling constant value are correlated with a *cis* configuration leading to the β epimer, whilst the larger ^{3}J-coupling constant correlated to a *trans*-axial configuration that is consistent with the α epimer (Figure 2.13). The protons, H-9 and H-10, are positioned either in a trans-diaxial (α) or in an axial-equatorial (β) position.[32,33] The β-epimer of **DHA** is represented by the singlet peak at 5.60 ppm assigned to the H-12 proton and the triplet (^{3}J = 3.3 Hz) at 5.30 ppm to the H-10 proton that couples to

H-9. The α-epimer has been assigned to the singlet at 5.38 ppm (H-12) and the triplet (^3J = 8.8 Hz) at 4.76 ppm (H-10), corresponding with previous literature findings.[32,34]

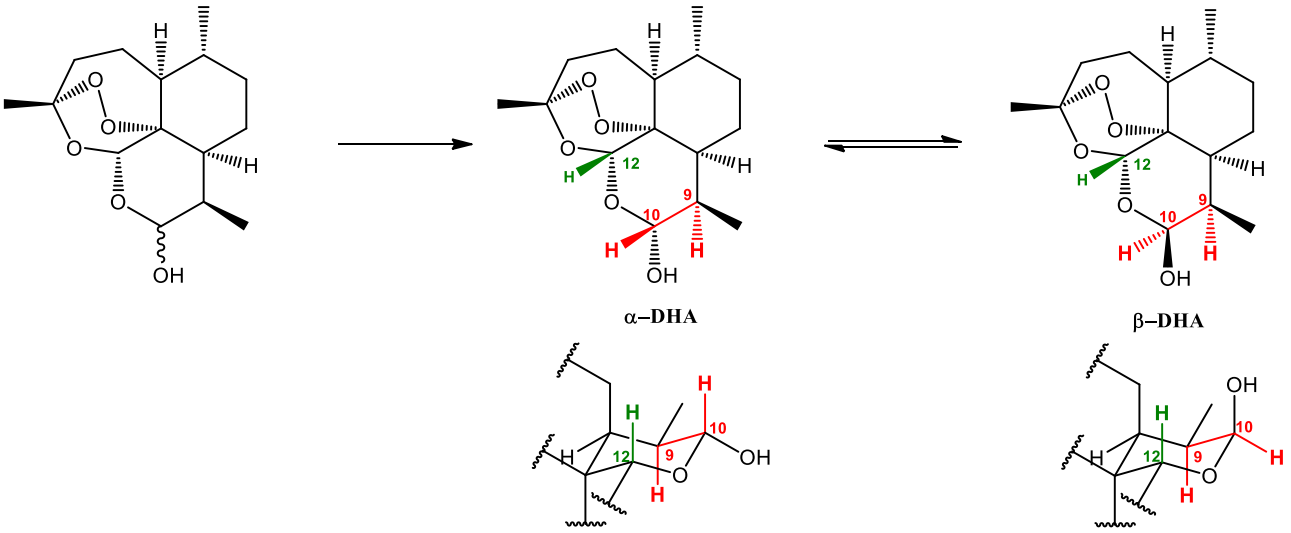

Figure 2.5. The epimerisation of **DHA.**

IR analysis of **intermediate 2** showed the characteristic azido-absorption band at 2105 cm^{-1}, and the disappearance of the hydroxyl absorption band. Comparing the ^{1}H-NMR spectra (**Figure 2.6**) with literature,[19,21] we obtained a mixture of isomers. The isomers were separated by column chromatography for ^{1}H-NMR characterisation. The three isolated isomers of **intermediate 2** were identified as: 9α,10β- (**intermediate 2a**), 9β,10α-azidoartemisinin (**intermediate 2b**) and 9β,10β- (**intermediate 2c**). The potassium iodide catalyst may have influenced the enantiomeric ratio, we obtained 1.2: 1: 16.5 (intermediates **2a**:**2b**:**2c**) respectively, compared to a ratio of 1:3:1 from a literature method that did not use potassium iodide or any catalyst.[19]

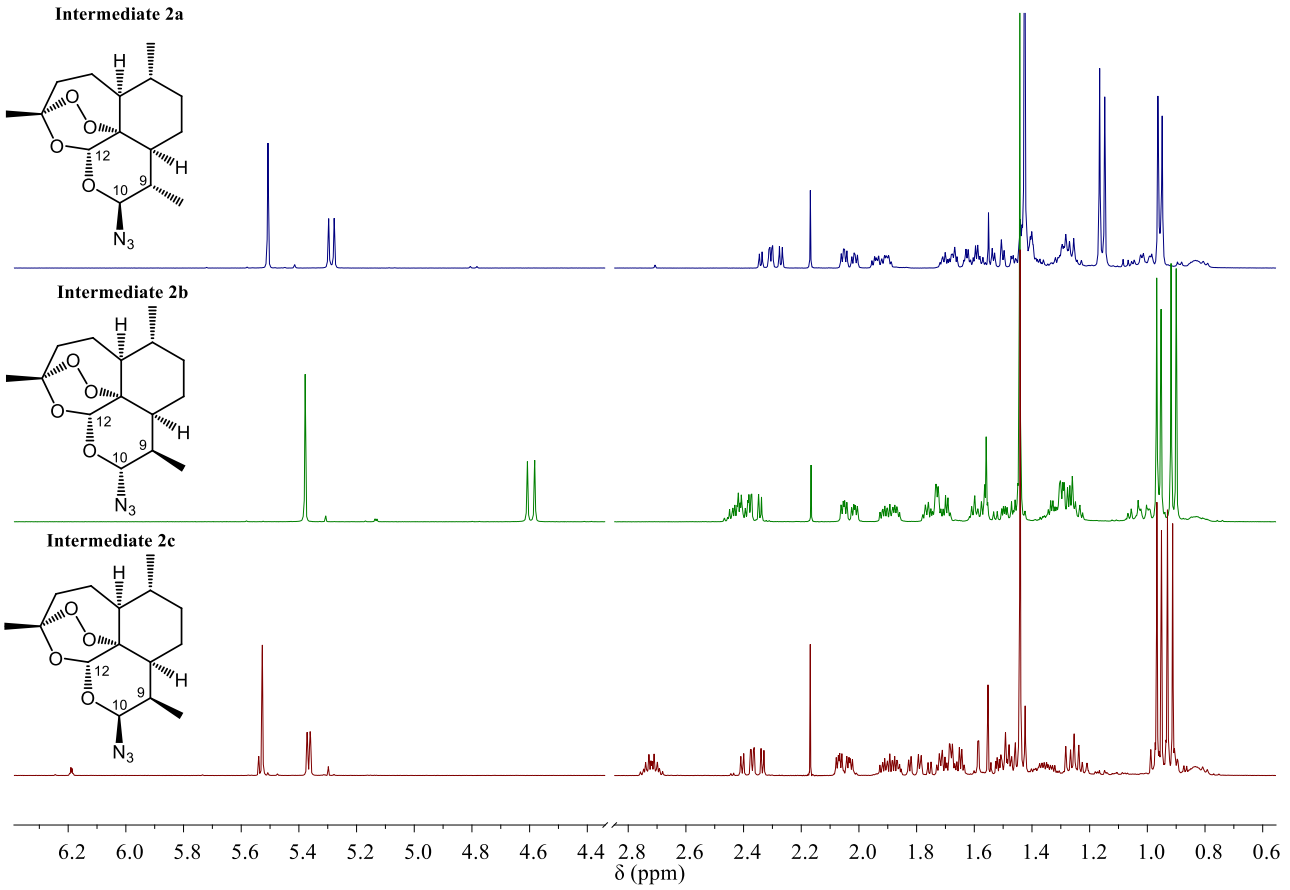

Figure 2.6. ^{1}H-NMR spectra ($CDCl_3$) of the isolated **ART-N_3. Intermediate 2a**: 9α,10β-azidoartemisinin (top); **Intermediate 2b**: 9β,10α-azidoartemisinin (middle); **Intermediate 2c**: 9β,10β-azidoartemisinin (bottom) with an hydroartemisinin impurity.

Evaluating the expansion spectra of **intermediate 2** (**Figure 2.7**)**: Intermediate 2a** was identified by the singlet at 5.51 ppm which was assigned to H-12 and H-10 to the doublet at 5.30 ppm with ^{3}J coupling to H-9 of 7.6 Hz. Isomer **intermediate 2b** showed the singlet resonating at 5.38 ppm for H-12 and doublet for H-10 at 4.61 ppm with ^{3}J coupling =10.2 Hz. **Intermediate 2c**, was found to be the major isomer and H-12 was assigned to the singlet at 5.53 ppm and a doublet for H-10, integrated for one proton at 5.37 ppm with ^{3}J coupling = 4.1 Hz.

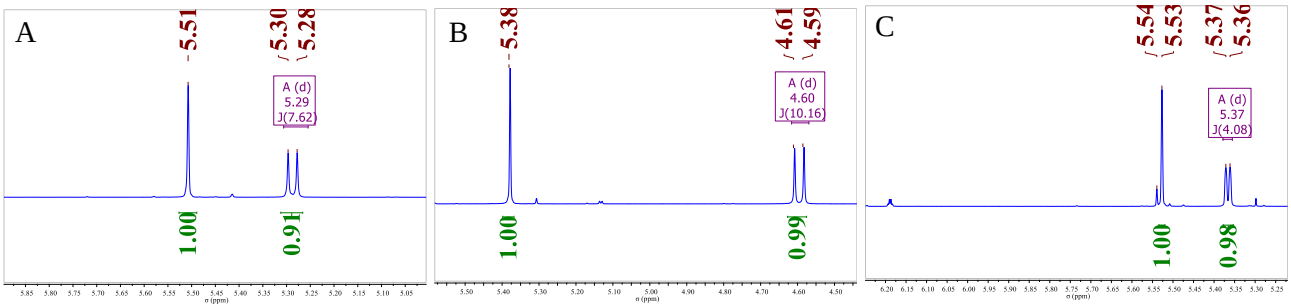

Figure 2.7. ^{1}H-NMR ($CDCl_3$) expansion spectra **of intermediate 2a** (A), **2b** (B) and **2c** (C).

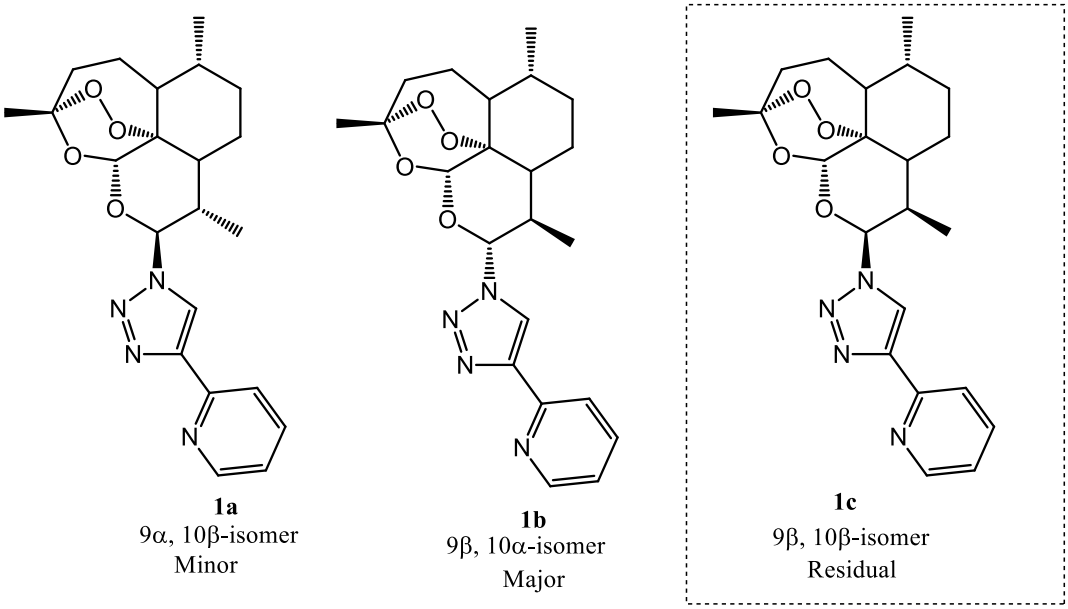

Figure 2.8. Chemical structures of the isomers of **compound 1.**

Purified through gravity, column chromatography afforded compound **1** as a mixture of three isomers, one of which was obtained in residual amount (**Figure 2.8**). Though reverse phase HPLC indicated a purity of more than 95%, further method development is required to separate the three isomers of compound **1** – two isomers co-eluted. ATR-IR spectroscopy revealed the loss of the strong azide absorption band 2105 cm^{-1}. The isomers were identified as follows: the minor 9α,10β-isomer (**1a**), the major 9β,10α-isomer (**1b**) and the and residual 9β,10β-isomer (**1c**). Low experimental yields of compound **1** could be explained from the apparent isomeric ratio observed in the ^{1}H-NMR spectra from **ART-N$_3$** and compound **1**. The ^{1}H-NMR indicated that **intermediate 2c** did not readily follow the Huisgen 1,3-dipolar cycloaddition reaction to produce **1c**. The isomeric mixture of **intermediate 2** consisted largely of **intermediate 2c**, hence a low overall yield was obtained for compound **1**. Similarly seen in a literature study,[19] it was stipulated that only a small amount of **intermediate 2c** reacts during the click reaction due to the sterically hindered azide group in the axial position (**Figure 2.9**).

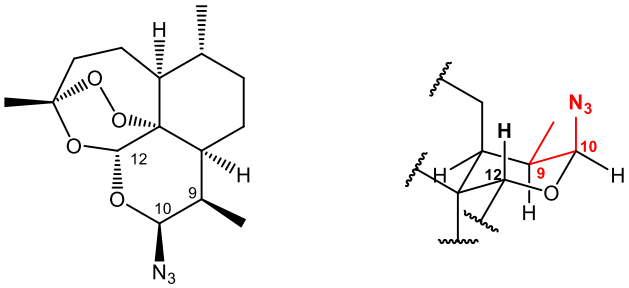

Figure 2.9. Intermediate 2c chemical structure and model.

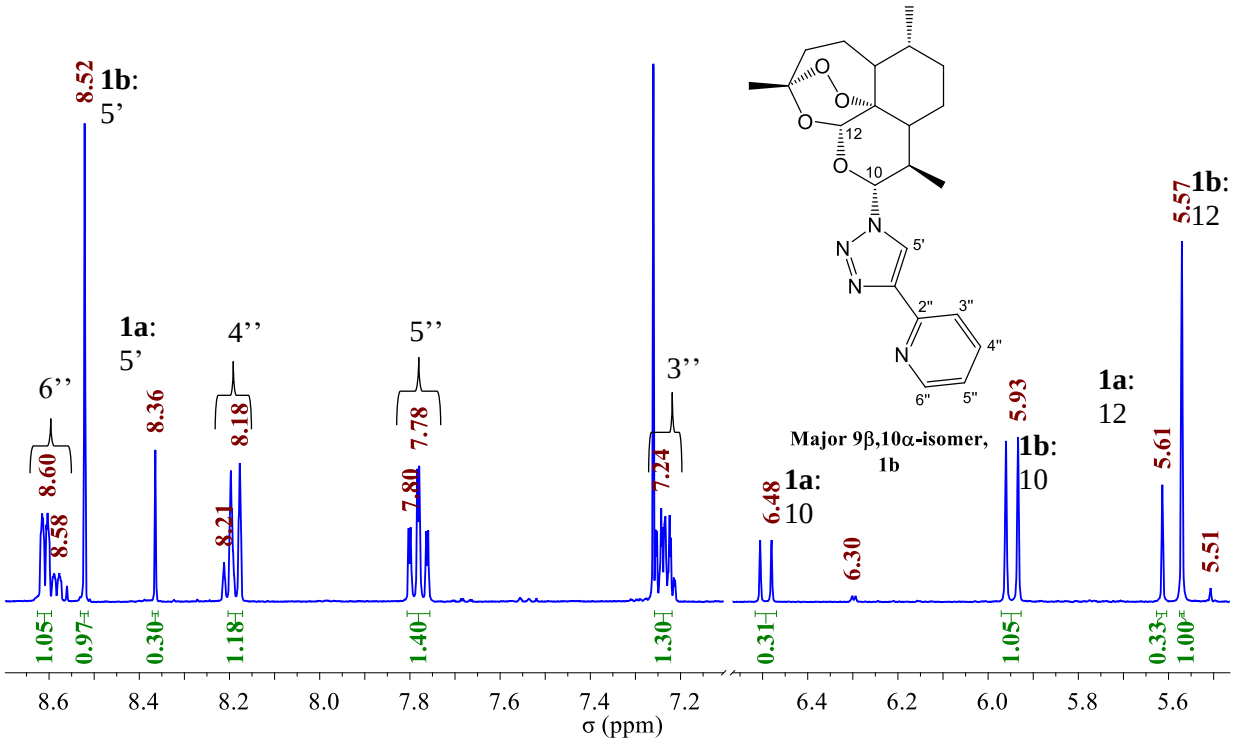

Figure 2.10. Expansion ^{1}H-NMR ($CDCl_3$, 400 MHz) spectrum of **compound 1**.

The expansion ^{1}H-NMR spectrum of compound **1** is seen in **Figure 2.10**: The full spectrum (see **appendix**) clearly indicated that no unreacted 2-ethynylpyridine was present,[35] as no methine proton signal was observed at 3.25 ppm. Literature articles that produced a benzene-triazole derivative of compound **1** and other 2-ethynyltriazoles assisted in assigning the isomers of compound **1**.[19,35] The pyridine ring was assigned: The signal that integrated for one proton as a doublet of doublet of doublets at 8.61 ppm was assigned to the proton at 6'' (see **Figure 2.11**). Proton at position 6'' is the most downfield in the aromatic ring due to distorted electron-density of the pyridine ring. Since there is less electron density *ortho* to the nitrogen (as resonance structures would suggest), it is apparent that proton at 6'' is at 8.61 ppm. The latter signal appeared as a doublet of doublet of doublets due to ^{3}J-coupling to proton 5'', ^{4}J-coupling to proton 4'' and although very unlikely, ^{5}J-coupling to proton H-3''. ^{5}J- coupling usually has < 1 Hz, and for this compound it displayed a splitting constant of 0.84 Hz.

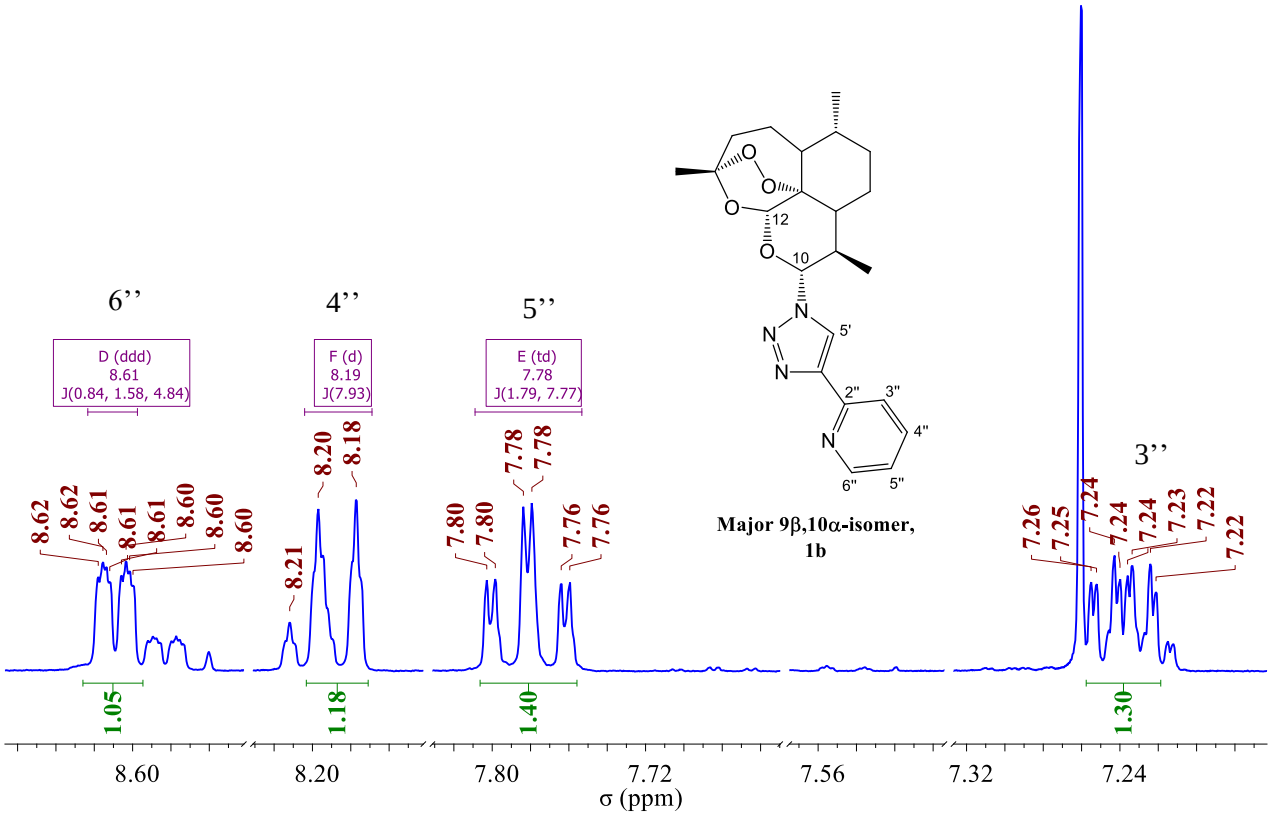

Figure 2.11. Expansion ^{1}H-NMR spectrum of **compound 1** between 8.6-7.2 ppm.

Since H-4'' is *para* to the pyridine nitrogen (has a slight positive-dipole), it was assigned to the doublet at 8.20 ppm. H-4'' had a ^{3}J-coupling = 7.93 Hz to H-3'' and H-5''. If looked closely, the doublet signal is slightly distorted/ unresolved due to a slightly different ^{3}J-splitting of H-3'' and H-5''. This ^{3}J-coupling could be correlated to the ^{3}J-splitting (7.77 Hz) observed in the triplet of doublets at 7.80 ppm, assigned to H-5''. ^{4}J-coupling of 1.80 Hz to H-3'' is observed. The H-3'' would then be assigned to the multiplet at 7.24 ppm, which nearly overlaps with the deuterated solvent peak. Further indication of a successful click-reaction is due to the appearance of the deshielded singlet peak at 8.52 ppm, which correlated with a methine triazole signal (H-5') of the benzylic-derivative of Cho S. *et al.*[19,35] The minor isomer, compound **1a**, has its methine singlet peak at 8.36 ppm (H-5'). The artemisinin moiety H-10 and H-12 were then assigned: For the major isomer, compound **1b**, the doublet at 5.95 ppm were assigned to the H-10 and the singlet at 5.57 ppm to H-12. Compound **1b** was assigned to the 9β,10α-isomer due to a 10.73 Hz ^{3}J-coupling constant of H-10 that was very similar to the 10α-benzene-triazole isomer from Cho *et al.*[19] The minor 9α,10β-isomer (**1a**) was assigned to the doublet at 6.51 ppm (^{3}J-coupling constant of 10.06 Hz) and singlet at 5.61 ppm for H-10 and H-12, respectively. Compound **1a**, too, had a similar ^{3}J-H-10 coupling constant to the 9α,10β-benzene-triazole isomer from Cho *et al.*[19] ESI^{+}-

MS data of the expected $[M+H^+]^+$ molecular ion value (413.2144 *m/z*) compared very well with the experimental value (413.2176 *m/z*) found.

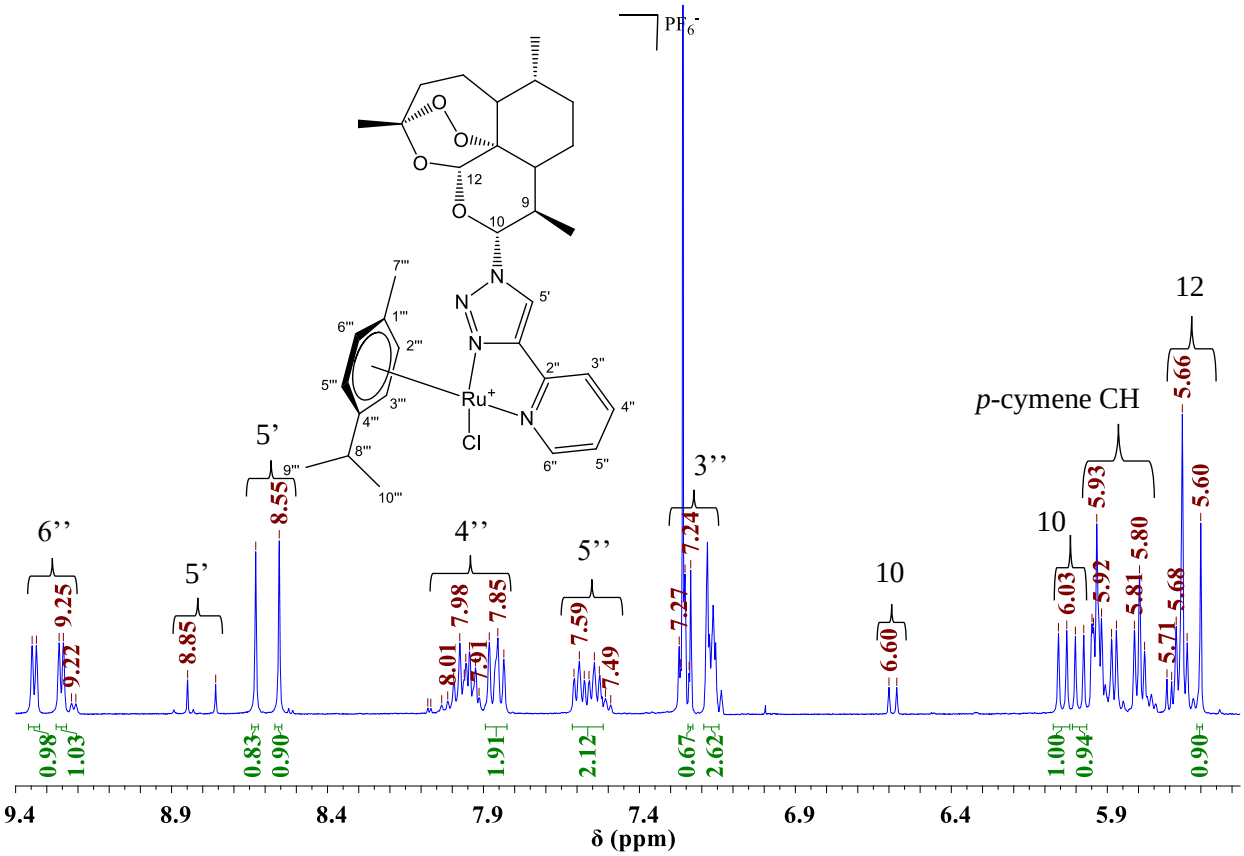

Figure 2.12. Expansion ^{1}H-NMR spectrum of **compound 2a** ($CDCl_3$).

Due to the complex chemical structure of **compound 2**, similar ruthenium complexes from literature study[36] were used to assist the assignment of protons for complex **2a** (**Figure 2.12**). 2D-^{1}H-NMR (COSY) performed on complex **2a** revealed three stereoisomers of the rutheno-cycle were present. Further 2D-^{1}H-NMR studies are required to fully assign which stereoisomers are present in the complex mixture. The ^{1}H-NMR suggests that complex **2a** has two different rutheno-isomers for both ligand precursors **1a** and **1b**, as four triazole methine proton signals are present at 8.85 and 8.76 (H-5' of complex of ligand **1a**); 8.63 and 8.55 ppm (H-5' of complex of ligand **1b**). However, it is unclear as to why H-10 of complex **2a** has two doublets (6.06 ppm to 5.98 ppm) with ^3J-coupling constant of 10.72 Hz (from ligand **1b**) yet only one doublet for H-10 at 6.60 ppm of ^3J-coupling constant of 10.05 Hz (from ligand **1a**). Furthermore, during reverse phase HPLC purity analysis, the chromatogram displayed four signals of interest that are observed as two sets of pairs. Compared to the HPLC chromatogram of ligand **1**, it is possible that the two quantifiable isomers from ligand **1a** and **1b** furnished two rutheno-stereoisomers for each of complex **2a**. Moreover, ESI$^+$-MS revealed a high abundance of the expected parent molecular ion of compound **2a** $[M\text{-}PF_6^-]^+$: 683.1947 *m/z* was found (expect value = 683.1933 *m/z*).

The integration was based on the major 10α-artemisinin isomer, of which its H-10 and H-12 protons were assigned to 6.05 ppm (doublet peaks coupling constant correlated to the 10α-isomer) and 5.60 ppm, respectively. Furthermore, only certain pyridine proton signals from different ruthenium complex isomers are

fully separated from each other, like the doublet peaks representing proton 5'' at 9.32 and 9.24 ppm (which integrated for one proton each). Some signals overlapped between 8.01 ppm – 7.83 ppm region. This multiplet integrated for two protons and not for the expected one proton, suggesting the presence of multiple isomers in the sample. The *p*-cymene methine protons (H-2'''; H-3'''; H-5'''; H-6''') resonate between 5.96 and 5.62 ppm as overlapping multiplets. The resulting forest of proton signals thus further suggest that the compound is a mixture of stereoisomers.

Complex **2b** displayed an absorbance band at 1581 cm^{-1} for the pyridine C=N stretch, compared to ligand **1** which displayed a band at 1571 cm^{-1} for its pyridine C=N stretch. The latter is indicative that the ruthenium moiety complexed through the nitrogen atoms of the ligand. However, the PF_6^- counter ion stretch which occurs at 835 cm^{-1} has a very weak signal when compared to complex **2a**. ESI^+-MS data revealed that complex **2b** had a similar expected molecular ion as **2a**, that resulted giving $C_{32}H_{42}IF_6N_4O_4PRu$ as $[M\text{-}PF_6^-]^+$ = 775.1298 *m/z* (expected = 775.1289 *m/z*).

The ^{1}H-NMR of **2b** is seen in **Figure 2.13**. Comparing **2b** with **2a**, it was noted that the proton H-10 displayed as two pairs of doublets at 6.59 ppm to 6.55 ppm whereas **2a** had a pair of doublets at 6.06 ppm to 5.98 ppm. Both doublets have a *J*-coupling constant to 10.2 Hz, which corresponds to the 10α position of the ligand for **2b**. This would indicate that **2a**, with a chlorido bond has isomers of 10β, whereas the iodo bond in **2b** produced 10α isomers. The *p*-cymene C-H protons could be assigned to the skew doublets at 5.73 ppm and 5.68 ppm respectively that did integrate for two protons each. It is clear from the ^{1}H-NMR spectra for complex **2b** that an improved purification method is required as unreacted ruthenium dimer is still present in the sample. Furthermore, the ^{1}H-NMR spectrum showed that a more extensive drying method is required, due to the prerence of the dichloromethane impurity at 5.30 ppm – this was after the compound was dried under high vacuum for 16 hours. It is difficult to assign proton H-12 in the multiplet region from 6.12 ppm to 5.66 ppm. The triazole proton H-5' is assigned to the singlet at 8.67 ppm which integrated well for one proton.

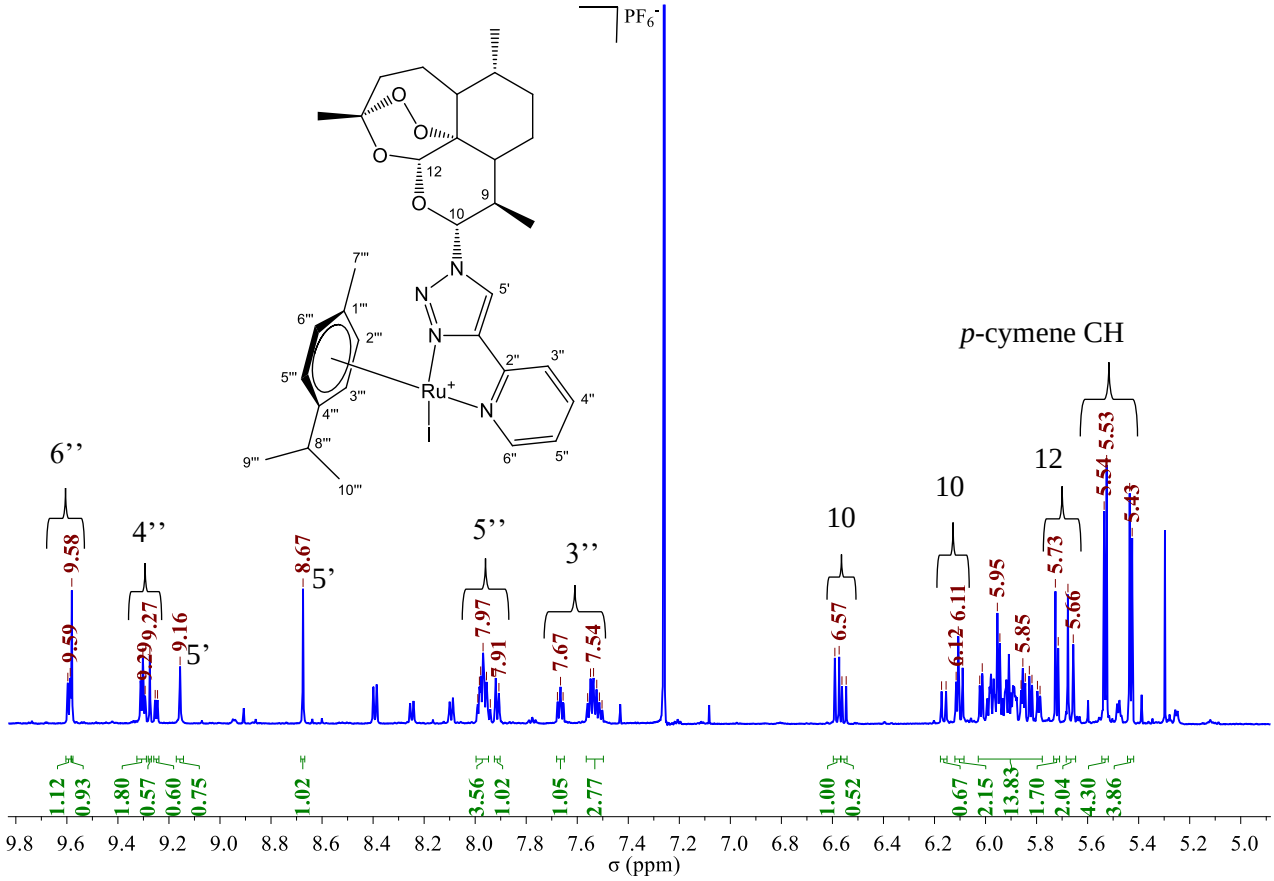

Figure 2.13. ^{1}H-NMR expansion spectrum of **complex 2b** ($CDCl_3$).

IR analysis confirmed the appearance of a weak 2089 cm^{-1} stretch of a sp C-C bond and the loss of the imino-bond at 1642 cm^{-1} that reduction to **intermediate 3** was successful. The proton NMR spectrum (**Figure 2.14**) displayed all proton signals of the desired amine (**intermediate 3**). This new compound was assigned to the signals as follows: The substituted cyclopentadiene ring (H-7 to H-10) protons was easily discerned from the unsubstituted ring (H-11 to H-15) protons. The triplet peaks at 4.21 ppm and 4.12 ppm were respectively H-7 & H-10 and H-8 & H-9, both sets of triplet peaks integrated for 2 protons. The singlet at 4.14 ppm was assigned to the unsubstituted cyclopentadienyl ring protons, H-11 to H-15. The characteristic methine proton, H-1, was assigned to the triplet at 2.26 ppm which coupled to H-3, which respectively was assigned to the doublet at 3.46 ppm – both triplet and doublet peaks had a *J* coupling constant of 2.42 Hz which corresponded to an allylic type ^{4}J coupling.

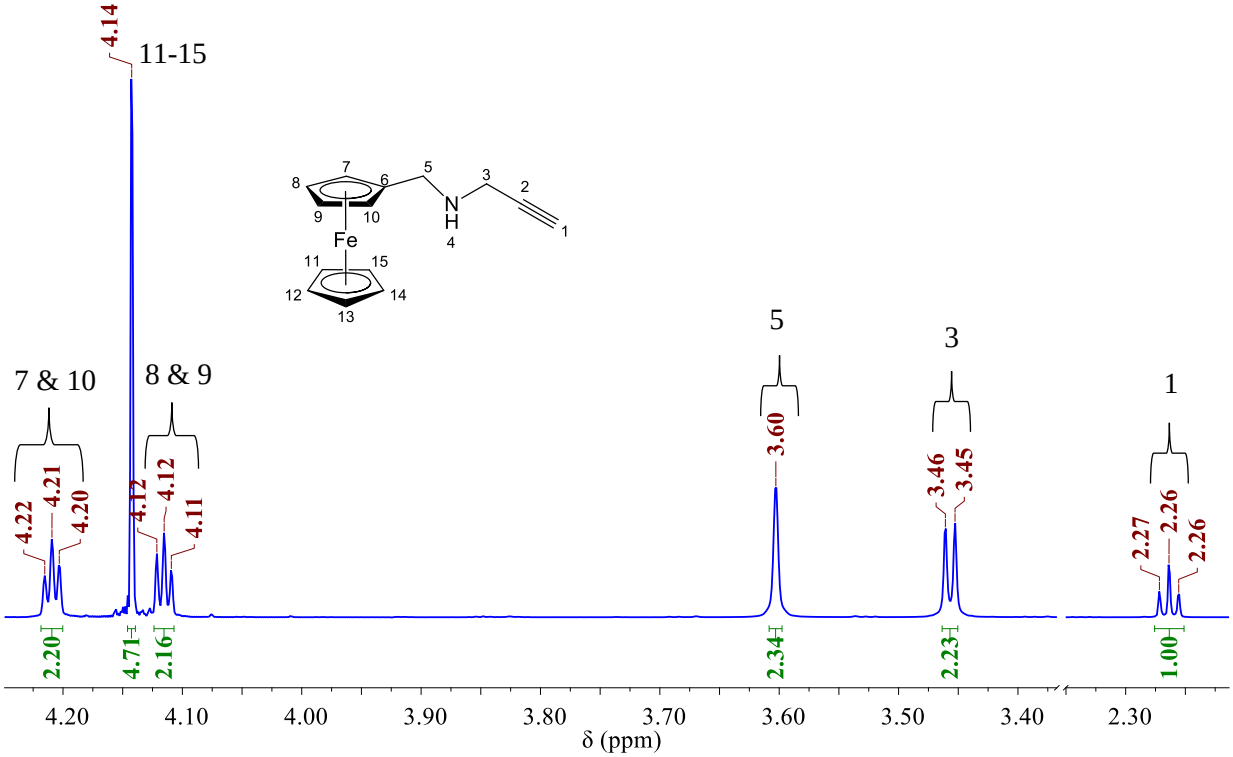

Figure 2.14. Expansion ^{1}H-NMR ($CDCl_3$) spectrum of **intermediate 3**.

Therefore, the singlet peak at 3.60, which roughly integrated for two protons was assigned to the methylene protons H-5. The amine proton of H-4, however, was not observed in this spectrum, as it may most likely be exchanging at a rapid rate with the water present in the sample – a strong water peak was observed at 1.51 ppm and a residual methylene chloride proton signal at 5.30 ppm (not shown in Figure 2.12). ^{13}C{^{1}H}-NMR of **intermediate 3** was analysed and all carbons were accounted for except an extra irregular secondary or quaternary carbon signal observed at 71.59 ppm – which does not correlate to any solvent impurity.

Similar to ligand **1**, two quantifiable isomers of triazole **3** were identified as the major 9β, 10α-isomer (**3b**) and the minor 9α, 10β-isomer (**3a**) present. The absence of the azide signal in the IR spectrum indicates that the reaction was successful.

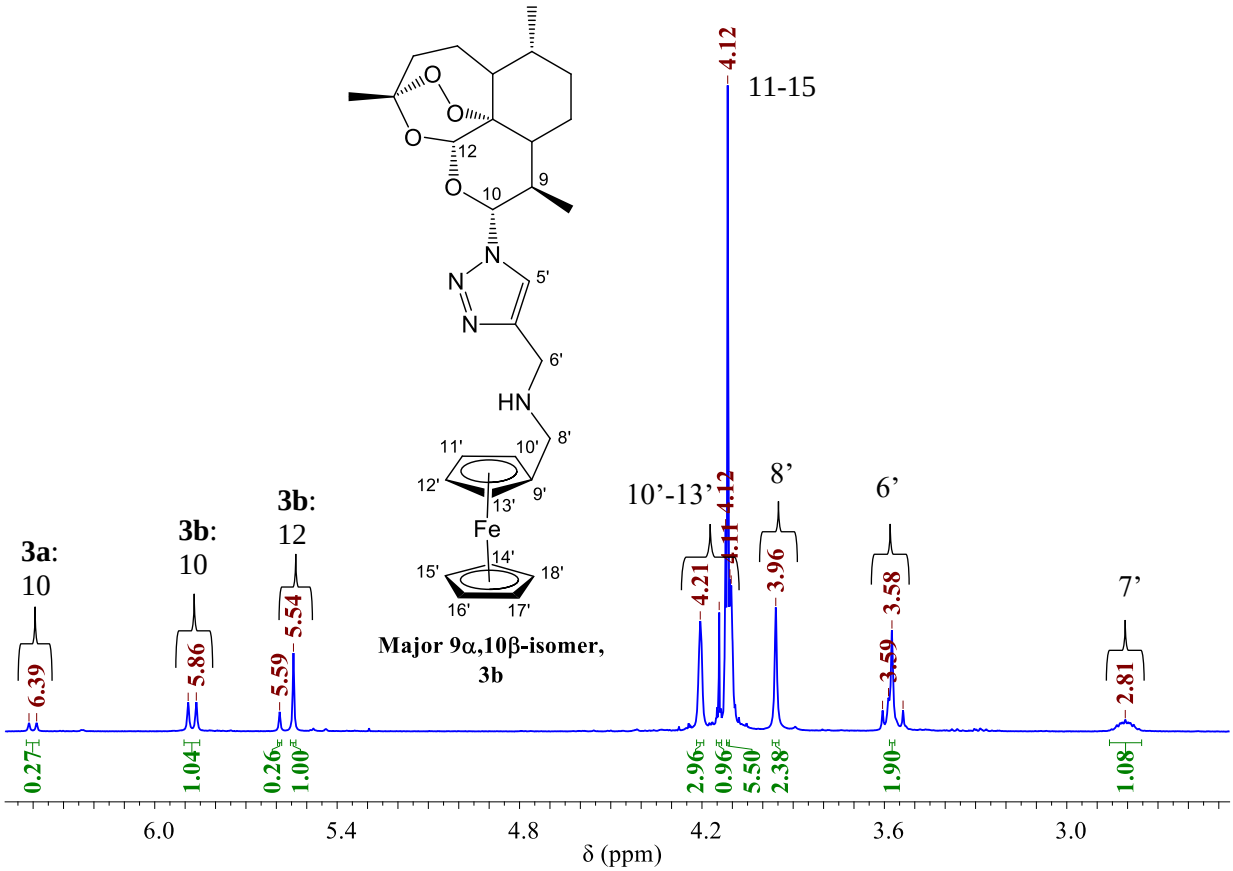

Figure 2.15. Expansion ^{1}H-NMR ($CDCl_3$, 400 MHz) spectrum of **compound 3.**

The ^{1}H-NMR (**Figure 2.15**) for compound **3** revealed a doublet at 5.88 ppm that corresponded to H-12 of the major 9β, 10α-isomer and a doublet at 6.40 ppm for the minor 9α, 10β-isomer. Therefore, the singlets for H-12 and H-5' were assigned to 5.54 ppm and 7.81 ppm respectively – for the major isomer. It is evident from the spectrum that the ferrocenyl moiety of compound **3** (4.21 to 3.54 ppm) of both isomers overlaps with one another, resulting in odd integrations. With an exception to the latter, proton H-6' displayed an unresolved singlet at 3.58 ppm with an integration of 1.90 (relatively good integration for 2H). Proton, H-8', was assigned to the singlet at 3.96 ppm and the amine proton at position 7' assigned to the broad singlet at 2.81 ppm The proton signals for the substituted cp-ring overlapped with the proton signal for the unsubstituted cp-ring to form a multiplet between 4.20-4.10 ppm.

APT-^{13}C{^{1}H}-NMR of compound **3** was performed and assigned. The artemisinin carbon signals were identified[19,35,37] and the carbon signals of the ferrocenyl moiety were identified[38,39] comparing it to the ^{13}C{^{1}H}-NMR spectrum of compound **1** (see **appendix**). It was noted that the carbon spectrum of compound **3** requires more time to acquire an improved carbon spectrum as no signal was observed to correspond to the triazole quaternary.[39] C-4' was not able to be observed as it could have overlapped with the carbon of the artemisinin moiety at 85.89 ppm. A slight positive signal is observed at 86.23 ppm however comparing well with the same carbon position of **intermediate 3**. Even with no observable methine carbon (C-5') we are certain that we produced compound **3** as its ESI^{+} mass spectrum correlated very well with its expected value (*m/z* calcd for $C_{29}H_{38}FeN_4O_4$ $[M+H^{+}]^{+}$: 563.2276, found 563.2325).

2.2.2. Artesunate-amido compounds (4-6)

2.2.2.1. Synthesis

Complexes **5** and **6** were prepared from artesunate (**intermediate 4**) as depicted in **Scheme 2.2**.

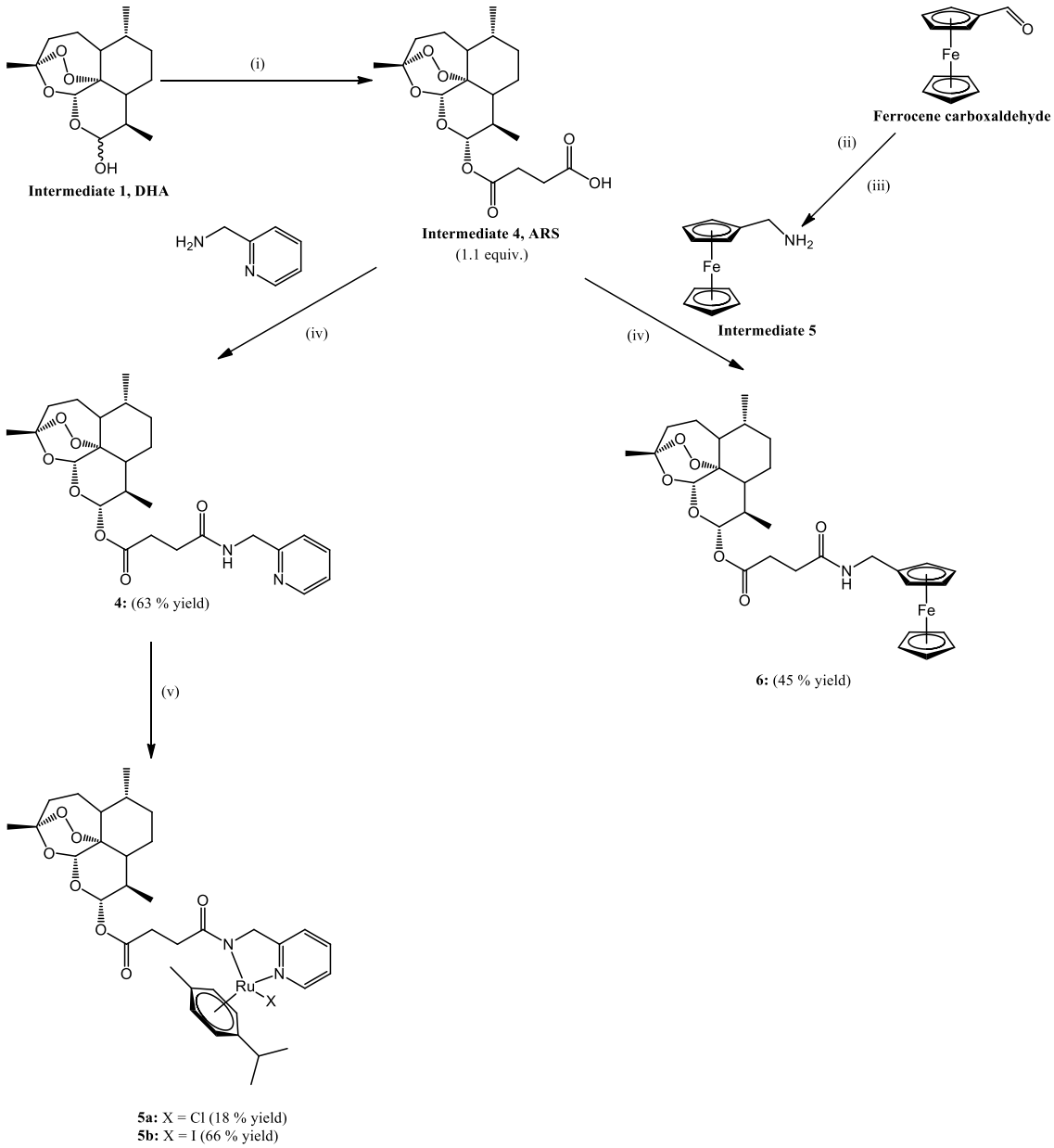

Scheme 2.2. Synthetic route to the artesunate-amido complexes 5 and 6. Reaction conditions: (i) Succinic anhydride (2.0 equiv.), Triethyl amine (1.1 equiv.), EtOAc, 22 h, rt.; (ii) NH_2OH-HCl (2.0 equiv.), NaOH (5.9 equiv.), EtOH, 2 h 30 min., 90 °C; (iii) $LiAlH_4$ (5.3 equiv.), THF, 8 h, rt; (iv) appropriate amine (1.0 equiv.), EDC (1.1 equiv.), HOBt (1.1 equiv.), DMAP (0.10 equiv.), DCM, 19 h 15 min, 0 °C – rt.; (v) RuX(OAC)(*p*-cymene) (1.0 equiv.), DCM, 1 h 30 min., rt. X = Cl or I.

Artesunate (**ARS, intermediate 4**), was synthesised by reaction of **DHA** (**intermediate 1**) with excess succinic anhydride, following a known procedure, quantitatively yielding the desired ester as a white sticky-fibrous solid.[23] ARS was then used for the synthesis of ligand **4** and complex **6**.

Two different synthetic routes were investigated, the first involved production of the acyl-chloride derivative of **ARS** which could be reacted with the appropriate amine and the second involved an N-(3-

Dimethylaminopropyl)-N′-ethylcarbodiimide hydrochloride (EDC)-coupled reaction. It was decided that the reaction conditions to the latter was more preferable as opposed to the synthesis of the acyl-chloride precursor since it is possible that it could possibly react/exchange with the ester linkage of nearby artesunate molecules. Ligand **4** and complex **6** were obtained in moderate yields. Future syntheses could optimise the reaction- and workup conditions. In order to prepare complex **6**, **intermediate 5** was prepared by reduction of ferrocene carboxaldehyde using a known literature method and was obtained in moderate yield.[40]

After attempting different methodologies where the ligand was directly reacted with the *p*-cymene dimer with the presence of a base proved unsuccessful, complexes **5a** and **5b** were successfully isolated using an appropriate acetate precursor (Scheme 4). Similar to the triazole complexes (**2a** and **2b**), the synthesis of the iodido-complex (**5b**) reacted much slower compared to complex **5a**.

2.2.2.2. Characterisation

Intermediate 4 (**ARS**) was easily characterised with IR spectroscopy by the appearance of a broad carbonyl absorption band at 1753 cm^{-1} due to overlapping ester and carboxylic acid carbonyl stretches. The ^{1}H-NMR spectrum (**Figure 2.16**) corresponded well to the literature ^{1}H-NMR spectra.[32] The doublet proton signal at 5.81 ppm with a ^{3}J coupling constant of 9.9 Hz was assigned to H-10 and correlates to a *cis* configuration, which indicated that the **α**-isomer of **ARS** was synthesized.

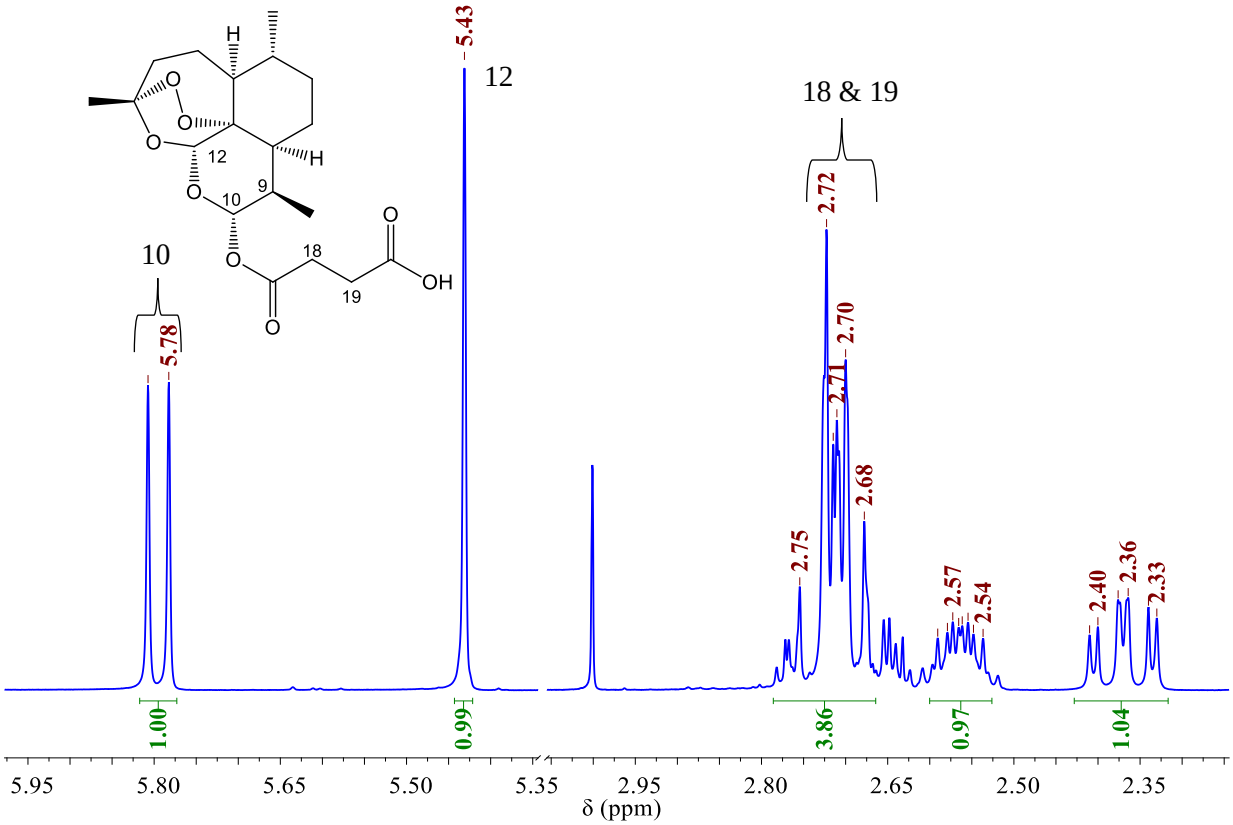

Figure 2.16. ^{1}H-NMR ($CDCl_3$, 400 MHz) spectrum of ARS (**intermediate 4**).

Literature shows that the **α**-isomer formation is predominant as the crystal structure of **ARS** shows that the **α**-isomer has a less crowded environment and that the ester would be more thermodynamically stable compared

to its **β**-isomer counterpart.[32] The presence of a multiplet between 2.75 and 2.68, integrated for 4 protons and is assigned to the methylene groups of protons H-18 and H-19.[32]

The IR spectrum of ligand **4** displayed both the carbonyl ester and carbonyl amide absorption bands at 1746 cm^{-1} and 1658 cm^{-1}, respectively. Furthermore, the pyridine C=N absorption band is also present at 1538 cm^{-1}.

From the ^{1}H-NMR spectrum (Figure 2.24) it is apparent that the artesunate methylene protons H-18 and H-19 as well as H-10 and H-12 do not shift much from their positions observed prior to derivatization. No evidence of isomerisation was found – H-10 is seen as a doublet at 5.80 ppm (*J*= 9.9 Hz) and H-12 as a singlet at 5.42 ppm. Three of the four pyridyl protons could be assigned, but the fourth proton signal, H-24, is most likely overlapping with the deuterated chloroform solvent signal. This is suspected because the H-24 signal should give either a doublet or a doublet of doublets, and the signal at 7.23 ppm integrated for one proton. The methylene protons, H-22, resonate as a doublet at 4.57 ppm likely due to coupling geminal coupling to the proton on the same carbon. The amide proton signal was also observed at 6.84 ppm as a broad singlet. ESI-MS data also revealed that the expected $[M+H^{+}]^{+}$ molecular ion was observed experimentally, found at 475.2439 *m/z* (calculated for $[M+H^{+}]^{+}$: 475.2400 *m/z*).

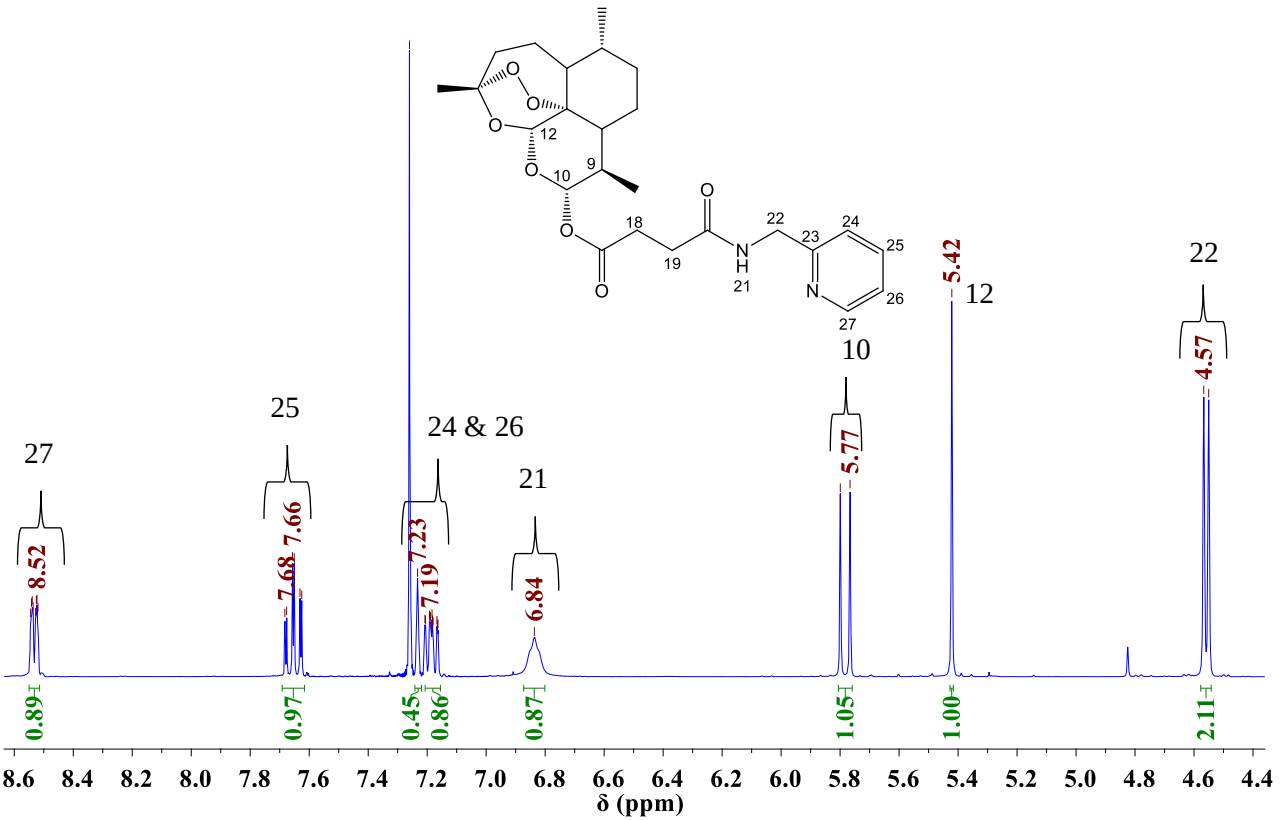

Figure 2.17. ^{1}H-NMR ($CDCl_3$) expansion spectrum of **compound 4.**

For the complexation of picolinamide ligands, literature shows that it is possible to isolate the *N,N*-configuration instead of the *N,O*-configuration by the addition of electron withdrawing groups.[41,42] A study also indicated that the *N,N*-configuration showed more promising biological activity against cancerous cell

lines compared to their *N,O*-configuration counterpart, moreover the *N,O*-coordinated compound hydrolysed.[41] Easily hydrolysable compounds generally indicate the loss of biological activity, and would be detrimental to our compounds.

Only the ^{1}H-NMR spectra compound **5b** would be discussed both **5a** and **5b** have similar spectra, contrary to compounds **2a** and **2b,** where the halogen on the ruthenium moiety influenced the isomeric mixture; only slight shifts for the pyridine ring for compounds **5a** and **5b** was observed. After extensive evaluation of the ^{1}H-NMR for **5b** (**Figure 2.18**), the following protons were assigned: Proton H-10 was assigned to the multiplet in the 5.82-5.76 ppm region; the complexity of the signal arising from multiple isomers in the sample. Moreover, multiple doublet signals for proton H-22 were observed at 4.55 – 4.44 ppm pointing to different metal stereoisomers. There is a definite downfield shift of the pyridyl proton resonances of H-24 to H-27 for complex **5b** compared to ligand **4**. Furthermore, for both compounds **5a** and **5b**, ESI^{+}-MS data revealed that both had a molecular ion of $[M\text{-}X]^{+}$ (where X = Cl or I), both compared very well within expected values: 709.2434 *m/z* for **5a** (calculated for $[M\text{-}Cl^{-}]^{+}$: 709.2427) and 709.2425 *m/z* (calculated as $[M\text{-}I^{-}]^{+}$: 709.2427) for **5b**.

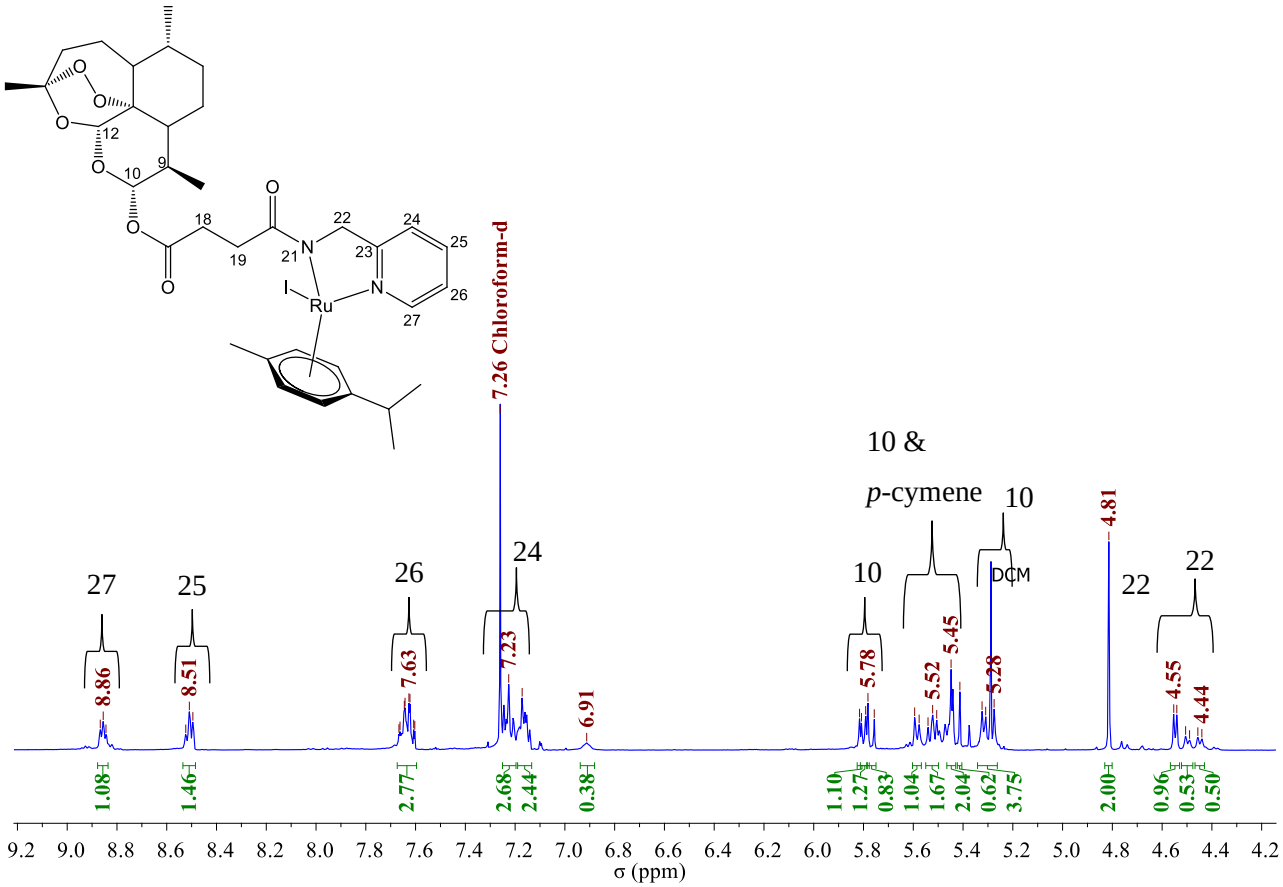

Figure 2.18. ^{1}H-NMR excerpt of **compound 5b** ($CDCl_3$).

After the ferrocene methylamine (**intermediate 5**) was synthesised from a known literature method,[40] the synthesis of complex **6** proceeded via an EDC coupled reaction.

Comparison of the IR spectra for ligand **4** and complex **6** to its reagents, clearly show that an amide functionality is present. The IR spectrum of complex **6** displayed both carbonyl C=O stretching frequencies

corresponding to the ester and amide functionalities at 1738 cm^{-1} and 1658 cm^{-1} respectively. A broad N-H bending absorption band is present at 1530 cm^{-1}.

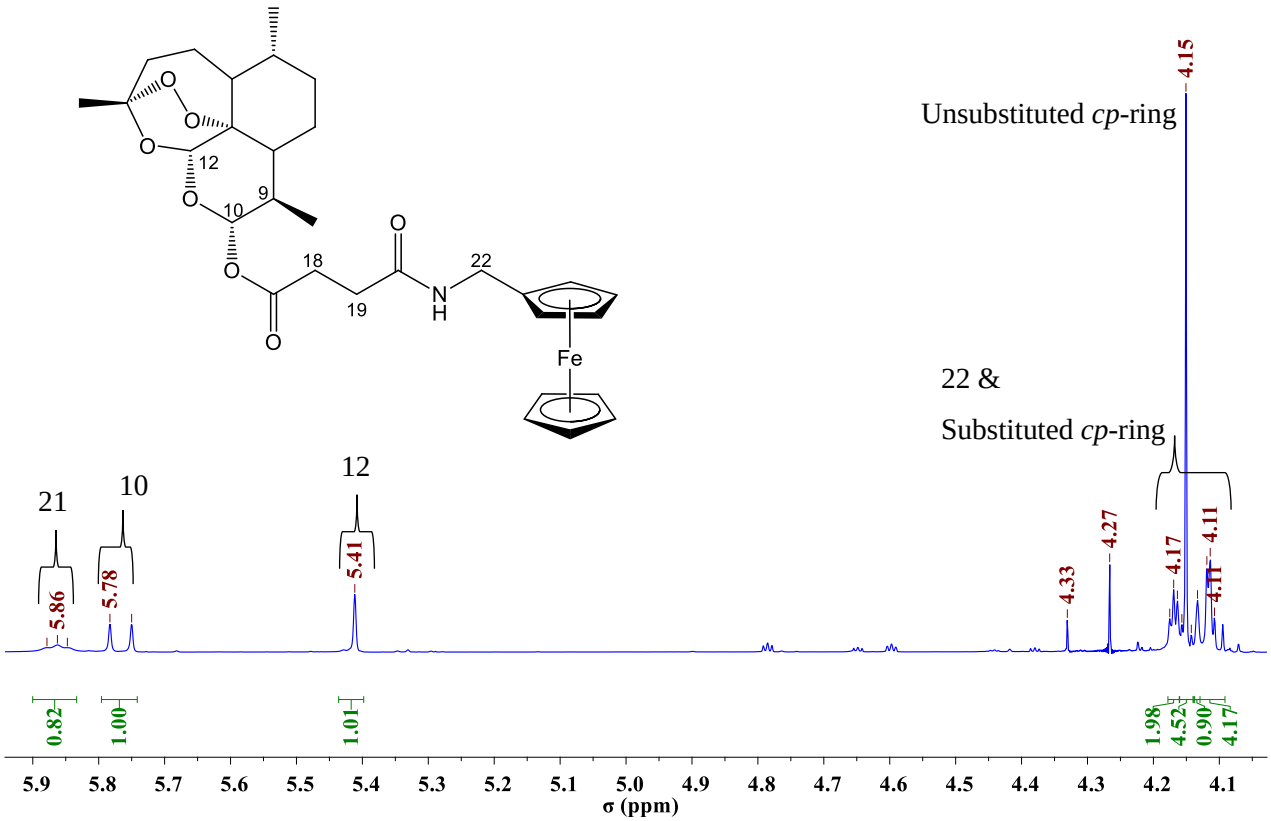

Figure 2.19. ^{1}H-NMR ($CDCl_3$, 300 MHz) expansion spectrum of **complex 6**.

Unreacted ferrocene species and ethyl acetate impurities was present in the ^{1}H-NMR spectrum (**Figure 2.19**). Compared to its artesunate precursor, complex **6** shows that the artesunate methylene protons H_{18} and H_{19} and protons H_{10} and H_{12} did not shift much from their original positions. Closer inspection of the H_{18} and H_{19} protons revealed that some distortion of the multiplicity of the proton peaks are present, indicating some restricted stereochemistry in this area. The doublet at 5.78 ppm, assigned to the H_{10} proton of compound **6** displayed a greater ^{3}J coupling to H_9, 9.67 Hz compared to artesunate with 7.30 Hz. Further studies are required to elucidate the larger ^{3}J coupling. Interestingly it was noticed that both the H_{10} doublet and the singlet at 5.41 ppm (H_{12}) is slightly upfield compared to artesunate, indicating increased shielding. The presence of the ethyl acetate impurity forced a skewed integrated ferrocene moiety, but identification of the mutliplets and singlets were satisfactory for characterisation. The substituted cyclopentadiene (Cp) ring was identified to the multiplet at 4.18 ppm, followed by the singlet assigned to the unsubstituted Cp ring at 4.15 ppm. The remaining protons of the substituted Cp ring and the methylene protons (H_{22}) overlap in the 4.13 to 4.09 ppm region as the relative integration roughly equates to 4 protons. Lastly, a very broad and weak unresolved triplet was observed at 5.86 ppm. This peak is most likely the proton on the N-H amide (H_{21}). ESI-MS data showed that the 581.2075 *m/z* was in most abundance as it too correlated with the expected molecular ion of $[M]^{+}$ calculated as 581.2076 *m/z*.

2.3. Conclusion:

Successful syntheses were performed, producing new compounds, which include compounds 1-6 and **intermediate 3**. Moreover, slight modifications and development to known literature methods, especially those which produced **intermediate 1** (ART-N_3), obtained higher yields, faster reaction time and slightly improved selectivity of the substitution reaction over the elimination side-reaction. However, method development to new "click-reactions" are required that would include the presence of peroxides. Considerable effort went into producing cleaner and higher yielding complexes of compounds **5a** and **5b**, with substituting the respective ruthenium dimers with ruthenium-acetate precursors. MS data was very informative to indicate that the complex compounds **2** and **5** were present, as purity continued to be a difficult challenge to overcome. Molecular ions for compounds **2** were identified as $[M\text{-}PF_6]^+$ and compounds **5** as $[M\text{-}X+H]^+$, where X = Cl or I. Further NMR characterisation is required to fully assign and elucidate compounds **2** and **5**. Although these complex molecules are not yet fully characterised and understood, it would provide a great opportunity for future work to elaborate on the current characterisation.

Purification of all compounds (precursors, intermediates and final complexes) was achieved using easily accessible silica or alumina gravity columns; however, a method is yet to be developed to achieve bio-assay approved purification levels with the ruthenium complexes, compounds **2** and **5**, with emphasis placed on the triazole complexes. Purification of the three identified isomers of **ART-N_3** was also achieved using silica gravity column chromatography, which normally requires specialised columns for separation. Further elaboration and development to the HPLC method is paramount, such as MS-coupled HPLC, due to evidence that the triazole compounds **2a** and **2b** and all artesunate linked compounds (**4-6)**, indicated interaction with the column and the solvent system used. The latter led to false purity results which would affect the data obtained during biological studies.

2.4. Experimental:

Chemicals and reagents. All reagent solvents were purchased from Sigma-Aldrich. Ammonium hexafluorophosphate (NH_4PF_6), copper (II) acetate monohydrate, copper (I) iodide, α-terpinene, dimethylformamide, ,chlorotrimethyl silane (TMSCl), N,N-Diisopropylethylamine (DIPEA), N-(3-Dimethylaminopropyl)-N′-ethylcarbodiimide hydrochloride (EDC), 2-ethynyl pyridine, ferrocene carboxaldehyde, glacial acetic acid, hydroxylamine hydrochloride, 1-Hydroxybenzotriazole hydrate (HOBt), lithium aluminium hydride ($LiAlH_4$), magnesium sulphate ($MgSO_4$), potassium iodide, propargyl amine sodium acetate, sodium azide, sodium borohydride ($NaBH_4$), succinic anhydride and sodium bicarbonate used were supplied from Sigma-Aldrich. Artemisinin (97 %) from Alfa Aesar. $RuCl_3{\cdot}3H_2O$ were purchased from Precious Metals Online. Deuterated solvents ($(CD_3)_2CO$, $CDCl_3$, MeOD-d_4 and DMSO-d_6) were purchased from Sigma-Aldrich. Solvents required for inert atmospheric reactions were dry distilled prior to use. TLC plates (MACHEREY-NAGEL, silica gel 60 F_{254} 0.20 mm, 20 x 20 cm) were used to monitor reactions, visualising with *p*-anisaldehyde or vanillin staining if it was required. Known compounds: dihydroartemisinin

(intermediate **1**), 10-azidoartemisinin (intermediate **2**), artesunate (intermediate **3**), [(*p*-Cymene)$RuCl_2$]$_2$, [(*p*-Cymene)RuI_2]$_2$, RuCl(OAc)(*p*-cymene), RuI(OAc)(*p*-cymene) and ferrocene methyl amine were synthesised according to literature procedures cited.[23,43–47]

Instrumentation. NMR spectra was collected on a Varian VNMRS 300 NMR Spectrometer and Varian ^{Unity}*Inova* 400 spectrometer at ambient room temperature using the residual solvent peak as an internal standard for ^{1}H-NMR spectra. The chemical shift (δ) is reported in parts per million. IR spectra were recorded on a Thermo Nicolet Avatar 330 FT-IR using an ATR ZnSe crystal or KBr plates or with a Bruker APLHA ATR on a diamond crystal.

General procedures. All glass apparatus was cleaned and dried in an oven prior to use. All reactions were performed under a fume hood and in the air unless stated otherwise. Microwave assisted reactions were performed in a CEM Discover SP Microwave reactor. Column chromatography was performed over Fluka Silica gel (70-230 mesh and 230-400 mesh), and unless stated, gravity column chromatography was used. HPLC was performed with an Agilent 1200 series with a Kinetex 5 µm C18, 100 Å, LC column (150 x 4.6 mm). **HPLC method:** 0.5 mL/min; 50 µL injection; with 0.1%TFA in both H_2O (A) and MeOH (B) – at 0 min (80% A:20% B) the gradient increases over 10 min to 10% A: 90% B, the gradient is kept at 10% A: 90% B for the next 15 min, then it increased to 100% B over the next 5 minutes before finally dropping to 80% A: 20% B over 1 min, and equilibrates for the next 5 minutes at 80% A: 20% B, afterwards proceeding with a 5 min post run before the next sample is injected. Solvents were removed *in vacuo*, with the use of a rotary evaporator whilst sample is in a water bath at 40 °C. Trace amount of solvent was removed with a high vacuum pump at 0.08 mm Hg.

Full IR and NMR spectra are given in the **appendix** document.

2.4.1. Methods:

2.4.1.1. Synthesis of [(*p*-Cymene)$RuCl_2$]$_2$:[43]

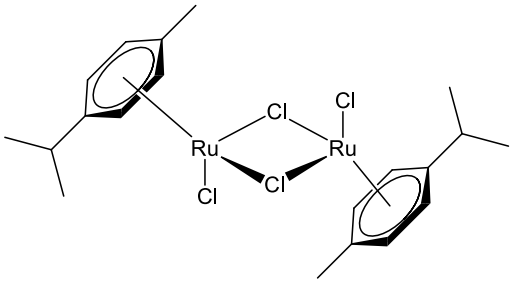

$RuCl_3 \cdot 3H_2O$ salt (507 mg, 1.94 mmol) was dissolved in dry MeOH (5 mL) in a 35 mL microwave vial. While stirring at room temperature, α-terpinene (0.88 mL, 5.43 mmol) was added. The microwave vial was then sealed and placed in the microwave reactor and allowed to react at 140 °C for 5 min. After the mixture cooled to room temperature, the contents were transferred to an Erlenmeyer flask and pentane (5 mL) was added. After a short vigorous shake, the layers were allowed to separate, and the pentane layer removed. The pentane wash was repeated twice more. The dark red microcrystalline solid was collected and washed with pentane (3x 5 mL) and dried under high vacuum that produced 313 mg (53 % yield).

2.4.1.2. Synthesis of [(*p*-cymene)RuI_2]$_2$: [45,48]

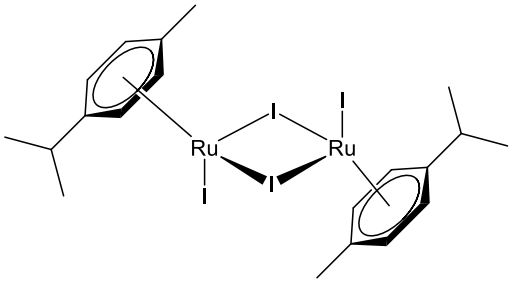

[(*p*-Cymene)$RuCl_2$]$_2$ (100 mg, 0.16 mmol) was dissolved in methanol (8 mL). While stirring, a solution of potassium iodide (271 mg, 1.63 mmol) in dH_2O (1 mL) was slowly added dropwise over 15 minutes to the Ru-dimer solution at room temperature. The reaction was allowed to stir under reflux (75 °C) for 2 hours. The suspension was transferred to a separatory funnel and diluted with additional methylene chloride (40 mL). The organic layer was washed with dH_2O (50 mL), dried over $MgSO_4$, filtered through celite and solvent evaporated under reduced pressure. A dark-red crystalline powder was obtained (152 mg, 95 % yield).

2.4.1.3. Synthesis of RuX(OAc)(*p*-cymene); X = Cl or I:

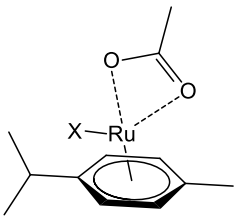

Method 1: [46] [(*p*-Cymene)$RuCl_2$]$_2$ (100 mg, 0.16 mmol) was dissolved/suspended in tertiary-amyl alcohol (17.5 mL). Cu(OAc)$_2$-mono-hydrate (1307 mg, 6.55 mmol) – crystals were crushed to a powder using a mortar and pestle – was transferred to the solution while stirring. The reaction was allowed to stir under reflux (105 °C) for 24 hours. After the reaction mixture cooled to room temperature, it was filtered through multiple columns of celite with tAmOH until unreacted copper acetate was removed. All solvent from the filtrate was evaporated under reduced pressure and dried under high vacuum to afford the amber-orange product (93 mg; 75 %). ^{1}H-NMR (300 MHz, $CDCl_3$, 25 °C): δ = 5.64 (d, 2H, *J* = 6 Hz, Ar-CH), 5.42 (d, 2H, *J* = 6 Hz, Ar-CH),2.97 (m, 1H, ^{i}PrCH-*p*-cymene), 2.31 (s, 3H, OAc-CH_3), 1.82 (s, 3H, *p*-cymene-CH_3), 1.39 (d, 6H, *J* = 7 Hz, ^{i}PrCH_3).

Preferred – Method 2:[47] Reaction performed under an inert atmosphere (N_2). [(*p*-Cymene)RuI_2]$_2$ (50 mg, 0.051 mmol) was suspended in dry methanol (4 mL). To it, while stirring, was added sodium acetate (12 mg, 0.14 mmol) dissolved in dry methanol (1 mL). Reaction was allowed to stir at reflux temperature (65 °C) for 3 hours. The reaction mixture was cooled to ambient temperature and filtered through celite. Afterwards, the solvent was evaporated under reduced pressure and dried under high vacuum. The crude material was then dissolved in dry DCM and filtered through celite. Filtrate was evaporated under reduced pressure and further dried under high vacuum. A dark purple solid was obtained (80 % yield) and was stored under inert gas.

2.4.1.4. Synthesis of dihydroartemisinin (**intermediate 1**):[23]

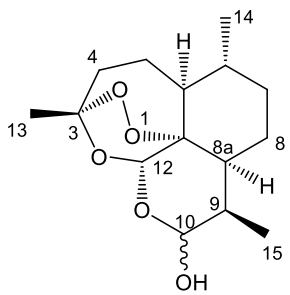

Artemisinin (3001 mg, 10.63 mmol) was suspended in dry methanol (70 mL) in a round bottom flask (100 mL). After the solution was cooled to *ca*. 0 °C with vigorous stirring, $NaBH_4$ (1248 mg, 32.97 mmol) was added in small increments over 40 minutes. The reaction was stirred for 3 hours and 50 minutes and monitored by TLC (20:0.5 dichloromethane:methanol) – staining with *p*-anisaldehyde or vanillin. The mixture quenched with a 30% acetic acid-methanol mixture (v/v; 1:1) to pH 5-6 after the reaction reached completion. The solvent was evaporated under reduced pressure and the

resulting off-white solid was extracted with ethyl acetate (6x 50 mL), dried over $MgSO_4$ and filtered. The solvent of the filtrate was evaporated under reduced pressure and the crude white product was dried under high vacuum after which, it was recrystallised three times from a 1:3 ethyl acetate:hexane solution. White fibrous needle-like crystals were obtained (2580 mg, 85 %). ATR-IR (ZnSe): 3363 cm^{-1}. ^{1}H-NMR (400 MHz, $CDCl_3$, 25 °C): δ = 5.60 (s, 1H, Hβ-12), 5.38 (s, 1H, Hα-12), 5.30 (t, 1H, *J* = 3.3 Hz, Hβ-10), 4.76 (t, 1H, *J* = 8.79 Hz, Hα-10); 2.95 (bs, 1H, H-DHA); 2.64-2.57 (m, 1H, H-DHA); 2.41-2.33 (m, 2H, H-DHA); 2.06-2.00 (m, 1H, H-DHA); 1.93-1.85 (m, 2H, H-DHA); 1.84-1.74 (m, 2H,H-DHA); 1.43 (s, 1H, H-DHA); 1.42 (s, 3H, H-DHA); 0.96-0.94 (m. 9H, H-DHA).

2.4.1.5. Synthesis of 10α/β-Azidoartemisinin (**intermediate 2**):[21]

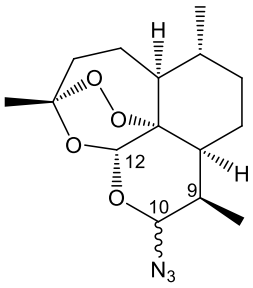

Dihydroartemisinin (506 mg, 1.78 mmol) and sodium azide (514 mg, 7.91 mmol) were suspended in dry dichloromethane (5 mL). While stirring, at *ca*. 0-5 °C, TMSCl (335 µL, 2.64 mmol) was added dropwise to the suspension over 5 minutes. Potassium iodide (78 mg, 0.47 mmol) was added to the reaction mixture, upon which the reaction mixture would turn from yellow to orange to red-orange colour. The reaction mixture was allowed to stir for 5 hours, whilst the ice bath slowly reach ambient temperature. The reaction was quenched with saturated sodium bicarbonate (10 mL). The reaction mixture was diluted with dichloromethane (20 mL) and washed the organic layer with brine (25 mL). The organic layer was then dried over $MgSO_4$, filtered and the solvent evaporated under reduced pressure. The brown crude oil product (569 mg) was purified on a silica column (70-230 mesh) using ethyl acetate and hexane as elution solvents. The silica column dimensions were: ±1 cm internal diameter, ±22 g silica. A crude purification, with 50:50:0.1 (ethyl acetate:hexane:triethylamine), yielded a diastereomeric mixture of **intermediate 2** (533 mg, 96 % yield) as a light yellow oil. A more refined silica column purification performed could isolate the isomers eluted with 1% ethyl acetate: hexane to 5% ethyl acetate:hexane. Isomers of **intermediate 2** were identified as: 9α, 10β-azidodihydroartemisinin (**intermediate 2a**) eluted first, 9β,10β-azidodihydroartemisinin (**intermediate 2c**) and lastly 9β,10α-azidodihydroartemisinin (**iintermediate 2b**). ATR-IR (ZnSe crystal): 2105 cm^{-1}. **Intermediate 2a**: ^{1}H NMR (400 MHz, $CDCl_3$) δ 5.51 (s, 1H, H-12), 5.30 (d, *J* = 7.6 Hz, 1H, H-10), 2.35-2.27 (m, 1H, H-ART-N_3), 2.06-2.01 (m, 1H, H-ART-N_3), 1.96-1.89 (m, 1H, H-ART-N_3), 1.72-1.66 (m, 1H, H-ART-N_3), 1.64-1.58 (m, 1H, H-ART-N_3), 1.54-1.47 (m, 1H, H-ART-N_3), 1.43 (bs, 6H, H-ART-N_3), 1.32-1.23 (m, 3H, H-ART-N_3), 1.17 (d, *J* = 7.0 Hz, 2H, H-ART-N_3), 0.96 (d, *J* = 6.0 Hz, 3H, H-ART-N_3). **Intermediate 2b**: ^{1}H NMR (400 MHz, $CDCl_3$) δ 5.38 (s, 1H, H-12), 4.61 (d, *J* = 10.2 Hz, 1H, H-10), 2.45-2.34 (m, 2H, H-ART-N_3), 2.06-2.01 (m, 1H, H-ART-N_3), 1.93-1.86 (m, 1H, H-ART-N_3), 1.78-1.68 (m, 2H, H-ART-N_3), 1.61-1.55 (m, 2H, H-ART-N_3), 1.45 (bs, 3H, H-ART-N_3), 1.34-1.22 (m, 4H, H-ART-N_3), 0.97 (d, *J* = 6.0 Hz, 3H, H-ART-N_3), 0.92 (d, *J* = 7.1 Hz, 3H, H-ART-N_3). **Intermediate 2c**: ^{1}H NMR (400 MHz, $CDCl_3$) δ = 5.53 (s, 1H, H-12), 5.37 (d, *J* = 4.1 Hz, 1H, H-10), 2.76-2.68 (m, 1H, H-ART-N_3), 2.41-2.33 (m, 1H, H-ART-N_3), 2.08-2.02 (m, 1H, H-ART-N_3), 1.93-1.85 (m, 1H, H-ART-N_3), 1.83-1.75 (m, 1H, H-ART-N_3), 1.73-1.64 (m, 3H, H-ART-N_3), 1.44 (bs, 4H, H-ART-N_3), 1.28-1.24 (m, 1jH, H-ART-N_3), 0.97 (d, *J* =6.3 Hz, 3H, H-ART-N_3), 0.93 (d, *J* = 7.3 Hz, 3H, H-ART-N_3).

2.4.1.6. Synthesis of compound **1**:[18]

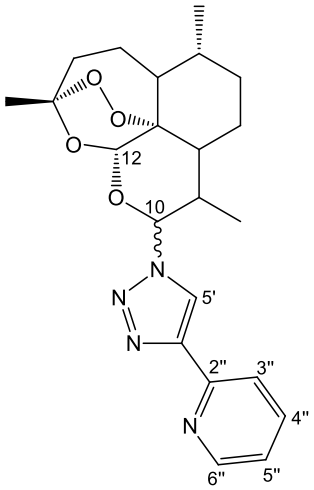

A mixture of **intermediate 1** (250 mg, 0.81 mmol) 2-ethynyl pyridine (74.2 µL, 0.74 mmol) was suspended in a 1:1 acetonitrile/H_2O mixture (2.5 mL). While stirring at room temperature, DIPEA (92.2 µL, 0.53 mmol) and CuI (22 mg, 0.12 mmol) was added respectively in that order. After the reaction vessel was cooled to *ca*. 0 °C in an ice bath, DIPEA (5 µL, 0.029 mmol), CuI (3 mg, 0.015 mmol) and then sodium ascorbate (12 mg, 0.063 mmol) was added respectively. The reaction was allowed to stir ca. 0 °C – rt. overnight (22 hours and 30 minutes). Saturated NH_4Cl (20 mL) was added and then extracted with ethyl acetate (3x15 mL). The organic layer was washed with brine (25 mL) and then dried over $MgSO_4$. The organic layer was filtered, and solvent removed under reduced pressure. After silica column purification was performed, the pure product was isolated as a mixture of isomers as a light yellow oil (69 mg, 21.4 %). The isomers were identified as **1a** (9α, 10β-isomer), **1b** (9β, 10α-isomer) and residual to no **1c** (9β, 10β-isomer). ATR-IR (ZnSe crystal): 3164 cm^{-1}, 2112 cm^{-1}, 1604 cm^{-1}, 1572 cm^{-1}, 1551 cm^{-1}. ^{1}H-NMR (300 MHz, $CDCl_3$): δ 8.61 (ddd, *J* = 4.9 Hz, 1.6 Hz, 0.8 Hz, 1H, H-6’’;10α), 8.52 (s, 1H, H-5’), 8.19 (d, *J* = 7.9 Hz, 1H, **1b:** H-4’’), 7.78 (td, *J* = 7.8, 1.8 Hz, 1H, **1b:** H-5’’), 7.25 – 7.21 (m, 1H, H-3’’), 5.95 (d, *J* = 10.7 Hz, 1H, **1b:** H-10), 5.57 (s, 1H, **1b:** H-12), 2.95-2.86 (m, 1H, H-ART), 2.46-2.38 (m, 1H, H-ART), 2.09-2.03 (m, 2H, H-ART), 1.97-1.90 (m, 1H, H-ART), 1.89-1.81 (m, 2H, H-ART), 1.79-1.72 (m, 2H, H-ART), 1.57-1.48 (m, 3H, H-ART), 1.42 (s, 3H, H-ART), 1.38-1.32 (m, 2H, H-ART), 1.01-0.99 (m, 4H, H-ART), 0.70 (d, *J* = 7.15 Hz, 3H, H-ART). ^{13}C NMR (101 MHz, $CDCl_3$): δ (ppm) = 150.35 (C-2’’), 149.54 (C-6’’), 149.01 (C-4’), 137.01 (C-5’), 123.04 (C-4’’), 120.46 (C-3’’), 119.89 (C-5’’), 104.92 (C-3), 92.26 (C-12), 86.10 (C-10), 79.89 (C-12a), 51.62 (C-5a), 45.60 (C-8a), 37.46(C-6), 36.24 (C-4), 34.08(C-7), 33.93 (C-9), 25.86 (C-15), 24.76 (C-5), 21.66 (C-8), 20.28 (C-14), 12.41 (C-16). HRMS (ESI^+): *m/z* calcd for $C_{22}H_{28}N_4O_4$ $[M+H^+]^+$: 413.2144, found 413.2176.

2.4.1.7. Synthesis of compound **2**:

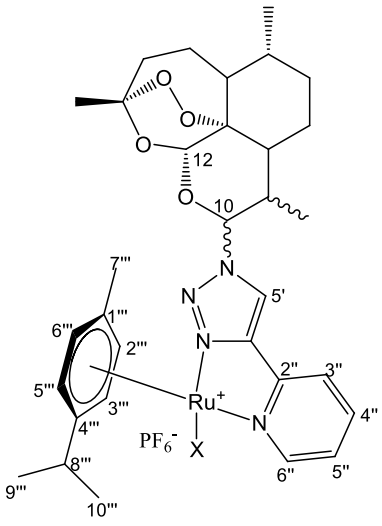

X = Cl (**2a**) or I (**2b**)

Compound **1** (68 mg, 0.16 mmol) was suspended in reagent grade methanol (10 mL). Whilst stirring at room temperature to the ligand solution, [Ru(*p*-cymene)Cl_2]$_2$ (50 mg, 0.082 mmol), dissolved in dichloromethane (5 mL) was added dropwise over 10 minutes. After 2 hour of stirring, NH_4PF_6 (27 mg, 0.17 mmol) was added to the complex and was allowed to stir for 50 minutes. All solvent was evaporated under reduced pressure, until dryness. The impure orange crystalline complex (166 mg) was filtered through a pad of celite with acetone. The solvent was removed under reduced pressure and dried under high vacuum. Reprecipitation was attempted with a toluene:hexane mixture to separate residual uncoordinated ligand from the complex. An orange powder-like precipitate (glitters like crystals) was obtained (113 mg, 84 % yield). ATR-IR (ZnSe crystal): 1622 cm^{-1}, 1582

cm^{-1}, 831 cm^{-1}. **2a:** ^{1}H NMR (400 MHz, $CDCl_3$) δ (ppm) = 9.35 (d, *J* = 5.5 Hz, 1H, H-6''), 9.26 (d, *J* = 5.5 Hz,1H, H-6''-isomer), 8.63 (s, 1H, H-5'-isomer), 8.55 (s, 1H, H-5'), 8.01-7.91 (m, , 3H, H-4''-isomers), 7.88-7.83 (m, 2H, H-4''-), , 7.61 (m, , 2H, H-5''-overlapping isomers), 7.18-7.16 (m, 3H, H-3''-overlapping isomers), 6.06 (d, *J* = 10.7 Hz, 1H, H-10 9β,10α), 6.00 (d, J = 10.7 Hz, H-10 9β,10α), 5.95-5.92 (m, 3H, *p*-cymene CH), 5.89 (d, *J* = 6.2 Hz, 1H, *p*-cymene CH), 5.81 (t, *J* = 6.5 Hz, 2H, *p*-cymene CH), 5.68-5.64 (m, 3H, *p*-cymene CH), 5.60 (s, 1H, H-12), 3.10 (m, 1H, H-ART), 2.94 (m, 1H, H-ART), 2.85-2.72 (m, 2H, ^{i}PrCH *p*-cymene), 2.48-2.39 (m, 2H, H-ART), 2.11-2.05 (m, 3H, H-ART), 1.98-1.93 (m, 3H, H-ART), 1.85-1.77 (m, 3H, H-ART), 1.59 (s, 4H, *p*-cymene-CH_3). 1.45 (s, 3H, H-ART), 1.41 (s, 3H, H-ART), 1.23 (d, *J* = 6.9 Hz, 3H, ^{i}PrCH_3 *p*-cymene), 1.20 (d, *J* = 7.0 Hz, 3H, ^{i}PrCH_3 *p*-cymene), 1.14 (d, *J* = 6.9 Hz, 4H, ^{i}PrCH_3 *p*-cymene), 1.09 (d, *J* = 6.9 Hz, 4H, ^{i}PrCH_3 *p*-cymene), 1.02-1.00 (m, 6H, H-ART), 0.82 (d, *J* = 7.1 Hz, 3H, H-ART), 0.76 (d, *J* = 7.1 Hz, 3H, H-ART isomer). ^{13}C{^{1}H}-NMR (101 MHz, $CDCl_3$) δ (ppm) = 155.94 (C-ART), 155.58 (C-ART isomer), 147.74 (C-ART), 147.50 (C-ART isomer), 146.89 (C-ART), 140.02 (C-ART), 139.95 (C-ART isomer), 129.15, 128.34, 127.06, 126.85, 125.41, 122.65 (C-ART), 122.46 (C-ART isomer), 105.65 (C-*p*-cymene), 105.24 (C-ART), 105.05 (C-ART isomer), 102.80 (C-*p*-cymene), 102.34 (C-*p*-cymene), 92.70 (C-ART), 92.57 (C-ART isomer), 88.16 (C-*p*-cymene), 87.97 (C-*p*-cymene), 86.10 (C-ART), 86.02 (C-ART isomer), 85.09 (C-*p*-cymene), 85.03 (C-*p*-cymene), 84.11, 84.08, 83.64, 83.28, 80.00 (C-ART), 51.50 (C-ART), 45.52 (C-ART), 37.37 (C-ART), 36.16 (C-ART), 33.98 (C-ART), 33.90 (C-ART), 31.19 (C-*p*-cymene), 25.82 (C-ART), 24.72 (C-ART), 22.52 (unreacted C-*p*-cymene), 22.43 (unreacted C-*p*-cymene), 21.87 (C-*p*-cymene), 21.76 (C-*p*-cymene isomer), 21.50 (C-ART), 20.25 (C-ART), 18.83 (C-*p*-cymene), 18.61 (C-*p*-cymene isomer) 12.43 (C-ART), 12.26 (C-ART isomer). HRMS (ESI^{+}): *m/z* calcd for $C_{32}H_{42}ClF_6N_4O_4PRu$ [M-PF_6^{-}]$^{+}$: 683.1933, found 683.1947. **2b**: ^{1}H-NMR (400 MHz ,$CDCl_3$) δ (ppm) = 9.60 (d, *J* = 5.7 Hz, 1H, H-6''), 9.31 (t, *J* = 5.3 Hz, 2H, H-4''), 9.27 (s, 1H, H-5' minor isomer), 9.16 (s, 1H, H-5' minor isomer), 8.67 (s, 1H, H-5' major isomer), 7.99-7.94 (m, 4H, H-5''), 7.68-7.66 (m, 1H, H-3''), 7.56-7.50 (m, 3H, H- 3''), 6.59 (d, *J* = 10.1 Hz, 1H, H-10), 6.56 (d, *J* = 9.9 Hz, 1H, H-10 isomer), 6.17 (d, *J* =10.6 Hz, 1H, H-10 isomer), 6.02-5.79 (unknown impurities), 5.73 (s, 1H, H-12), 5.72 (s, 1H, H-12 isomer), 5.68 (s, 1H, H-12 isomer), 5.66 (s, 1H, H-12 isomer), 5.54 (d, *J* = 5.9 Hz, 4H, *p*-cymene CH), 5.44 (d, *J* = 5.9 Hz, 4H, *p*-cymene CH), 5.30 (DCM impurity), 3.17-3.14 (m, 1H, H-ART), 3.04-2.98 (m, 6H, H-ART), 2.86-2.82 (m, 1H, ^{i}PrCH *p*-cymene), 2.39-2.34 (unreacted impurities), 1.56 (s, 8H, *p*-cymene-CH_3). 1.49 (s, 3H, H-ART), 1.47 (s, 4H, H-ART), 1.42 (s, 2H, H-ART), ,1.25 (d, *J* = 7.0 Hz, 17H, H-ART), 1.22 (m, 3H, H-ART), 1.21 (m, 4H, H-ART), 1.19-1.18 (m, 3H, H-ART), 1.16 (m, 2H, H-ART), 1.15 (d, *J* = 6.9 Hz, 4H, ^{i}PrCH_3 *p*-cymene), 1.05 (d, *J* = 6.9 Hz, 4H, ^{i}PrCH_3 *p*-cymene), 1.03 (d, *J* =6.2 Hz, 4H, ^{i}PrCH_3 *p*-cymene), 1.00-0.99 (m, 6H, H-ART), 0.82 (d, *J* = 7.1 Hz, 3H, H-ART), 0.76 (d, *J* = 7.1 Hz, 3H, H-ART). HRMS (ESI^{+}): *m/z* calcd for $C_{32}H_{42}IF_6N_4O_4PRu$ [M-PF_6^{-}]$^{+}$: 775.1289, found 775.1298.

2.4.1.8. Synthesis of **intermediate 3**:[49]

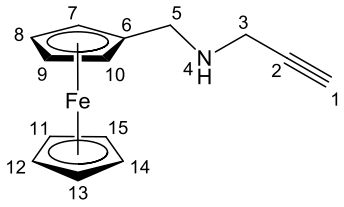

This reaction was performed under inert (N_2) gas. Ferrocene carboxaldehyde (202 mg, 0.94 mmol) was dissolved in methanol (5 mL). Propargyl amine (75 µL, 1.17 mmol) was added to the solution. A few activated 3A molecular sieves were added and then allowed the reaction to stir at room temperature in the dark (covered flask in foil) for 24 hours. The reaction mixture was filtered to remove the sieves and evaporated all solvent under reduced pressure. The crude mixture was extensively dried under reduced pressure at 40 °C to remove residual unreacted amine. The crude imine was redissolved in methanol (5 mL) and cooled to *ca*. 0 °C. While stirring, sodium borohydride (73 mg, 1.94 mmol) was added stepwise in small amounts over 15 minutes to the reaction mixture. The reaction was allowed to stir for 1 hour, monitored with TLC (5 % MeOH:DCM; ninhydrin stain). After all the methanol was evaporated under reduced pressure, the mixture was suspended in dH_2O (20 mL) and extracted with dichloromethane (3x 15 mL). The combined organic layer was washed with brine (25 mL) and saturated sodium bicarbonate (25 mL). The organic layer was dried over $MgSO_4$, filtered and solvent evaporated under reduced pressure until dryness. The dark orange-red oil crude product mixture was purified with silica column chromatography: fluka silica (70 – 230 mesh). Solvent system: 10:01:90 (EtOAc:Et_3N:DCM). The pure product was obtained as a dark red solid (205 mg, 86% yield). ATR-IR (ZnSe crystal): 3899 cm^{-1}, 3302 cm^{-1}, 2093 cm^{-1}. ^1H NMR (400 MHz, $CDCl_3$) δ (ppm) = 4.21 (*t*, *J*= 4.21 Hz, 2H,H-7 & H-10); 4.12 (*t*, *J*= 4.21 Hz, 2H,H-8 & H-9); 4.14 (*s*, 5H, H-8-H-15); 3.60 (*s*, 2H,H-5); 3.46 (*t*, *J*=2.42 Hz, 2H, H-3); 2.27 (*t*, *J*=2.42 Hz, 1H, H-1). $^{13}C\{^1H\}$-NMR (101 MHz, $CDCl_3$) δ (ppm) = 86.18 (C-2); 82.34(C-6); 68.55 (C-11-C-15); 68.46 (C-1); 67.98(C-7-C-10); 47.51(C-5); 37.68(C-3). HRMS (ESI^+): *m/z* calcd for $C_{14}H_{15}FeN$ $[M]^+$: 253.0554, found 253.0545.

2.4.1.9. Synthesis of compound **3**:[50]

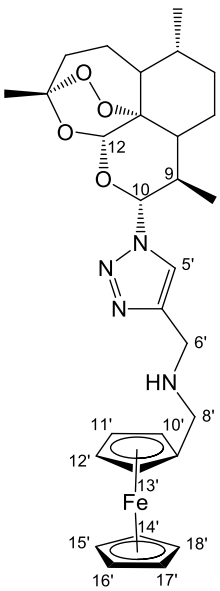

Major 9β,10α–isomer: 3b

A mixture of 10α/β-Azidoartemisinin (**Intermediate 2**) (100 mg, 0.32 mmol) and ferrocenyl-propargyl amine (**Intermediate 3**) (75 mg, 0.29 mmol) was suspended in a 1:1 acetonitrile/H_2O mixture (2.5 mL). While stirring at room temperature, DIPEA (92.2 µL, 0.53 mmol) and CuI (22 mg, 0.12 mmol) was added respectively in that order. After the reaction vessel was cooled to *ca*. 0 °C in an ice bath, DIPEA (5 µL, 0.029 mmol), CuI (3 mg, 0.015 mmol) and then sodium ascorbate (12 mg, 0.063 mmol) were added respectively. The reaction was allowed to stir ca. 0 °C – rt. overnight (18 h). Saturated NH_4Cl (20 mL) was added and then extracted with ethyl acetate (3x15 mL). The organic layer was washed with brine (25 mL) and then dried over $MgSO_4$. The organic layer was filtered, and solvent removed under reduced pressure. After silica column purification was performed, pure product yielded 41.6 % (69 mg); brown-orange sticky semi-oil. Isomers were identified as a minor 9α, 10β-isomer (**3a**) and a major 9β, 10α-isomer (**3b**). ATR-IR (ZnSe crystal): 3080 cm^{-1}, 1732 cm^{-1}, 1639 cm^{-1}. ^1H NMR (400 MHz, $CDCl_3$) δ (ppm) = 7.81 (s, 1H, **3b:** H-5'), 7.67 (s, 1H, **3a:** H-5'), 6.40 (d, *J* = 10.1 Hz, **3a:** H-10), 5.88 (d, *J* = 10.7 Hz, 1H, **3b:** H-10), 5.59 (s, 1H, **3a:** H-12), 5.54 (s, 1H, **3b:**

H-12), 4.20 (bs, "4H", sub-Cp, both isomers), 4.14 (m, 2H, **3b:** sub-Cp), 4.12 (s, 2H, **3a:** unsub-Cp), 4.12 (s, 5H, **3b:** unsub-Cp), 4.10 (m, 4H, H- both isomers), 3.96 (bs, "3H", H8' both isomers) 3.57 (bs, "3H", H6' both isomers), 2.83-2.78 (m, 1H, H-ART), 2.45-2.37 (m, 2H, H-ART), 2.13-2.04 (m, 2H, H-ART), 2.04 (s, 1H, H-ART), 1.96-1.91 (m, 3H, H-ART), 1.87-1.77 (m, 8H, H-ART), 1.78-1.69 (m, 3H, H-ART), 1.58-1.49 (m, 4H, H-ART), 1.44 (s, 2H, H-ART isomer), 1.42 (s, 4H, H-ART), 1.37-1.33 (m, 3H, H-ART), 1.27-1.24 (m, 2H, H-ART), 1.08-1.05 (m, 2H, H-ART), 1.01-0.99 (m, 8H, H-ART), 0.65 (d, J = 7.1 Hz, 3H, H-ART). ^{13}C NMR (101 MHz, $CDCl_3$) δ (ppm) = 104.89 (C-ART), 103.00 (C-ART), 92.17 (C-ART), 85.89 (C-ART), 82.35 (C9'), 79.97 (C-ART), 68.54 (C14'-18'), 68.00 (C10'-13'), 51.58 (C-ART), 48.46 (C8'), 45.57 (C-ART), 44.36 (C6'), 37.45 (C-ART), 36.23 (C-ART), 34.06 (C-ART), 33.86 (C-ART), 25.88 (C-ART), 24.74 (C-ART), 21.63 (C-ART), 20.27 (C-ART), 12.40 (C-ART). HRMS (ESI$^+$): *m/z* calcd for $C_{29}H_{38}FeN_4O_4$ $[M+H^+]^+$: 563.2276, found 563.2325.

2.4.1.10. Synthesis of artesunate (**intermediate 4**):[23]

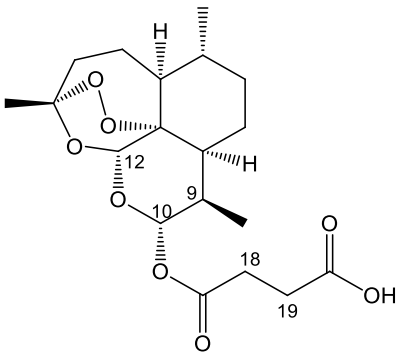

This reaction was performed under inert (N_2) gas. Dihydroartemisinin (1002 mg, 3.52 mmol) was suspended in ethyl acetate (7 mL), cooled in an ice bath. Whilst stirring vigorously, triethylamine (0.54 mL, 3.87 mmol) was added to the cooled suspension. Succinic anhydride (705 mg, 7.04 mmol) was added step-wise in small amounts to the reaction mixture over 45 minutes. After the reaction mixture stirred vigorously for 10 minutes, the ice bath was removed, and the reaction was allowed to vigorously stir at room temperature for 2 hours and 45 minutes. The reaction was quenched adding cold dH_2O (10 mL) followed by acidification with 2 N H_2SO_4 to pH 5. The aqueous layer was thoroughly extracted with ethyl acetate (5x 25 mL). The organic layer was washed once with dH_2O (75 mL) before drying over $MgSO_4$. The organic layer was filtered and then evaporated all solvent under reduced pressure. ATR-IR (ZnSe crystal): 1753 cm^{-1}. ^{1}H NMR (400 MHz, $CDCl_3$) δ = 5.79 (d, J = 9.9 Hz, 1H, H-10), 5.43 (s, 1H, H-12), 2.75-2.68 (m, 4H, H-18, H19), 2.59-2.54 (m, 1H, H-ART), 2.41-2.33 (m, 1H, H-ART), 2.04 (s, 1H, H-ART), 1.92-1.85 (m, 1H, H-ART), 1.80-1.69 (m, 2H, H-ART), 1.65-1.59 (m, 1H, H-ART), 1.50-1.45 (m, 1H, H-ART), 1.43 (s, 3H, H-ART), 1.39-1.35 (m, 1H, H-ART), 1.31-1.23 (m, 2H, H-ART), 1.06-0.99 (m, 1H, H-ART), 0.97 (d, J = 6.0 Hz, 3H, H-ART), 0.85 (d, J = 7.1 Hz, 3H, H-ART).

2.4.1.11. Synthesis of compound **4**:[51]

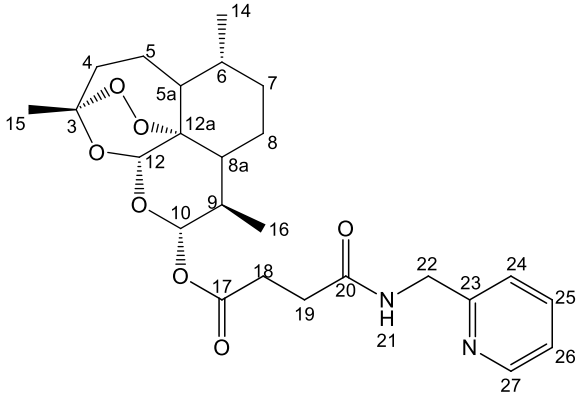

Artesunate (254 mg, 0.66 mmol) was transferred to a round bottom flask and dissolved in dichloromethane (2.5 mL). After the solution was cooled to *ca*. 0 °C, 2-picolylamine (67.5 µL, 0.66 mmol), EDC (126 mg, 0.66 mmol), HOBt (12%w/w H_2O, 101 mg; "89 mg", 0.66 mmol) & 4-dimethylaminopyridine (8 mg, 0.064 mmol) was added respectively to the solution. The reaction was allowed to stir overnight (19 hours 15 minutes) to room temperature.

The reaction mixture was diluted with dichloromethane (25 mL) and washed with sat. $NaHCO_3$ (25 mL x 2), followed with brine (25 mL). The organic layer was dried over $MgSO_4$, filtered and evaporated all solvent until dryness. The off-white crude solid material (300 mg) was purified with gravity silica chromatography. Solvent system: ethyl acetate: triethyl amine: methanol – 100:0.1:0; 95:0.1:5. A pure light bubbly solid was obtained (203 mg, 63% yield). ATR-IR (KBr): 1751 cm^{-1}, 1707 cm^{-1}, 1664 cm^{-1}, 1594 cm^{-1}, 1571 cm^{-1}, 1546 cm^{-1}, 1036 cm^{-1}. ^1H NMR (300 MHz, $CDCl_3$) δ (ppm) = 8.53 (ddd, *J* = 4.9, 1.7, 0.9 Hz, 1H, H-pyridine), 7.65 (td, *J* = 7.7, 1.8 Hz, 1H, H-pyridine), 7.21 – 7.16 (m, 1H, H-pyridine), 5.78 (d, *J* = 9.9 Hz, 1H, H-10), 5.42 (s, 1H, H-12), 4.56 (d, *J* = 5.0 Hz, 2H, H-22), 2.90-2.52 (m, 6H, H-18 & H-19), 2.42-2.31 (m, 1H, H-ART), 2.06-1.98 (m, 1H, H-ART), 1.93-1.85 (m, 1H, H-ART), 1.79-1.67 (m, 3H, H-ART), 1.64-1.58 (m, 1H, H-ART), 1.42 (s, 3H, H-ART), 1.39-1.25 (m, 3H, H-ART), 0.96 (d, *J* = 6.0 Hz, 3H, H-ART), 0.85 (d, *J* = 7.1 Hz, 3H, H-ART). ^{13}C NMR (101 MHz, $CDCl_3$) δ (ppm) = 171.81 (carbonylC-ARS), 171.29 (carbonylC-ARS), 156.50 (methineC-Pyr), 149.10 (methineC-Pyr), 136.87 (methineC-Pyr), 122.43 (methineC-Pyr), 122.09 (methineC-Pyr), 104.56 (C-ART), 92.25 (C-ART), 91.60 (C-ART), 80.22 (C-ART), 77.16 (C-ART), 51.68 (C-ART), 45.35 (C-ART), 44.66 (methyleneC-Pyr), 37.39 (C-ART), 36.34 (C-ART), 34.21 (C-ART), 31.90 (C-ART), 30.82 (methyleneC-ARS), 29.77 (methyleneC-ARS), 24.70 (C-ART), 22.11 (C-ART), 20.33 (C-ART), 12.16 (C-ART). HRMS (ESI^+): *m/z* calcd for $C_{25}H_{34}N_2O_7$ $[M+H^+]^+$: 475.2400, found 475.2439.

2.4.1.12. Synthesis of compound **5**:

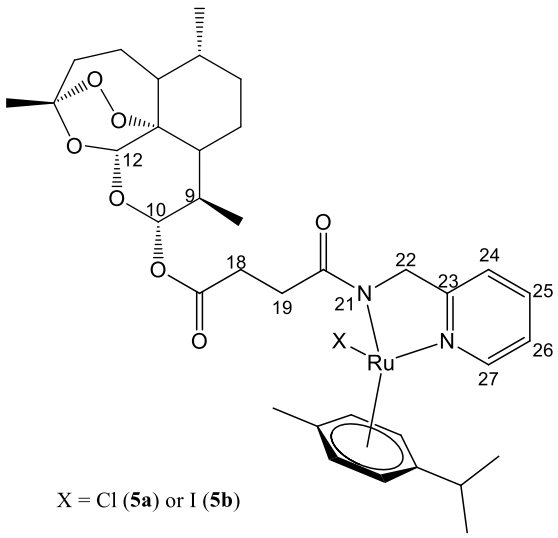

X = Cl (**5a**) or I (**5b**)

This reaction was performed under inert conditions (N_2). Compound **9** (51 mg, 0.11 mmol) was dissolved in dry dichloromethane (4 mL). Appropriate ruthenium acetate (35 mg, 0.11 mmol) was added to the ligand while stirring. The reaction was allowed to stir at room temperature until full conversion was achieved (1.5 hours). Note: Reaction time for compound **5b** was 19.5 hours. All solvent of the reaction mixture was evaporated under reduced pressure until dryness. The crude product was purified with gravity alumina neutral chromatography. Solvent system: 100 % DCM; then 1% MeOH:DCM; then 5 % MeOH:DCM. A relatively pure compound was obtained (**5a**: 15 mg, ; **5b**: 34 mg). **5a:** ATR-IR (ZnSe): 1743 cm^{-1}, 1663 cm^{-1}, 1543 cm^{-1}. ^1H NMR (400 MHz, $CDCl_3$) δ (ppm) = 8.84 (d *J* = 5.3 Hz, 1H, H-27), 8.07- 7.87 (m, 2H, H-25), 7.70 (t, *J* = 7.6 Hz, 1H, H-26), 7.11 (d, *J* = 2.4 Hz, 1H, H-24), 5.87-5.77 (m, 3H, H-10), 5.64-5.54 (m, 4H, *p*-cymene CH), 5.46- 5.42 (m, 4H, H-12 & *p*-cymene CH), 4.46-4.39 (m, 1H, H-22), 3.02-2.95 (m, 3H, H-18, H-19 & ^{i}PrCH *p*-cymene), 2.74-2.56 (m, 6H, H-ART), 2.40- 2.33 (m, 3H, H-ART), 2.27-2.26 (m, unreacted impurities), 2.03-2.00 (m, 3H, H-ART), 1.90-1.86 (m, 4H, H-ART), 1.70 (bs, 12H, *p*-cymene-CH_3), 1.42-1.41 (m, 6H, H-ART), 1.26-1.19 (m, 9H, H-ART & ^{i}PrCH_3 *p*-cymene), 1.13 (d, *J* = 6.9 Hz, 5H, ^{i}PrCH_3 *p*-cymene), 0.97 (d, *J* = 6.0 Hz, 10H, H-ART), 0.92 (d, *J* = 7.2 Hz, 4H, H-ART), 0.89 (d, *J* = 7.0 Hz, 4H, H-ART).. HRMS (ESI^+): *m/z* calcd for $C_{35}H_{47}ClN_2O_7Ru$ $[M-Cl^-]^+$: 709.2427, found 709.2434. **5b:** ATR-IR (ZnSe): 1742 cm^{-1},

1703 cm^{-1}, 1571 cm^{-1}, 1541 cm^{-1}. ^{1}H NMR (400 MHz, $CDCl_3$) δ (ppm) = 8.87-8.84 (m, 1H, H-27), 8.52-8.50 (m, 1H, H-25), 7.67-7.60 (m, 3H, H-26), 7.25-7.21 (m, 3H, H-24), 7.17-7.14 (m, 2H, H-24), 5.82-5.76 (m, 3H, H-10 mixture of isomers), 5.59-5.58 (m, 1H, *p*-cymene CH), 5.54-5.51 (m, 2H. *p*-cymene CH), 5.45-5.44 (m, 2H, H-12 mixture of isomers), 5.41 (s, 1H, H-12 isomer), 5.32-5.31 (m, 1H, *p*-cymene CH), 4.81 (s, 2H, H-22), 4.55 (d, *J* = 4.9 Hz, 1H, H-22), 4.51 (d, *J* = 6.3 Hz, 1H, H-22), 4.46 (d, *J* = 6.4 Hz, 1H, H-22), 3.05- 2.90 (m, 3H, H-18, H-19 & ^{i}PrCH *p*-cymene), 2.80 (s, 4H, H-ART), 2.64-2.53 (m, 4H, H-ART), 2.46 (d, *J* = 7.0 Hz, 3H, H-ART), 2.40-2.32 (m, 3H, H-ART), 2.03-1.99 (m, 5H, H-ART), 1.90-1.86 (m, 3H, H-ART), 1.80-1.68 (m, 5H, H-ART), 1.63-1.58 (m, 3H, H-ART & *p*-cymene-CH_3), 1.41 (bs, 8H, H-ART), 1.16-1.13 (m, 7H, ^{i}PrCH_3 *p*-cymene), 0.96-0.94 (m, 9H, H-ART), 0.91-0.87 (m, 5H, H-ART), 0.83 (d, *J* = 7.2 Hz, 2H, H-ART). (,. ^{13}C NMR (101 MHz, $CDCl_3$) δ (ppm) = 177.58, 177.12, 173.25, 171.79 (C-ART),, 171.33 (C-ART),, 164.16, 156.55 (C-ART),, 155.59, 154.54, 149.68 (C-ART),, 149.04 (C-ART),, 137.83, 136.92 (C-ART),, 136.74 (C-ART),, 129.04, 126.34, 123.44, 122.65, 122.42 (C-ART),, 122.14 (C-ART), 122.02 (C-ART), 120.35, 120.29, 106.29 (C-*p*-cymene), 106.24 (C-*p*-cymene), 104.53 (C-ART), 104.48 (C-ART), 98.75 (C-*p*-cymene), 98.22 (C-*p*-cymene), 92.22 (C-ART), 91.89 (C-ART or C-*p*-cymene), 91.83 (C-ART or C-*p*-cymene), 91.57 (C-ART), 87.84 (C-*p*-cymene), 86.27 (C-*p*-cymene), 86.09 (C-*p*-cymene), 84.26 (C-*p*-cymene), 83.85 (C-*p*-cymene), 82.68, 82.30, 80.25 (C-ART),, 58.93, 52.62, 51.70 (C-ART), 45.39 (C-ART), 44.62 (C-ART), 43.62 (C-*p*-cymene), 37.38 (C-ART), 36.36 (C-ART), 34.22 (C-ART), 31.97 (C-*p*-cymene), 31.86 (C-ART), 31.56 (C-*p*-cymene), 30.77 (C-ART), 29.74 (C-ART), 28.41 (C-*p*-cymene), 26.09 (C-ART isomer), 26.03 (C-ART), 24.66 (C-ART), 23.32 (C-*p*-cymene), 22.13 (C-ART), 21.44 (C-*p*-cymene), 21.37 (C-*p*-cymene isomer), 20.33 (C-ART), 12.34 (C-ART), 12.13 (C-ART isomer). HRMS (ESI^+): *m/z* calcd for $C_{35}H_{47}IN_2O_7Ru$ $[M\text{-}I^-]^+$: 709.2427, found 709.2425.

2.4.1.13. Synthesis of **intermediate 5**:[40]

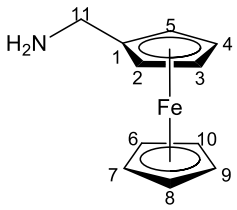

Ferrocene carboxaldehyde (251 mg, 1.17 mmol) was dissolved with sodium hydroxide (280 mg, 7.00 mmol) and hydroxylamine hydrochloride (167 mg, 2.41 mmol) in ethanol (12.5 mL) under inert gas. The reaction was allowed to stir for 3 hours at reflux temperature (90 °C). After the reaction cooled down to ambient temperature, the reaction mixture was diluted with dH_2O (25 mL) and extracted with dichloromethane (20 mL x 4). The organic layer was dried over $MgSO_4$, filtered and evaporated all solvent under vacuum.

Under inert conditions, the crude orange-red oxime was dissolved in dry tetrahydrofuran (9 mL) and was added dropwise, over 10 minutes, to a stirring solution of $LiAlH_4$ (234 mg, 6.17 mmol) in dry THF (9 mL). After the reaction stirred for 5 hours at room temperature, dH_2O (25 mL) was slowly added to quench the reaction. The product was extracted with diethyl ether (20 mL x 3) and washed with brine (25 mL). The organic layer was dried over $MgSO_4$, filtered and evaporated all solvent under vacuum. ATR-IR (ZnSe crystal): 1585 cm^{-1}. ^{1}H NMR (300 MHz, $CDCl_3$) δ (ppm) = 4.17 (m, 2H, substituted-Cp), 4.14 (s, 5H, unsubstituted-Cp), 4.12 (m, 2H, substituted-Cp), 3.59 (s, 2H, H-11).

2.4.1.14. Synthesis of compound **6**:[51]

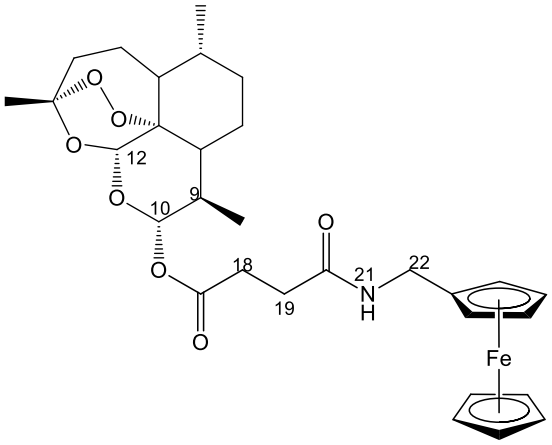

Artesunate (254 mg, 0.66 mmol) was transferred to a round bottom flask and dissolved in dichloromethane (2.5 mL). After the solution was cooled to *ca*. 0 °C, ferrocene methylamine (77 mg, 0.36 mmol), EDC (74 mg, 0.38 mmol), HOBt (12%w/w H_2O, 60 mg, 0.39 mmol) & 4-dimethylaminopyridine (5 mg, 0.043 mmol) was added respectively to the solution. The reaction was allowed to stir overnight (16 hours 30 minutes) to room temperature. The reaction mixture was diluted with dichloromethane (25 mL) and washed with sat. $NaHCO_3$ (25 mL x 2), followed with brine (25 mL). The organic layer was dried over $MgSO_4$, filtered and evaporated all solvent until dryness. The orange/yellow crude solid material (186 mg) was purified with gravity silica chromatography. Solvent system: ethyl acetate: triethyl amine: methanol – 100:0.1:0; 97:0.1:3. A second silica column purification was performed to separate an impurity that had a near identical R_f value to the target compound: Hexane: triethyl amine: ethyl acetate; 25:0.1:75. A orange-yellow oil/solid was obtained (95 mg, 45.7% yield). ATR-IR (ZnSe crystal): 1738 cm^{-1}, 1658 cm^{-1}, 1530 cm^{-1}, 1015 cm^{-1}. ^{1}H NMR (300 MHz, $CDCl_3$) δ (ppm) = 5.86 (s, 1H, H-21), 5.78 (d, *J* = 9.67 Hz, 1H, H-10), 5.41 (s, 1H, H-12), 4.17 (m, 2H, substituted-Cp), 4.15 (s, 5H, unsubstituted-Cp), 4.13-4.09 (m, 4H, substituted-Cp & H-22), 2.85-2.67 (m, 2H, H-ART), 2.62-2.31 (m, 4H, H-ART), 1.92-1.83 (m, 1H, H-ART), 1.79-1.73 (m, 3H, H-ART), 1.70-1.67 (m, 1H, H-ART), 1.64-1.57 (m, 1H, H-ART), 1.42 (s, 3H, H-ART), 1.27 (t, *J* = 7.2 Hz, 2H, H-ART), 0.96 (d, *J* = 5.9 Hz, 3H, H-ART), 0.85 (d, *J* = 7.1 Hz, 3H, H-ART). ^{13}C NMR (101 MHz, $CDCl_3$) δ (ppm) = 171.92 (carbonylC-ARS), 170.63 (carbonylC-ARS), 104.57 (C-ART), 92.30 (C-ART), 91.61 (C-ART), 84.81 (C- substituted-Cp), 80.22 (C-ART), 68.68 (C-unsubstituted-Cp), 68.34-68.25 (C-substituted-Cp), 51.68 (C-ART), 45.34 (C-ART),39.08 (C-22), 37.39 (C-ART), 36.34 (C-ART), 34.20 (C-ART), 31.90 (C-ART), 30.93 (methyleneC-ARS), 29.85 (methyleneC-ARS), 24.70 (C-ART), 22.12 (C-ART), 20.33 (C-ART), 12.22 (C-ART). HRMS (ESI^+): *m/z* calcd for $C_{30}H_{39}FeNO_7$ $[M]^+$: 581.2076, found 581.2075.

2.5. References:

1 M. Schlitzer, *ChemMedChem*, 2007, 2, 944–986.

2 World Health Organization, *Guidelines for the treatment of malaria*, 2015.

3 G. Gasser and N. Metzler-Nolte, *Curr. Opin. Chem. Biol.*, 2012, 16, 84–91.

4 R. K. Haynes and S. Krishna, *Microbes Infect.*, 2004, 6, 1339–1346.

5 J. Wang, L. Huang, J. Li, Q. Fan, Y. Long, Y. Li and B. Zhou, *PLoS One*, 2010, **5**, e9582.

6 S. Krishna, A. C. Uhlemann and R. K. Haynes, *Drug Resist. Updat.*, 2004, **7**, 233–244.

7 J. Li and B. Zhou, *Molecules*, 2010, **15**, 1378–1397.

8 M. A. Biamonte, J. Wanner and K. G. Le Roch, *Bioorganic Med. Chem. Lett.*, 2013, 23, 2829–2843.

9 T. Nguyen Le, W. M. De Borggraeve, P. Grellier, V. C. Pham, W. Dehaen and V. H. Nguyen, *Tetrahedron Lett.*, 2014, **55**, 4892–4894.

10 D. S. Torok and H. Ziffer, *Synthesis and reactions of 11-azaartemisinin and derivatives*, 1995, vol. 36.

11 S. Jana, S. Iram, J. Thomas, S. Liekens and W. Dehaen, *Bioorganic Med. Chem.*, 2017, **25**, 3671–3676.

12 N. Acton, J. M. Karle and R. E. Miller, *J. Med. Chem.*, 1993, **36**, 2552–2557.

13 D. Meyer, T. Smeilus, D. Pliatsika, F. Mousavizadeh and A. Giannis, *Bioorganic Med. Chem.*, 2017, **25**, 6098–6101.

14 M. A. Avery, P. Fan, J. M. Karle, J. D. Bonk, R. Miller and D. K. Goins, *J. Med. Chem.*, 1996, **39**, 1885–1897.

15 R. Gaur, H. S. Cheema, Y. Kumar, S. P. Singh, D. K. Yadav, M. P. Darokar, F. Khan and R. S. Bhakuni, *RSC Adv.*, 2015, **5**, 47959–47974.

16 P. M. O'Neill, M. Pugh, A. V. Stachulski, S. A. Ward, J. Davies and B. K. Park, *J. Chem. Soc. Perkin 1*, 2001, **1**, 2682–2689.

17 H. C. Kolb, M. G. Finn and K. B. Sharpless, *Angew. Chemie - Int. Ed.*, 2001, **40**, 2004–2021.

18 L. H. Binh, N. T. T. Van, V. T. Kien, N. T. T. My, L. Van Chinh, N. T. Nga, H. X. Tien, D. T. Thao and T. K. Vu, *Med. Chem. Res.*, 2016, **25**, 738–750.

19 S. Cho, S. Oh, Y. Um, J. H. Jung, J. Ham, W. S. Shin and S. Lee, *Bioorganic Med. Chem. Lett.*, 2009, **19**, 382–385.

20 L. L. Wang, L. Kong, H. Liu, Y. Zhang, L. Zhang, X. Liu, F. Yuan, Y. Li and Z. Zuo, *Eur. J. Med. Chem.*, , DOI:10.1016/j.ejmech.2019.111665.

21 L. Xie, X. Zhai, L. Ren, H. Meng, C. Liu, W. Zhu and Y. Zhao, *Design, synthesis and antitumor activity of novel artemisinin derivatives using hybrid approach*, 2011, vol. 59.

22 T. Efferth, M. R. Romero, A. Rita Bilia, A. Galal Osman, M. ElSohly, M. Wink, R. Bauer, I. Khan, M. Camilla Bergonzi and J. J.G. Marin, *World J. Tradit. Chinese Med.*, 2016, **2**, 1–23.

23 S. Buzzi, A. Presser and M. von Freyhold, *Determining Viable Protocols for the Derivatisation of Artemisinin into Dihydroartemisinin and into Artesunate*, 2017.

24 H. C. Kolb, M. G. Finn and K. B. Sharpless, *Angew. Chemie - Int. Ed.*, 2001, **40**, 2004–2021.

25 B.-Y. Lee, S. R. Park, H. B. Jeon and K. S. Kim, *Tetrahedron Lett.*, 2006, **47**, 5105–5109.

26 N. Moitra, J. J. E. Moreau, X. Cattoën and M. Wong Chi Man, *Chem. Commun.*, 2010, **46**, 8416.

27 K. Asano and S. Matsubara, *Org. Lett.*, 2010, **12**, 4988–4991.

28 C. Wang, D. Ikhlef, S. Kahlal, J. Y. Saillard and D. Astruc, *Coord. Chem. Rev.*, 2016, 316, 1–20.

29 W. Cabri, I. D'Acquarica, P. Simone, M. Di Iorio, M. Di Mattia, F. Gasparrini, F. Giorgi, A. Mazzanti, M. Pierini, M. Quaglia and C. Villani, *J. Org. Chem.*, 2011, **76**, 4831–4840.

30 F. J. Smit, R. A. van Biljon, L.-M. Birkholtz and D. D. N'Da, *Eur. J. Med. Chem.*, 2015, **90**, 33–44.

31 J. P. Joubert, F. J. Smit, L. du Plessis, P. J. Smith, D. D. N'Da and D. D. N'da, *Eur. J. Pharm. Sci.*, 2014, **56**, 16–27.

32 A. Presser, A. Feichtinger and S. Buzzi, *Monatshefte für Chemie - Chem. Mon.*, 2017, **148**, 63–68.

33 B. T. Mott, A. Tripathi, M. A. Siegler, C. D. Moore, D. J. Sullivan and G. H. Posner, *J. Med. Chem.*, 2013, **56**, 2630–2641.

34 X. Fan, V. Sans, P. Yaseneva, D. D. Plaza, J. Williams and A. Lapkin, *Org. Process Res. Dev.*, 2012, **16**, 1039–1042.

35 M. R. R. Prabhath, J. Romanova, R. J. Curry, S. R. P. Silva and P. D. Jarowski, *Angew. Chemie Int. Ed.*, 2015, **54**, 7949–7953.

36 B. S. Uppal, A. Zahid and P. I. P. Elliott, *Eur. J. Inorg. Chem.*, 2013, 2571–2579.

37 A. Pathak, D. Jain and R. Sharma, *Indian J. Chem. Sect. B …*, 1995, **34**, 992–993.

38 V. Sai Sudhir, N. Y. Phani Kumar and S. Chandrasekaran, *Tetrahedron*, 2010, **66**, 1327–1334.

39 J. Camponovo, J. Ruiz, E. Cloutet and D. Astruc, *Chem. - A Eur. J.*, 2009, **15**, 2990–3002.

40 A. Baramee, A. Coppin, M. Mortuaire, L. Pelinski, S. Tomavo and J. Brocard, *Bioorganic Med. Chem.*, 2006, **14**, 1294–1302.

41 S. H. van Rijt, A. J. Hebden, T. Amaresekera, R. J. Deeth, G. J. Clarkson, S. Parsons, P. C. McGowan and P. J. Sadler, *J. Med. Chem.*, 2009, **52**, 7753–7764.

42 A. Ashraf, M. Hanif, M. Kubanik, T. Söhnel, S. M. F. Jamieson, A. Bhattacharyya and C. G. Hartinger, *J. Organomet. Chem.*, 2017, **839**, 31–37.

43 J. Tönnemann, J. Risse, Z. Grote, R. Scopelliti and K. Severin, *Eur. J. Inorg. Chem.*, 2013, 4558–4562.

44 A. E. Fields, D. Zurwell, C. W. Padgett and B. Quillian, *J. Organomet. Chem.*, 2017, **846**, 66–73.

45 K. E. Jolley, G. J. Clarkson and M. Wills, *J. Organomet. Chem.*, 2015, **776**, 157–162.

46 S. Allu and K. C. K. Swamy, *J. Org. Chem.*, 2014, **79**, 3963–3972.

47 M. Melchart, A. Habtemariam, S. Parsons, S. A. Moggach and P. J. Sadler, *Inorganica Chim. Acta*, 2006, **359**, 3020–3028.

48 A. E. Fields, D. Zurwell, C. W. Padgett and B. Quillian, *J. Organomet. Chem.*, 2017, **846**, 66–73.

49 Z. Jia, S. Wei and Q. Zhu, *Biol. Pharm. Bull.*, 2010, **33**, 725–728.

50 A. R. Hamann, C. de Kock, P. J. Smith, W. A. L. van Otterlo and M. A. L. Blackie, *Bioorg. Med. Chem. Lett.*, 2014, **24**, 5466–5469.

51 J. A. Gurak, K. S. Yang, Z. Liu and K. M. Engle, *J. Am. Chem. Soc.*, 2016, **138**, 5805–5808.

Chapter 3: Biological studies of organometallic artemisinins

3.1. Introduction:

Although an optimised synthesis method in early drug discovery is important, pharmacological studies are equally, if not more important, to identify the properties of possible drug candidates for treatment of diseases like malaria. Along with the interactions of the drug with its target , the interactions with other unanticipated targets (e.g. healthy cells) need to be investigated.[1] As such, the word "target" can be applied broadly for investigations of specific sub-structures or specific disruptions in biological pathways. Essential preclinical studies include testing the solubility of the potential drug candidates in an appropriate biological buffer system and determining the efficacy of the potential drug candidate against the target without harming the host.[1] Extensive research has been done to mimic biological environments for different organisms,[1–3] such as to mimic salt concentrations and the appropriate pH at which the target exists.

As described in chapter one, due to the lack of bioavailability, artemisinin and its derivatives has been administered to patients in combination with other slower acting drugs, since the introduction of the artemisinin based combination therapy (ACT) as the recommended treatment against malaria by the WHO in 2006 [4,5] Praised by its excellent pharmacodynamic properties to selectively target infected red blood cells and high efficacies,[3,6,7] research for new artemisinin derivatives are in high demand to improve bioavailability (and other pharmacokinetic properties) with rising artemisinin resistant *Plasmodium falciparum* strains.[8–11]

It is imperative to investigate the new artemisinin compounds synthesised (Compounds **1-6**) during this research for their solubilities in the appropriate buffer system, efficacies against *P. falciparum* and toxicity to healthy human cells. Interestingly, increasing evidence of artemisinin derivatisation studies revealed that it can achieve high efficacies against other diseases, especially cancer treatment research.[12–18] Therefore, our drug candidates were tested against two bacteria, *Escherichia coli* and the notorious methicillin resistant *Staphylococcus aureus* strain. Artemisinin displayed activity against the MRSA strain by L. Lin and co-workers.[13] However, it is important to note that they used cyclodextrin to increase the solubility of artemisinin for the assays. Compounds **1-6** as well as their synthetic precursors (**Figure 3.1**) were screened for activity.

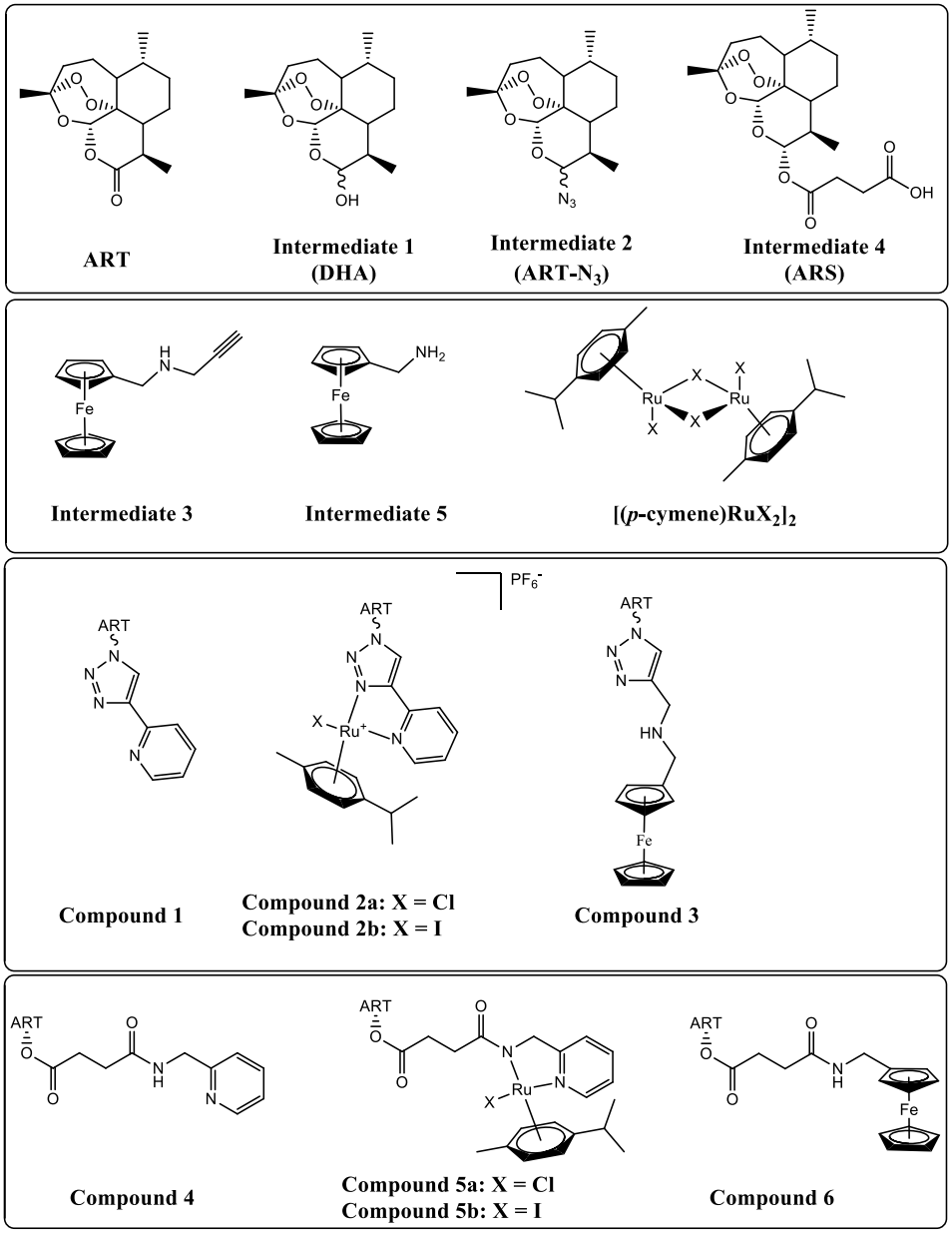

Figure 3.1. Chemical structures of compounds synthesised and tested.

3.2. Discussion:

3.2.1. Turbidimetric assay:

Solubility is an important property for early drug candidate development, as *in vitro* and *in vivo* tests require the compounds to be stable and to dissolve in the buffer systems in which they are placed where they are evaluated for other properties such as biological activity and toxicology.[2,19] Since artemisinin species are praised for its great solubility in biological media,[20] we aimed to maintain its aqueous solubility after derivatisation.

The aqueous solubility of the compounds was performed in a microtiter plate in triplicate measurements, reading turbidity at 620 nm, in biologically relevant buffers, PBS (**Table 3.1**) and HEPES (**Table 3.2**). The compounds were tested in 2% DMSO which mimics the physiological conditions used during anti-plasmodial

assay and cytotoxicity tests discussed later in this chapter. Reserpine and hydrocortisone were used in this study as controls, with reserpine compared as an insoluble compound and hydrocortisone as a soluble compound, **Figure 3.2**.

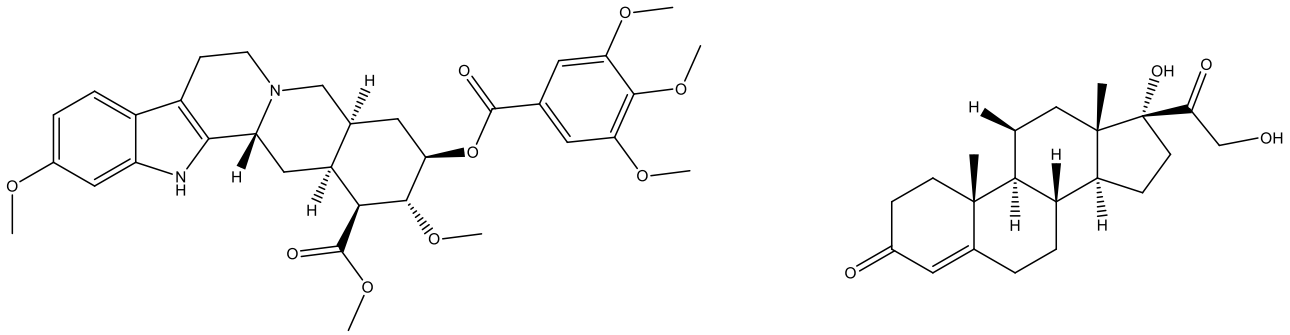

Reserpine **Hydrocortisone**

Figure 3.2. Chemical structures of reserpine and hydrocortisone used as controls for solubility assay.

To obtain an early insight into the solubility of the compounds synthesised, the turbidity assay procedure followed the extended kinetic solubility approach.[2] Such methods should be performed multiple times as the data can be affected by external factors such as temperature and time.[2] The solubility of the compounds were evaluated to be within a range around the point of inflection on the solubility graph of compound **1** in PBS and DMSO (see **Figure 3.3** as an example).

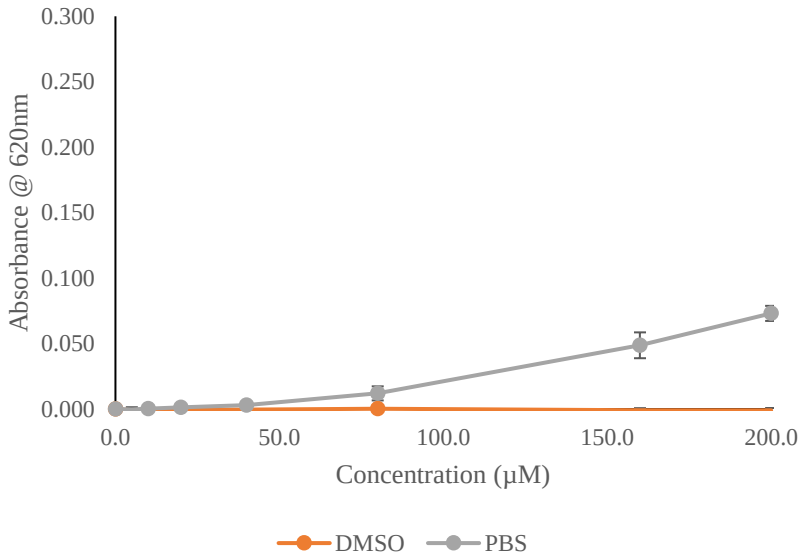

Figure 3.3. Solubility graph of compound 1 at room temperature.

The solubility data for all compounds is shown in **Table 3.1** and **Table 3.2.** As was expected, ARS was more soluble than the other artemisinin precursors: ART, DHA and ART-N_3 in both PBS and HEPES although data suggested that ART-N_3 is slightly more soluble in HEPES than PBS. It is apparent that ARS is the most soluble of the four artemisinin precursors tested, due to its polar carbonyl groups and hydroxyl group, capable for more hydrogen bonding in the aqueous environment. Overall, compounds had similar solubilities in both PBS and HEPES. Data for both the triazole compounds (**1**-**3**) and amide-ester compounds (**4**-**6**) clearly indicated that the addition of the organometallic moieties decreased the solubility when compared to their respective artemisinin precursors. The decrease in solubility most likely due to the increased size or mass of the chemical

structures. The effect of increased size becomes more evident after observing the loss of solubility of compounds **1** and **4** after complexation to ruthenium. Contrary to the initial expectation, the triazole compounds **2a** and **2b**, which are both salts, have low solubility, which could be explained due to its rigid chemical structure. Compounds **2a** and **2b** might even form adducts with the HEPES and PBS buffers, yet further experimental data is required to elucidate this statement. The influence of molecular size on solubility is further confirmed with the data of **intermediate 3** (solubility of >200 µM), compared to the triazole compound **3**(solubility of 10-20 µM). The UV-Vis spectra of the organometallic compounds **2a**, **3**, **5a** and **6** and intermediates **3** and **5** confirmed that they do not absorb at 620 nm, therefore no interference at 620 nm would be observed due to the compounds. The amide-ester compounds (**4**-**6**) are slightly more soluble than the triazole compounds (**1**-**3**). This could be due to the carbon chain linking the artemisinin moiety to the organometallic moiety or pyridine moiety, granting a higher degree of freedom for movement in the molecule than with the rigid triazole group. Moreover, the triazole compounds are more hydrophobic than the amide ester chain linker.

Table 3.1. Solubility data of artemisinin species in performed in PBS at pH 7.4.

Compound	**ART**	**DHA**	**ART-N_3**	**ARS**
Solubility (µM)	80-160	80-160	80-160	>200
Solubility (µg/mL)	22.6-45.2	22.7-45.5	24.7-49.5	>76.9
Compound	**Compound 1**	**Compound 2a**	**Compound 2b**	**Compound 3**
Solubility (µM)	40-80	20-40	10-20	10-20
Solubility (µg/mL)	16.5-33.0	16.6-33.1	9.2-18.4	5.6-11.2
Compound	**Compound 4**	**Compound 5a**	**Compound 5b**	**Compound 6**
Solubility (µM)	80-160	10-20	10-20	20-40
Solubility (µg/mL)	38.0-75.9	7.4-14.9	8.4-16.7	11.6-23.3
Compound	**Intermediate 3**	**Intermediate 5**	**[(*p*-cymene)$RuCl_2$]$_2$**	**[(*p*-cymene)RuI_2]$_2$**
Solubility (µM)	>200	80-160	80-160	80-160
Solubility (µg/mL)	>50.6	17.2-34.4	49.0-98.0	78.3-156.5
Compound	**Reserpine**	**Hydrocortisone**		
Solubility (µM)	20-40	80-160		
Solubility (µg/mL)	12.2-24.3	29.0-58.0		

Table 3.2. Solubility data of artemisinin species performed in HEPES buffered to pH 7.0

Compound	**ART**	**DHA**	**ART-N_3**	**ARS**
Solubility (µM)	80-160	80-160	>200	>200
Solubility (µg/mL)	22.6-45.2	22.7-45.5	>61.9	>76.9
Compound	**Compound 1**	**Compound 2a**	**Compound 2b**	**Compound 3**
Solubility (µM)	40-80	20-40	10-20	10-20
Solubility (µg/mL)	16.5-33	16.6-33.1	9.2-18.4	5.6-11.2
Compound	**Compound 4**	**Compound 5a**	**Compound 5b**	**Compound 6**
Solubility (µM)	80-160	10-20	20-40	20-40
Solubility (µg/mL)	38.0-75.9	7.4-14.9	16.7-33.4	11.6-23.3
Compound	**Intermediate 3**	**Intermediate 5**	**[(*p*-cymene)$RuCl_2$]$_2$**	**[(*p*-cymene)RuI_2]$_2$**
Solubility (µM)	>200	80-160	80-160	80-160
Solubility (µg/mL)	>50.6	17.2-34.4	49.0-98.0	78.3-156.5
Compound	**Reserpine**	**Hydrocortisone**		
Solubility (µM)	20-40	80-160		
Solubility (µg/mL)	12.2-24.3	29.0-58.0		

Compounds with solubilities within the range of 10 µg/mL – 60 µg/mL, are acceptable for further studies,[21] as it will become apparent how solubility affected the efficacies against *P. falciparum* and the bacteria tested. However, the lipophilicity of these compounds are yet unknown, as it is a good measure for absorption and permeability of the compounds to cross the cell membranes of the organisms. The tolerance of these compounds should thus be tested in future studies.[1] Stability of these low solubility compounds may also have a great effect in bioavailability.

3.2.2. Biological studies against Plasmodium falciparum

All compounds of this study were tested against two *P. falciparum* strains, 3D7 (chloroquine sensitive) and Dd2 (chloroquine resistant). The percent inhibition of parasitic proliferation for each compound was determined, normalised and plotted against a control, Puromycin, giving a sigmoidal dose response curve for which the IC_{50} values were obtained.

Comparing the anti-plasmodial results (**Table 3.3**), it is found that the amide-ester compounds (**4-6**) performed better than triazole compounds (**1-3**). The ruthenium dimers and ferrocene intermediates (intermediate **3** and **5**) are inactive against the malarial strains. Compounds **2a**, **2b** and **3** and compounds **5a**, **5b** and **6** displayed a great improvement, compared to their respective precursors, **intermediates 3** and i**ntermediate 5** and the respective ruthenium dimers. This observation confirms that the organometallic moieties alone are unable to either permeate the infected red blood cells and/or parasite, nor do they yield any reactivity against any possible target in the parasite. Interestingly, the ruthenium complexes (**2a**, **2b** and **5a**, **5b**) were not as active as their respective ligands, compounds **1** and **4**. Low purity could be one explanation for this result. However, the IC_{50} values obtained are far smaller than the approximate solubilities of the compounds, for example: compound **2b** has a solubility between 10-20 µM, while it achieved an IC_{50} of 120.8 ± 36.1 nM. It is possible that the ligands, compounds **1** and **4**, are able to bind to the iron in haem,[6,22] allowing the artemisinin moiety into close proximity to other haem molecules, therefore increasing the chance that the endoperoxide bridge of the artemisinin moiety would activate. This may then also continue to possibly interrupt the formation of hemozoin in the acidic food vacuole, leading to a build-up of toxic free haem in the parasite. The Ru-iodido complexes (**2b** and **5b**) performed better than their chlorido-derivatives (**2a** and **2b**), which indicated that a more polar

halogen group on the metal centre increased the activity against *P. falciparum*. The biological data strongly suggested that ferrocene derivatives (compounds **3** and **6**), moreover the artesunate derivative (compound **6**, IC_{50} (Dd2 = 3.0 ± 1.6 nM) held the best potential for further studies. Further evaluation of the biological data could be elaborated with the use of resistance index (RI). RI is a measure of how the biological activity of a drug compound is affected between a drug sensitive strain and a drug resistant strain. This could be interpreted whether or not the drug compound retains its biological activity when tested against a drug-resistant strain. All compounds tested were surprisingly more active against the chloroquine resistant strain (Dd2) than the chloroquine sensitive strain (3D7). The latter resulted in RI values < 1.0, indicative of low to no cross-resistances between the parasitic strains. One could highlight that complex **2a** showed the lowest RI value of all artemisinin-organometallic compounds, slightly more potent than ARS (RI = 0.31).

Table 3.3. Anti-plasmodial assay data indicating IC_{50} against chloroquine sensitive (3D7) and chloroquine resistant (Dd2) P. *falciparum* strains.

	IC_{50} (nM) (±SD)				**IC_{50} (nM) (±SD)**		
Compound[a]	**3D7**	**Dd2**	**RI[b]**	**Compound**	**3D7**	**Dd2**	**RI**
ART	10.4 (3.8)	4.7 (1.0)	0.45	**Compound 1**	6.5 (0.8)	3.3 (1.2)	0.51
DHA	0.6 (0.0)	0.4 (0.0)	0.68	**Compound 2a**	245.0 (36.8)	70.9 (2.6)	0.29
ARS	2.6 (0.7)	0.8 (0.2)	0.31	**Compound 2b**	120.8 (36.1)	69.8 (9.0)	0.58
ART-N_3	5.8 (0.8)	4.4 (0.4)	0.76	**Compound 3**	7.8 (3.2)	4.8 (0.6)	0.61
Intermediate 3	1380 (198.0)	693.0 (58.0)	0.50	**Compound 4**	1.4 (0.2)	0.6 (0.1)	0.43
Intermediate 5	215.5 (57.3)	99.8 (15.8)	0.46	**Compound 5a**	84.2 (3.7)	33.4 (3.7)	0.40
[(*p*-cymene)$RuCl_2$]$_2$	5830.0 (858.6)	3530.0 (670.0)	0.61	**Compound 5b**	30.3 (7.2)	14.2 (4.6)	0.47
[(*p*-cymene)RuI_2]$_2$	9135.0 (770.7)	2495.0 (49.5)	0.27	**Compound 6**	6.1 (1.1)	3.0 (1.6)	0.49

[a]See figure 3.1. for chemical structures.
[b]RI = IC_{50}Dd2/IC_{50}3D7

3.2.3. Toxicity studies

All compounds were subsequently screened against the HEK293 (Human embryonic kidney) cell line to ascertain if the compounds are toxic to healthy human cells.

The HEK toxicity data was consolidated into **Table 3.4**, as seen below. An interesting result observed for **intermediate 1** was that it is not only active against the *P. falciparum* strains 3D7 and Dd2, but also showed low to no activity on the healthy cells. Four of the twelve compounds tested were entirely inactive against HEK cells. The ferrocenyl compounds, **intermediate 3 and intermediate 5,** were inactive, but compounds **3** and **6** showed low activity against the healthy cells. It is promising that compounds 3 and 6 showed high anti-plasmodial activity while being relatively non-toxic to healthy cells. The iodido-complexes (**2b** and **5b**) were slightly more cytotoxic against HEK cells than their respective chloride counterparts (**2a** and **5a**). In conclusion, our compounds show very little toxicity against healthy cells.

Table 3.4. HEK inhibition studies of compounds.

Compound[a]	IC_{50} (µM) (±SD)	% Inhibition at 80 µM	Compound	IC_{50} (µM) (±SD)	% Inhibition at 80 µM
ART	-	IA[b]	**Compound 1**	5.975 (.091)	-
DHA	14.250 (3.04)	-	**Compound 2a**	13.250 (1.48)	-
ARS	10.000 (0.14)	-	**Compound 2b**	9.165 (0.59)	-
ART-N_3	-	57	**Compound 3**	-	102
Intermediate 3	-	IA	**Compound 4**	13.450(1.20)	-
Intermediate 5	-	IA	**Compound 5a**	-	32
[(*p*-cymene)$RuCl_2$]$_2$	-	IA	**Compound 5b**	-	69
[(*p*-cymene)RuI_2]$_2$	-	IA	**Compound 6**	-	102

[a]See figure 2 for chemical structures.
[b]IA = Inactive

3.2.4. Biological studies against bacteria

The solubility of compounds synthesised in Milner-Hilton broth, used to mimic biological conditions during anti-bacterial assays, was very low. The compounds **1-3, 5** and the [(*p*-cymene)RuI_2]$_2$ dimer were insoluble in the biological buffer system used for the anti-bacterial assay.

One literature study of L. Lin *et al*.[13] showed promising results against the MRSA bacterial strain (more than 99% loss of cell population after 4 days of incubation), after binding artemisinin to β-cyclodextrin. The article would indicate that artemisinin affected the Entner-Doudoroff Pathway (EMP), which is an essential metabolic pathway for catabolising glucose. In this pathway it seems to disrupt the three kinase enzymes that is responsible to produce adenosine triphosphate (ATP) – the "energy currency" of the cell.

Biological data against the *S. aureus* strain (Xen36) and *E. coli* strain (BL21) are shown in **Table 3.5**. The values reported here represent the percentage growth of bacteria after incubation with each compound at 500 µM. A high percent value indicates that the compound has no effect inhibiting the growth of the bacteria. The data indicates that the majority of the compounds have no activity against the bacterial strains. Compound **4** displayed the lowest percentage growth of all the compounds. As shown in **Table 3.5**, some compounds were insoluble in the assay media and could not be tested (value given as "IS"). Therefore, it is clear that when it comes to bacterial research, more thought needs to be put into the best structural aspects needed to solubilise these compounds in the multi component medium used for the bacterial assays. Artemisinin and our derivatives also struggled with aqueous solubility with the buffer medium used for anti-bacterial assay, as similarly reported by L. Lin *et al*.[13] and H. Cui *et al*.,[23] These researchers, as explained in chapter 1, that the solubility of artemisinin is increased with either encapsulation with a highly soluble nanoparticle or β-CD or requires to be administered in combination with an active anti-bacterial agent to improve absorption of artemisinin into the bacteria.

Table 3.5. Anti-bacterial assay % growth data of compounds tested against *E. coli* (BL21) and *S. aureus* (Xen36) at 500 µM.

	% growth at 500 µM (±SD)			% growth at 500 µM (±SD)	
Compound[a]	**BL21**	**Xen36**	**Compound**	**BL21**	**Xen36**
ART	93.0 (1.8)	IA	**Compound 1**	IS	IS
DHA	77.7 (3.7)	IA	**Compound 2a**	IS	IS
ARS	80.4 (3.4)	IA	**Compound 2b**	IS	IS
ART-N_3	88.5 (0.5)	IA	**Compound 3**	IS	IS
Intermediate 3	89.1 (1.9)	IA	**Compound 4**	53.0 (2.3)	70.8 (2.8)
Intermediate 5	IA	IA	**Compound 5a**	67.8 (0.5)	IA
[(*p*-cymene)$RuCl_2$]$_2$	81.0 (1.7)	IA	**Compound 5b**	NA	NA
[(*p*-cymene)RuI_2]$_2$	IS	IS	**Compound 6**	IS	IS

[a]See Figure 3.13.1 for chemical structure.
[b]IA = inactive
[c]IS = Insoluble
[d]N/A = not available

3.3. Conclusion and future work:

It is evident that the compounds studied show promising biological efficacies against the *P. falciparum* parasite. It is indicative that the compounds that contained ferrocene are the better alternative organometallic group for further studies. Moreover, it also indicates that amide-esters are not only slightly more soluble, but also have a higher efficacy against *P. falciparum*. Lastly, the compounds tested against bacteria indicate that although it is possible to slightly inhibit bacteria, a transport or carrier system must be developed if further studies would show that our compound is unable to enter the bacterial cells freely.

3.4. Experimental:

Chemicals and consumables. HEPES, PBS tablets, reserpine, hydrocortisone and DMSO were purchased from Sigma-Aldrich. Micro-pipette tips and microtiter plates were supplied from Lasec.

Instrumentation. Thermo Scientific Multiscan Go plate reader was used for turbidimetric assay analysis.

3.4.1. Turbidimetric assay:

Turbidimetric assay of the drug candidates was performed with either Phosphate buffered saline (PBS) or (4-(2-hydroxyethyl)-1-piperazineethanesulfonic acid) (HEPES). The PBS tablet was dissolved in distilled H_2O which yielded 10 mM phosphate buffer, 2.7 mM potassium chloride and 137 mM sodium chloride at pH 7.4. 0.025 mM HEPES was prepared with distilled $H_2O$and adjusted to pH 7.0 with diluted sodium hydroxide. Both buffer solutions were stored overnight in a fridge (5°C) before use the next day – and was discarded after 14 days. Both buffers and DMSO were filtered through a syringe filter (0.45 µm pore size, 25 mm diameter) right before use. Hydrocortisone solution and reserpine were used as controls. The drug candidates and controls were prepared in 10 mM stock solutions, each dissolved in high purity dimethyl sulfoxide (99.5%) and filtered through a syringe filter (0.45 µm pore size, 25 mm diameter). A serial dilution (between 10 mM and 0.25 mM) in triplicate of each drug candidate was prepared in a 96-well plate (200 µL). 4 µL of each concentration in the dilution series was then transferred to another 96-well plate (200 µL) for a 50x dilution with either DMSO, PBS or HEPES. Each compound had a corresponding blank in triplicate which consisted of 4 µL DMSO and 196 µL of the corresponding solvent (DMSO, PBS or HEPES). The microtiter plates were incubated with a lid on at an ambient temperature for 2 hours before analysed at 620 nm.

3.4.2. Antiplasmodial assay[24]

The compounds were evaluated using the confocal image analysis assay. Compounds were solubilized in DMSO to a final concentration of 5 mM. The stock compounds were then diluted further in DMSO to generate 3 doses per log dose response dilutions within 384-well polypropylene compound storage plates. The dose response dilution plates were then diluted 1 µL into 25 µL of sterile water and 5 µL transferred into 384-well imaging plates.

The *P. falciparum* 3D7 and Dd2 strains were kept in a continuous culture (RPMI supplemented with, 25 mM Hepes, 50 µg/mL hypoxanthine, 2.5 mg/mL Albumax II® plus 5% human serum) with sorbitol synchronization performed over two successive intra erythrocytic lifecycles to provide ring-stage parasites for use within the assays. On the day of assay, the ring-stage parasite culture was adjusted to 2% parasitaemia and 0.3% haematocrit and 45 µL of which was added to the compound-containing imaging plates. The assay plates were incubated for 72 h at 5% O_2, 5% CO_2 and 90% N_2. The plates were removed from incubation and allowed to equilibrate at room temperature prior to staining with 4',6-diamidino-2-phenylindole (DAPI). The imaging assay plates were then imaged on the Opera confocal imaging system. Using Accapella scripting software, the number of classified parasites was determined for each assay well. Percentage inhibition of parasite proliferation was calculated and normalized to assay control data of 0.4% DMSO and 5 µM Puromycin.

Percentage inhibition of parasite numbers (normalized to 5 µM puromycin) was plotted against log concentration of the compounds using a 4-parameter log dose, non-linear regression analysis, with sigmoidal dose response (variable slope) curve fit using Prizm 4.0. No constraints were placed on the top, bottom or Hill slope of the curve fit in the graphing software.

3.4.3. Human embryonic kidney (HEK293) mammalian cell toxicity

HEK293 cells were cultured in DMEM culture media supplemented with 10 % Foetal Bovine Serum (FBS). The cells were harvested and dispensed into 384 well sterile black, clear base microtiter plates at 2000 cells/well (45 µL). The plates were left to settle and the cells attached overnight in a standard tissue culture incubator at 5% CO_2, 37 °C and 60% humidity. After overnight incubation, 5 µL of the diluted compound (as described in the section, "Evaluation of *in vitro* activity against *P. falciparum* asexual blood stages") was added to the cell containing plates and incubated for a further 72 h. After incubation the supernatant from the wells was removed and 40 µL of 40 µM resazurin in DMEM media (FBS free) added to all wells. The plates were incubated for 6 h and then measured for fluorescent intensity using the PerkinElmer Envision. The data was analysed as in the *Plasmodium falciparum* methods section 3.3.2.

3.4.4. MIC assay

Minimum inhibitory concentrations (MICs) of compounds, discussed in this chapter, towards *Staphylococcus aureus* Xen36 and *Escherichia coli* BL21 were determined using the broth microdilution method according to guidelines of the Clinical and Laboratory Standards Institute (CLSI, 2015).[23] Milner-Hilton (MH) broth (Thermo Fisher Scientific) was inoculated (5 $\log_{10}$ CFU/ml) and incubated under static conditions at 37 °C for 24 h. Bacterial susceptibility towards compounds was determined at concentrations ranging from 500 µM to 0.977 µM. After incubation, bacterial growth (absorbance at 600 nm) was determined using the TECAN SPARK® multimode microplate reader (Tecan Group, Männedorf, Switzerland) and compared to controls (no anti-metabolites and inoculated media). The MICs were defined as the lowest concentration that inhibited visible growth, and IC_{50} as the concentration that inhibited 50 % of visible growth.

3.5. References:

1 J. P. Hughes, S. S. Rees, S. B. Kalindjian and K. L. Philpott, *Br. J. Pharmacol.*, 2011, **162**, 1239–1249.

2 T. Sou and C. A. S. Bergström, *Drug Discov. Today Technol.*, 2018, 27, 11–19.

3 J. Yang, Y. He, Y. Li, X. Zhang, Y. K. Wong, S. Shen, T. Zhong, J. Zhang, Q. Liu and J. Wang, *Pharmacol. Ther.*, 2020, **216**, 107697.

4 WHO, *World Malaria report 2020: 20 years of global progress and challenges*, World Health Organization, 2020.

5 H. Betram, W. B. Thomas, a K. J. Forest, M. John and World Health Organization, *Guidelines for the treatment of malaria*, .

6 P. A. Stocks, P. G. Bray, V. E. Barton, M. Al-Helal, M. Jones, N. C. Araujo, P. Gibbons, S. A. Ward, R. H. Hughes, G. A. Biagini, J. Davies, R. Amewu, A. E. Mercer, G. Ellis and P. M. O'Neill, *Angew. Chemie Int. Ed.*, 2007, **46**, 6278–6283.

7 G. A. Balint, *Artemisinin and its derivatives: An important new class of antimalarial agents*, 2001, vol. 90.

8 A. Mukherjee, S. Bopp, P. Magistrado, W. Wong, R. Daniels, A. Demas, S. Schaffner, C. Amaratunga, P. Lim, M. Dhorda, O. Miotto, C. Woodrow, E. A. Ashley, A. M. Dondorp, N. J. White, D. Wirth, R. Fairhurst and S. K. Volkman, *Malar. J.*, 2017, **16**, 1–12.

9 J. Birnbaum, S. Scharf, S. Schmidt, E. Jonscher, W. A. Maria Hoeijmakers, S. Flemming, C. G. Toenhake, M. Schmitt, R. Sabitzki, B. Bergmann, U. Fröhlke, P. Mesén-Ramírez, A. B. Soares, H. Herrmann, R. Bártfai and T. Spielmann, *Science (80-.).*, 2020, **367**, 51–59.

10 M. J. Njokah, J. N. Kang'Ethe, J. Kinyua, D. Kariuki and F. T. Kimani, *Malar. J.*, , DOI:10.1186/s12936-016-1443-y.

11 A. M. Dondorp, F. M. Smithuis, C. Woodrow and L. von Seidlein, *Trends Parasitol.*, 2017, **33**, 353–363.

12 S. Jana, S. Iram, J. Thomas, S. Liekens and W. Dehaen, *Bioorganic Med. Chem.*, 2017, **25**, 3671–3676.

13 L. Lin, X. Mao, Y. Sun and H. Cui, *Microb. Pathog.*, 2018, **118**, 66–73.

14 J. Lemire, A. Alhasawi, V. P. Appanna, S. Tharmalingam and V. D. Appanna, *J. Appl. Microbiol.*, 2017, **123**, 798–809.

15 P. L. Páez, M. C. Becerra and I. Albesa, *FEMS Microbiol. Lett.*, 2010, **303**, 101–105.

16 T. Efferth, *Semin. Cancer Biol.*, 2017, 46, 65–83.

17 W. E. Ho, H. Y. Peh, T. K. Chan and W. S. F. Wong, *Pharmacol. Ther.*, 2014, 142, 126–139.

18 Z. Li, Q. Li, J. Wu, M. Wang and J. Yu, *Molecules*, 2016, 21.

19 N. Wyttenbach, J. Alsenz and O. Grassmann, *Pharm. Res.*, 2007, **24**, 888–898.

20 P. Newton, Y. Suputtamongkol, P. Teja-Isavadharm, S. Pukrittayakamee, V. Navaratnam, I. Bates and N. White, *Antimicrob. Agents Chemother.*, 2000, **44**, 972–977.

21 L. Di and E. H. Kerns, *Drug-Like Properties: Concepts, Structure Design and Methods from ADME to Toxicity Optimization*, 2016.

22 T. J. Egan, K. R. Koch, P. L. Swan, C. Clarkson, D. A. Van Schalkwyk and P. J. Smith, *J. Med. Chem.*, 2004, **47**, 2926–2934.

23 H. Cui, X. Chen, M. Bai, D. Han, L. Lin and M. Dong, *ACS Appl. Mater. Interfaces*, 2019, **11**, 47299–47310.

24 S. Duffy and V. M. Avery, *Am. J. Trop. Med. Hyg.*, 2012, **86**, 84–92.

Chapter 4: Conclusions and future work

4.1 Summary and conclusions:

The incorporation of organometallic fragments into known drugs is becoming a thriving area for anti-microbial drug discovery. While metal complexes show promising biological activity, further studies need to be carried out to fully understand their mode of action on the intended biological target. Nevertheless, this project has built new ways in which the sesquiterpene lactone, artemisinin, could be further derivatised with organometallic moieties. Artemisinin based compounds are very interesting indeed and have been found useful in numerous other applications – such as cancer treatments, protozoan treatments and even anti-viral activities - since its introduction as an antimalarial drug.

Various routes were devised to synthesise artemisinin derivatives to couple with organometallic moieties. Previous studies have laid a foundation to pursue ferrocenyl and ruthenium *p*-cymene moieties as they have great potential for antiplasmodial drug development. Triazole derivatisation artemisinin and amide derivatisation of artesunate were pursued to link the artemisinin moiety to the organometallic groups. The triazole group drug candidates focussed on chemical stability and ease of synthesis; however, it was discovered to be challenging to synthesise and overcome purification limitations. The second group of artemisinin derivatives hoped to achieve increased solubility of the final products by maintaining the activity of the compounds against *Plasmodium falciparum*.

The synthesis of the required artemisinin azide precursor for the click-reaction had its own challenges to overcome. After identification of competing reactions (namely, between the elimination of the hydroxyl group and/or the substitution of the said group with the azide), some optimisation to the reaction conditions were achieved. The new method reduced the reaction time of this substitution time from 24 hours to 5 hours with high yield and purity. However, results indicated that the catalyst used during the reaction (potassium iodide), may be substituted with chloride on the trimethylsilyl moiety *in situ,* thereby producing TMSI. This facilitates the azide substitution which in turn influenced the enantiomeric ratio. The optimisation of a method to produce the labile azide isomer for click-reactions would ideally be sought after, for example: excluding the catalyst from the reaction, to reduce waste of artemisinin.

Similarly, to the substitution reaction, much method development was studied in order to perform a click-reaction with reproducible results. None of the click-reactions performed could reach full conversion. Small-scale test reactions, without competing for an alkyne, revealed that the Copper(I) iodide catalyst readily reacted with the artemisinin precursors, oxidising the copper catalyst and rendering it unreactive to proceed with the Huisgen 1, 3-dipolar cycloaddition reaction. Unable to overcome this fundamental limitation and the influence of the enantiomeric ratio of the ART-N_3, generally low yields between 8%-21% for compound **1** was obtained and 16%-42% yield for compound **3** was obtained. It is speculated that the higher yield for compound **3** was obtained due to a less constricted terminal alkyne, a better facilitated coordination to the copper catalyst that coordinated to the azide, compared to the 2-ethynyl pyridine terminal alkyne. Synthesis of compound **3** could

not be achieved without the synthesis of a new ferrocenyl compound, **intermediate 3**. **Intermediate 3** was successfully synthesised and obtained in high yield (86%) and purity (>99%) after its imine precursor was discovered to be highly unstable during purification.

The synthesis of the ruthenium triazole compounds **2a** and **2b** was easily obtained, however purification of these compounds continued to be challenging. Purification was attempted but was unsuccessful, likely due to the very bulky and complex structure that these compounds have. The rate of complexation of the ruthenium metal to the artemisinin ligand was much faster for the chlorido-dimer compared to the iodido-dimer. NMR- and MS data of these compounds confirmed that the desired compounds were synthesised.

The artesunate derivatives (compound **4** and **6**) were much easier to obtain than the triazole compounds. Moderately good yields (51%-60%) with high purity were obtained. Yet, much investigation had to be scrutinised till it was discovered that the HPLC method is not fully optimised for artesunate derivatives. Synthesis of ruthenium compounds **5a** and **5b** was a difficult challenge to overcome, as the facile method used to synthesise compounds **2a** and **2b** could not be applied. This led to the use of ruthenium p-cymene acetate precursors that proceeded in a cleaner reaction, with little side-reactions observed with TLC. Purification of the ruthenium artesunate compounds were realised with gravity column chromatography with alumina. Purification of compounds **5a** and **5b** was possible with column chromatography, due to the fact that the molecules are neutral, not like the salts, compounds **2a** and **2b**.

Before the compounds synthesised (**1-6**) could be tested against *P. falciparum*, their solubility was analysed in the appropriate buffer systems. The turbidimetric assays, performed in both PBS and HEPES, revealed that the artesunate derivatives (compounds **4-6**) were more soluble than the triazole compounds **1-3**. Moreover, the binding of the organometallic moieties (intermediates **3** and **5** and respective ruthenium *p*-cymene dimers) to the artemisinin precursors, only decreased the solubility of the final compounds. The loss of solubility of the compounds would seem to not have a detrimental effect on their biological activities against the *P. falciparum* strains. Biological data revealed that all artemisinin compounds had greater activities against the chloroquine resistant strain, Dd2, compared to the chloroquine sensitive strain, 3D7. Furthermore, ferrocenyl compounds **3** and **6** were the most active in their respective organometallic sub-groups (triazole and artesunate derivatives). Complexation of the ligands to the ruthenium moieties led to a loss of biological activity (up to a 60-fold decrease) against both *P. falciparum* strains. The loss of activity could not be properly elucidated as only solubility data was available. The high activity of the ligand compounds **1** and **4**, with compound **4** with the highest biological activity (Dd2 IC_{50} = 0.6 nM), was most surprising of all, since they do not possess any organometallic moiety, but an open cavity where it could coordinate with a free metal or organometallic group. It is speculated that compounds **1** and **3** bind to some unknown metal moiety inside the parasitic cell that facilitates the Fenton type reaction.

Results obtained during this project will help steer future research incorporating organometallic groups into the artemisinin structure, which could lead to new antiplasmodial agents.

4.2 Future work:

Numerous analyses and characterisation are yet to be performed on the compounds synthesised in this project. One of these is to optimise the click-reactions with peroxide containing compounds, since several experimental conditions were changed to maintain reproducible results. Isolation and separation of pure triazole isomers may indicate which holds more activity against *P. falciparum*. It is paramount, for future characterisation and biological studies, that purification methods must be developed to obtain pure artemisinin ruthenium half-sandwich complexes (**2** and **5**). Furthermore, the complex ^{1}H-NMR spectra of the ruthenium complexes, compounds **2** and **5**, require further elucidation with 2D-NMR experiments, such as NOESY, to investigate whether there are any through space coupling responsible for the complex proton signals observed in the ^{1}H-NMR spectra. Far-IR would also help identify future ruthenium half-sandwich complexes as it would give an indication at which element it chelated to - for example: our artesunate compound **5** could coordinate through either carbonyl oxygen or the amide nitrogen. This may also explain the complex ^{1}H-NMR signals as different ruthenium regioisomers present *in situ*. Moreover, HPLC method optimisation could be performed to be "soft" on hydrolytically liable groups such as compounds **4-6,** or search perform specialised techniques such as LC-MS to elucidate the presence of the fragments which could further elucidate the complex NMR spectra. Due to the influence water has on the compounds synthesised, especially on the hydrolytically liable compounds **4-6** as revealed during HPLC purification, investigations into aqua species of the ruthenium half-sandwich complexes must be performed. These aqua species that may form during biological studies, may influence the efficacies and other pharmacokinetic properties.

The importance of the endoperoxide bridge in the artemisinin compounds synthesised (**1-6**) could be investigated by substituting the artemisinin moiety with a similar structure as seen in **Figure 4.1** below. This could elucidate how different organometallic moieties or ligands influence biological activities.

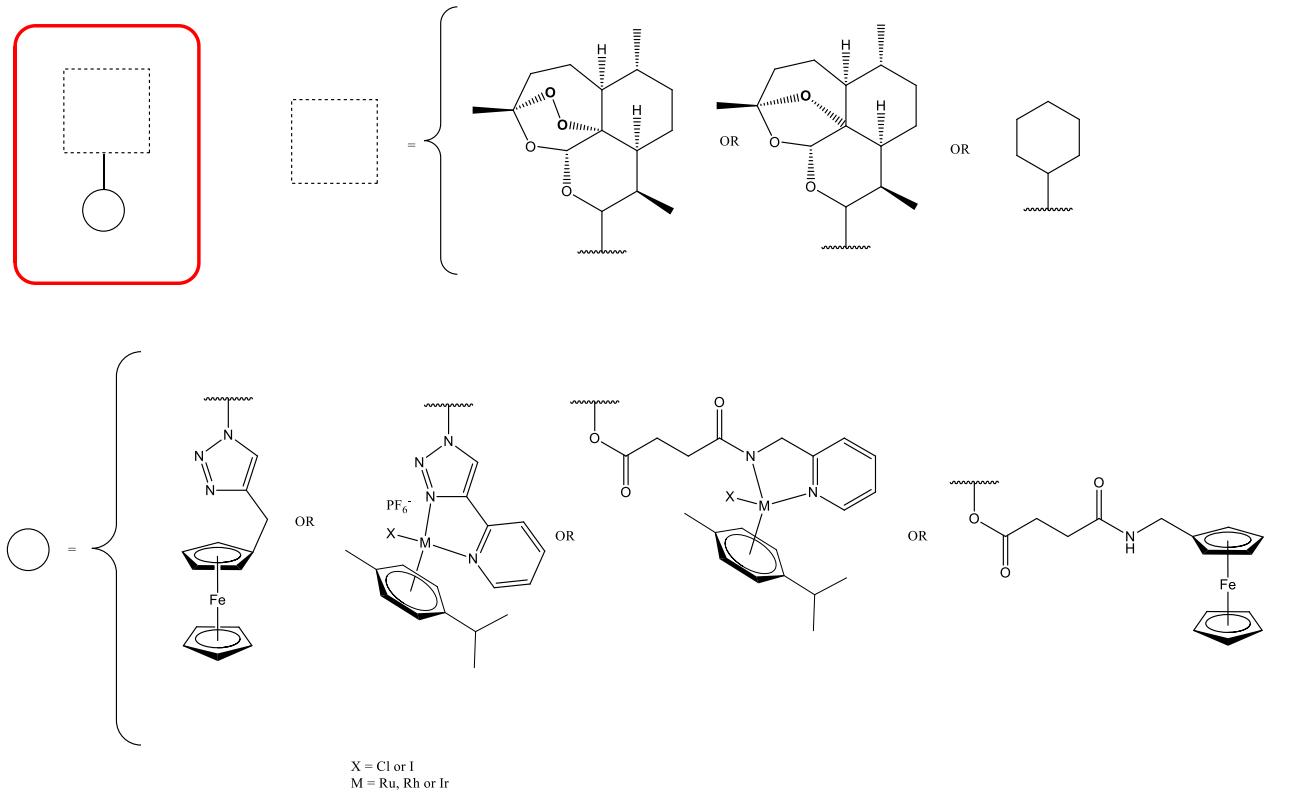

Figure 4.1. Proposed structures to test importance of organometallic moieties.

Artemisinin's mode of action could also be investigated performing specialised assays that could test for the production of ROS species, and further elucidate whether artemisinin has a detrimental effect on the glutathione redox pathway – the major anti-oxidant defence for *P. falciparum*. Proteomic studies could also be performed to identify specific bio-molecules the artemisinin derivatives might bind covalently or non-covalently to. Furthermore, cyclic voltammetry can also be performed to identify the oxidation states of the ruthenium or iron or other transition metals in the organometallic moiety, to elucidate with further research how the oxidation state of said organometallic moieties could influence properties such as biological activities.

Further investigations into antibacterial activity could stem new possible artemisinin drugs, able to have a broad spectrum. These compounds could also be screened against cancer cell lines and other microbial borne diseases.

Finally, due to the increasing evidence from biological studies, more artesunate derivatives and relatable C-10 derivatives could be synthesised (**Figure 4.2**), as studies suggested that the bioavailability or stability of the C-10 artemisinin compounds significantly differs with the chemical group attached to it. In this respect, acetal vs. non-acetal C-10 derivatives could be synthesised to compare their respective pharmacological properties.

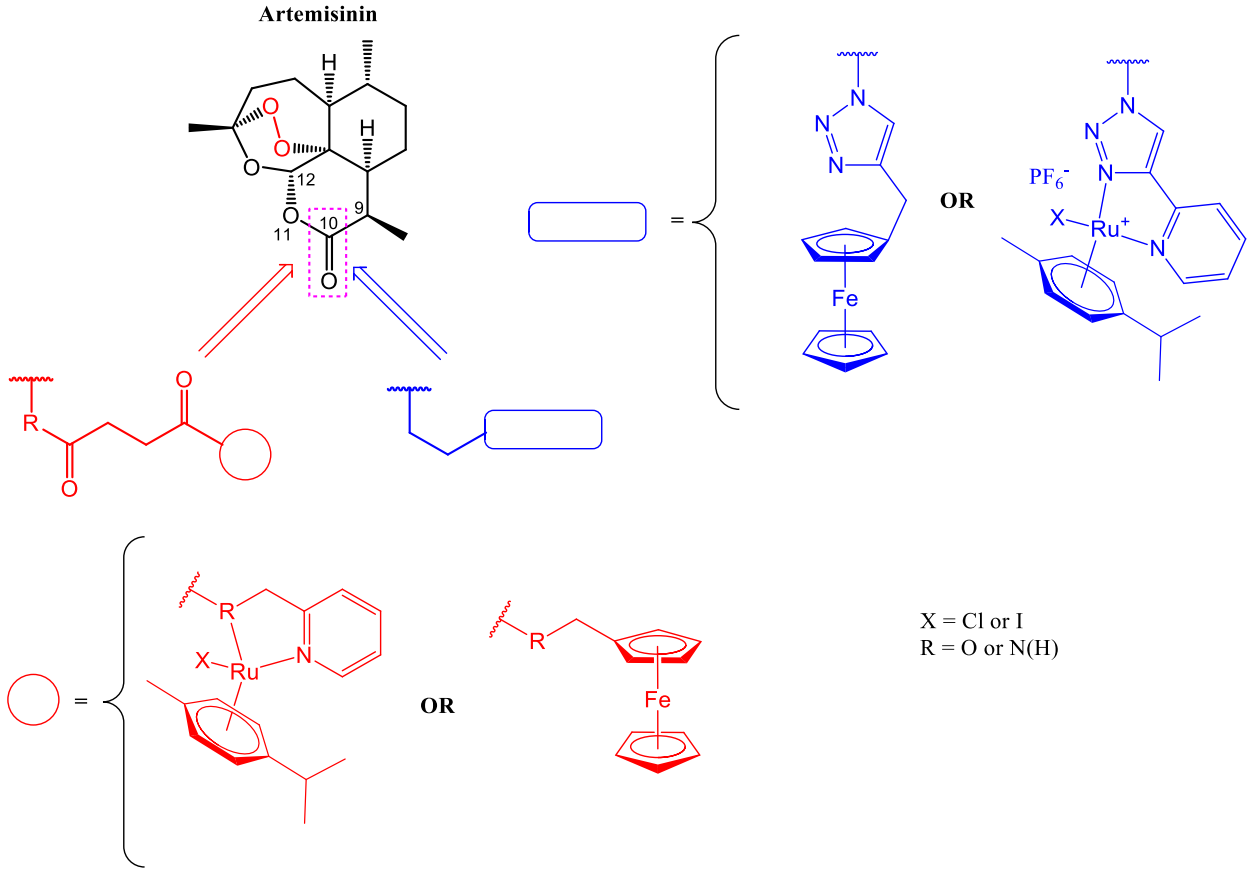

Figure 4.2. Proposed future artemisinin derivatives**.**

Appendix

1. Intermediate 1 (DHA):

IR

ATR-KBr window

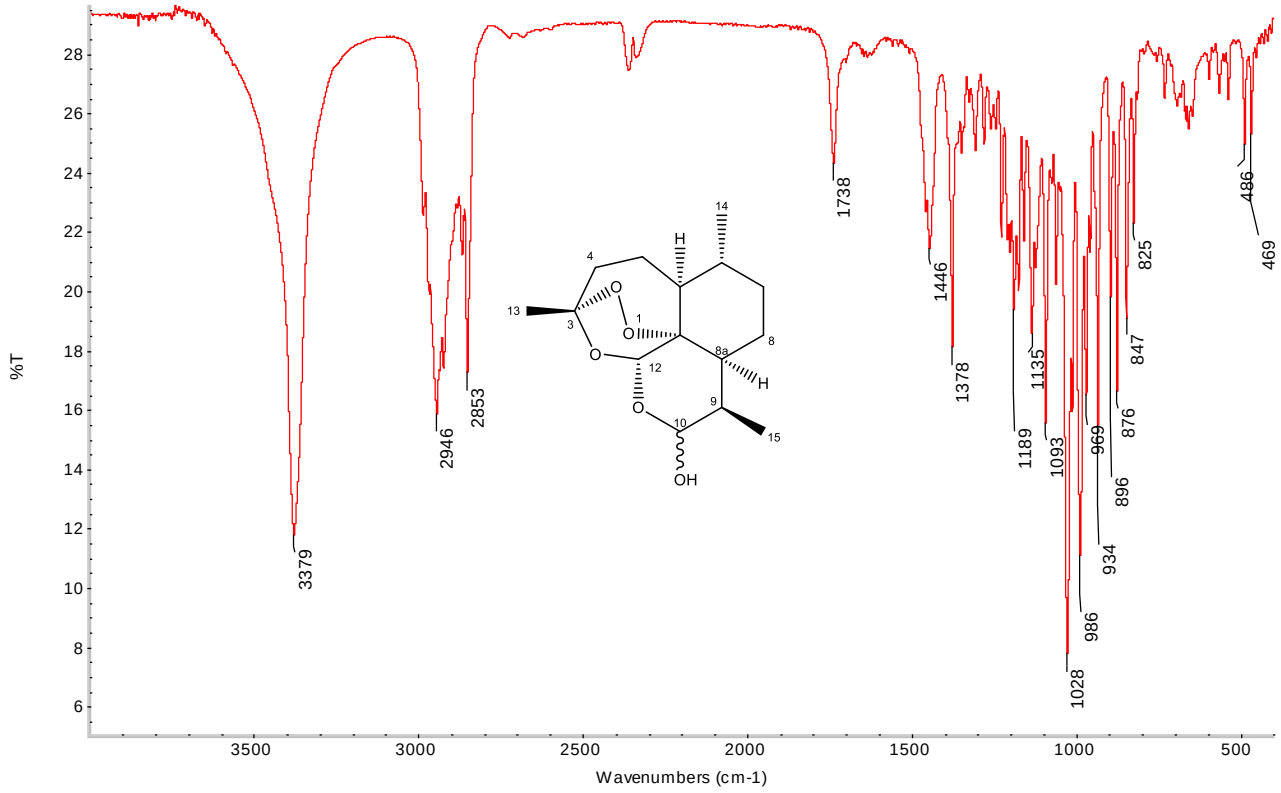

^{1}H-NMR:

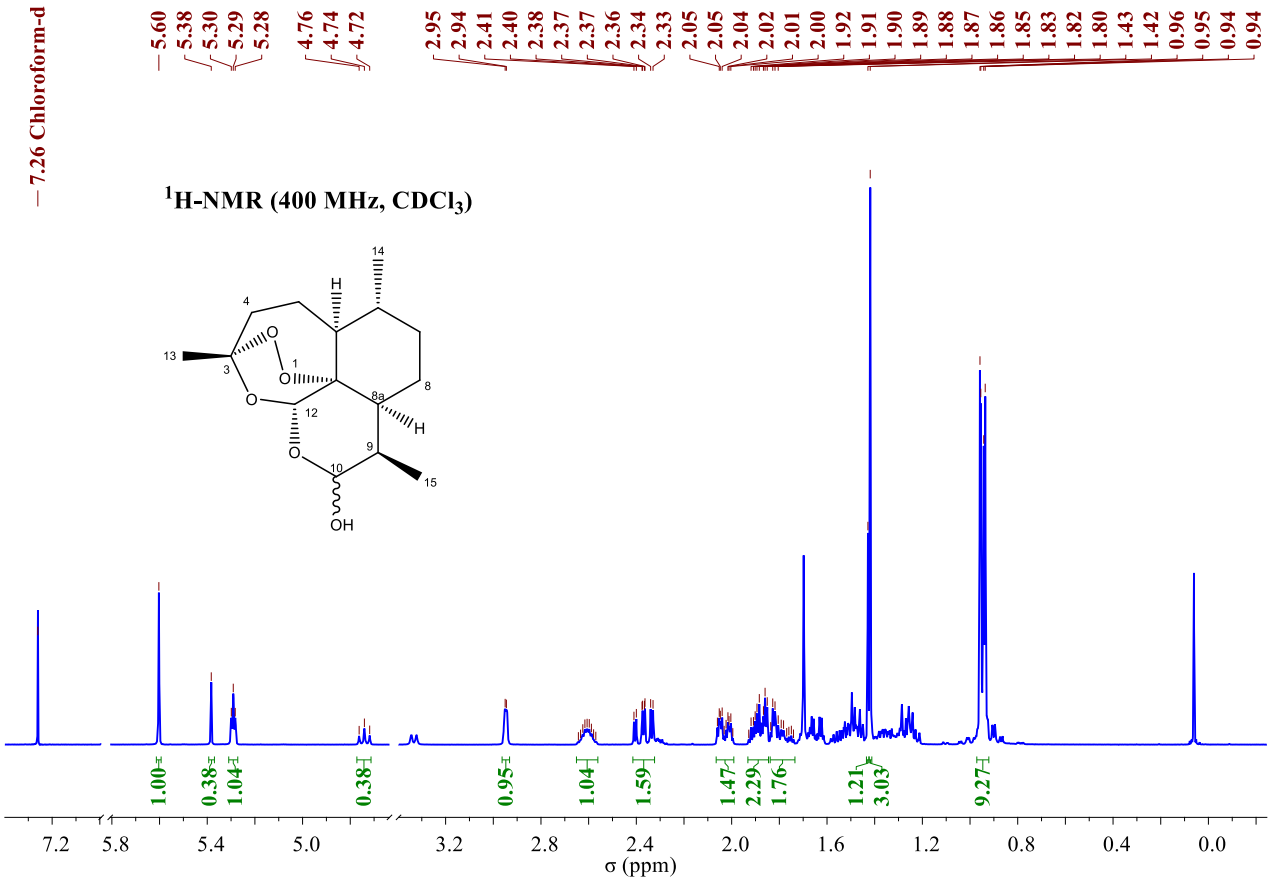

2. Intermediate 2 (ART-N_3):

IR

ATR-KBr window

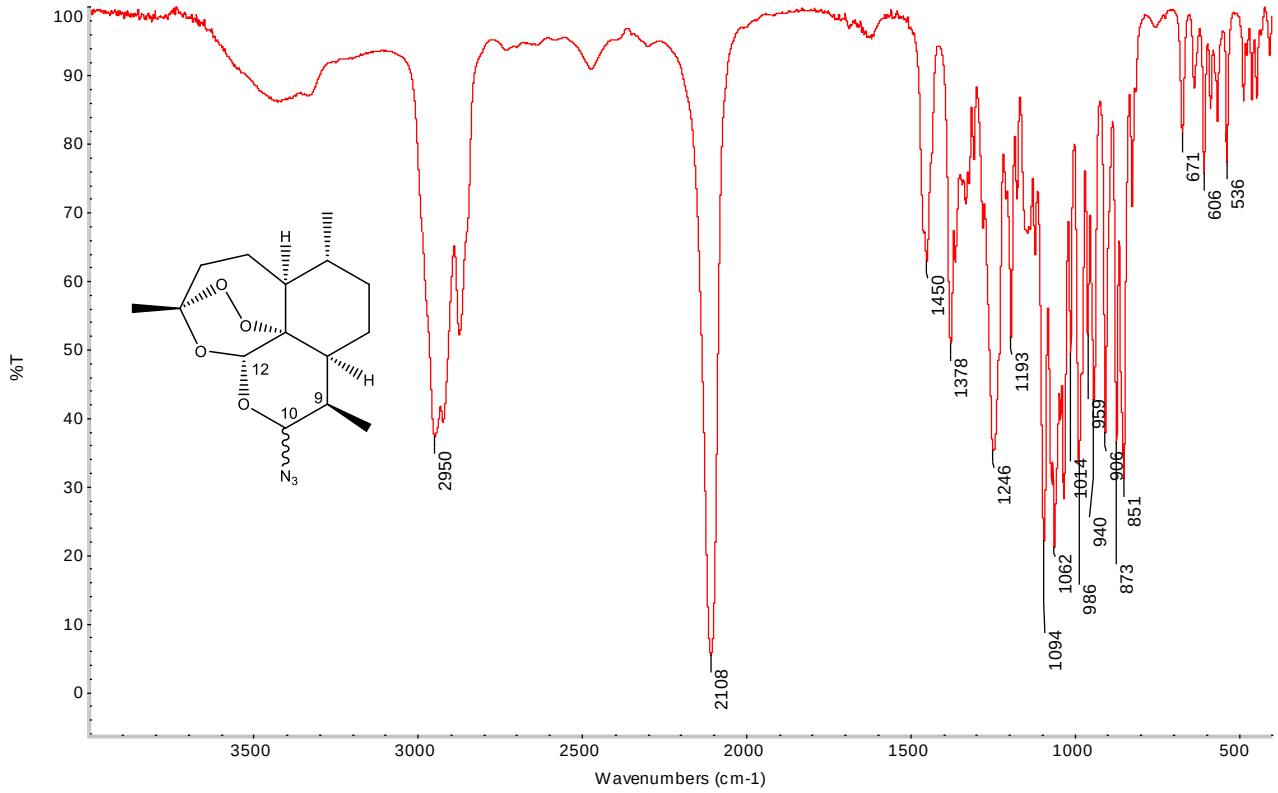

^{1}H-NMR:

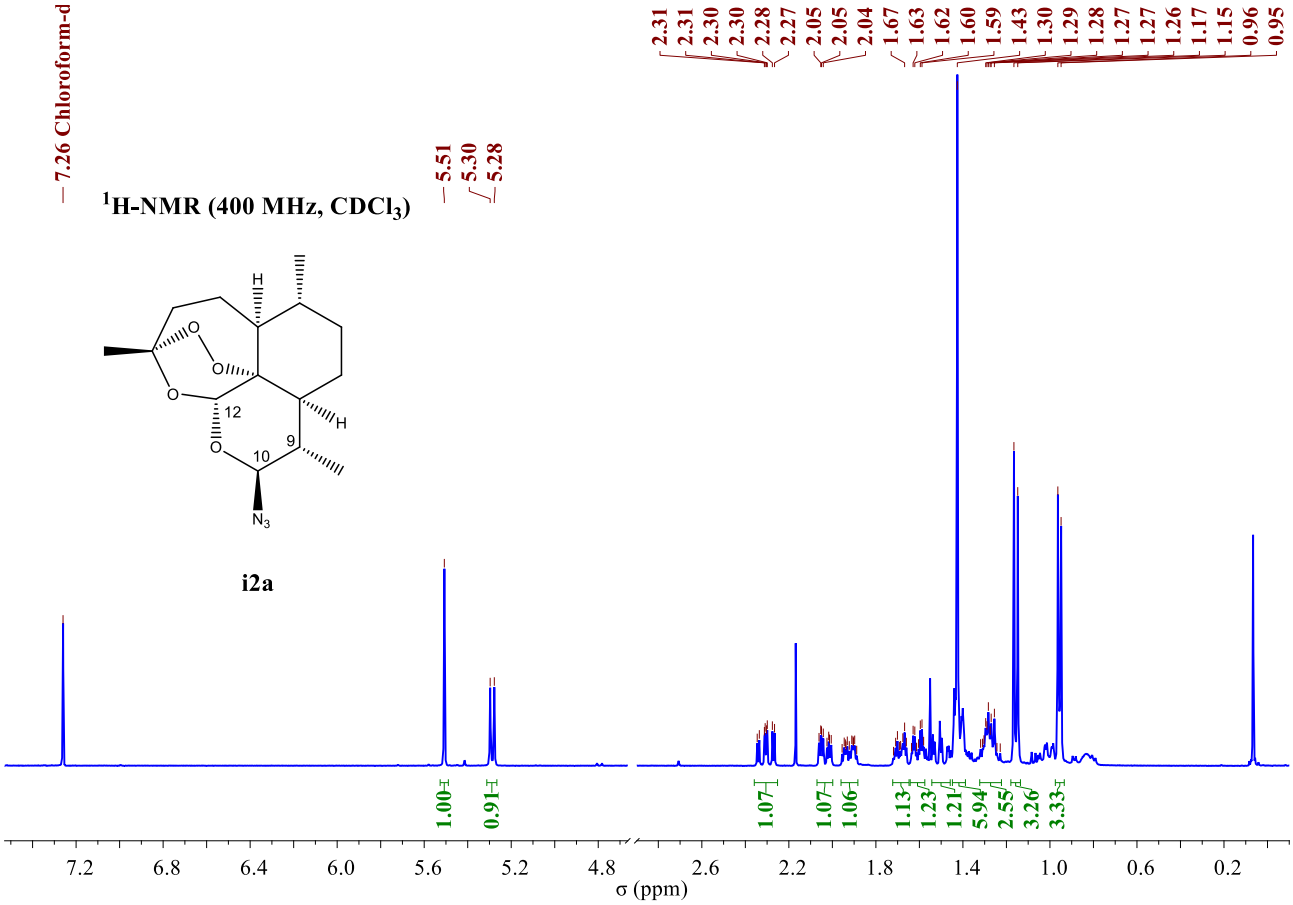

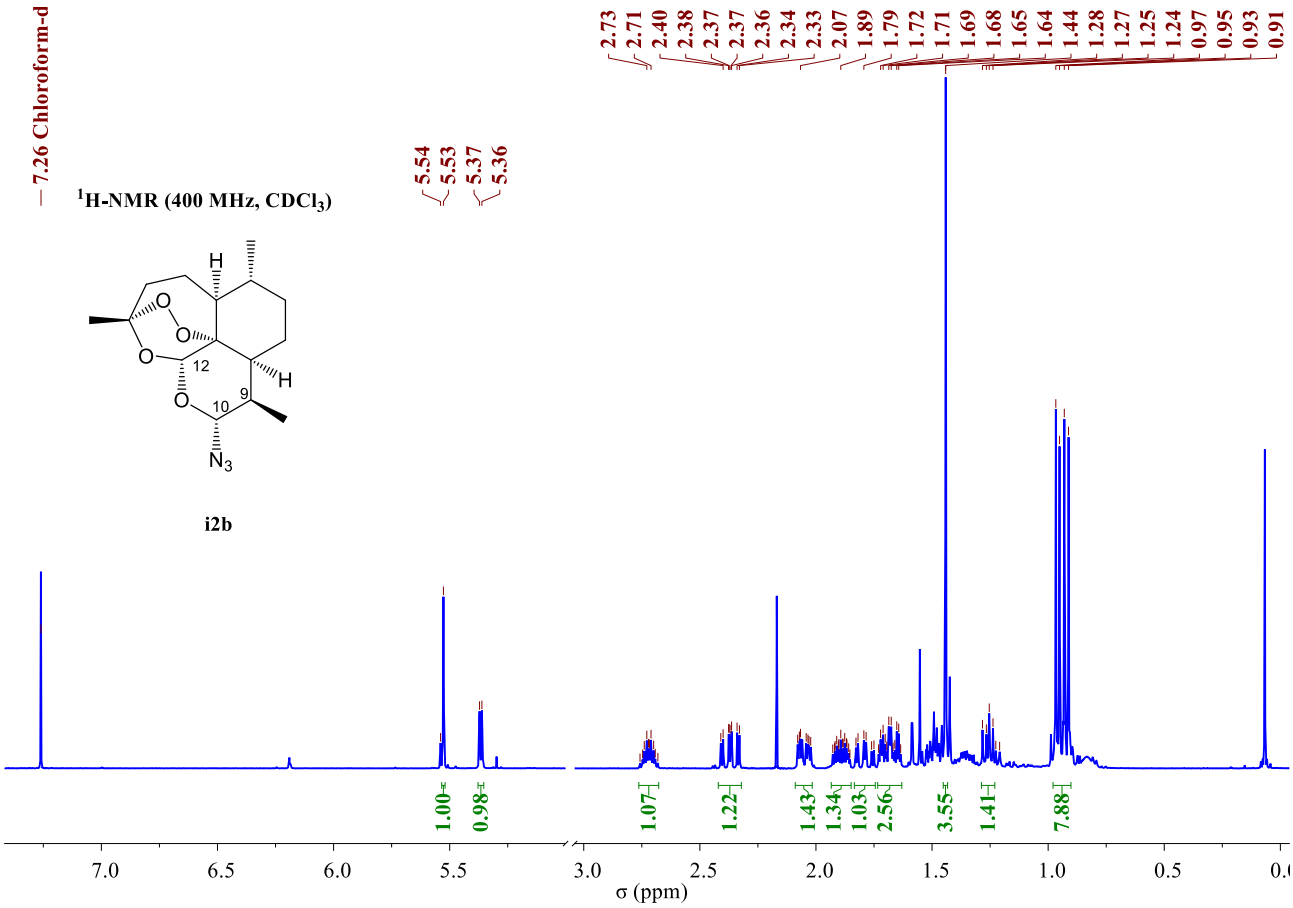

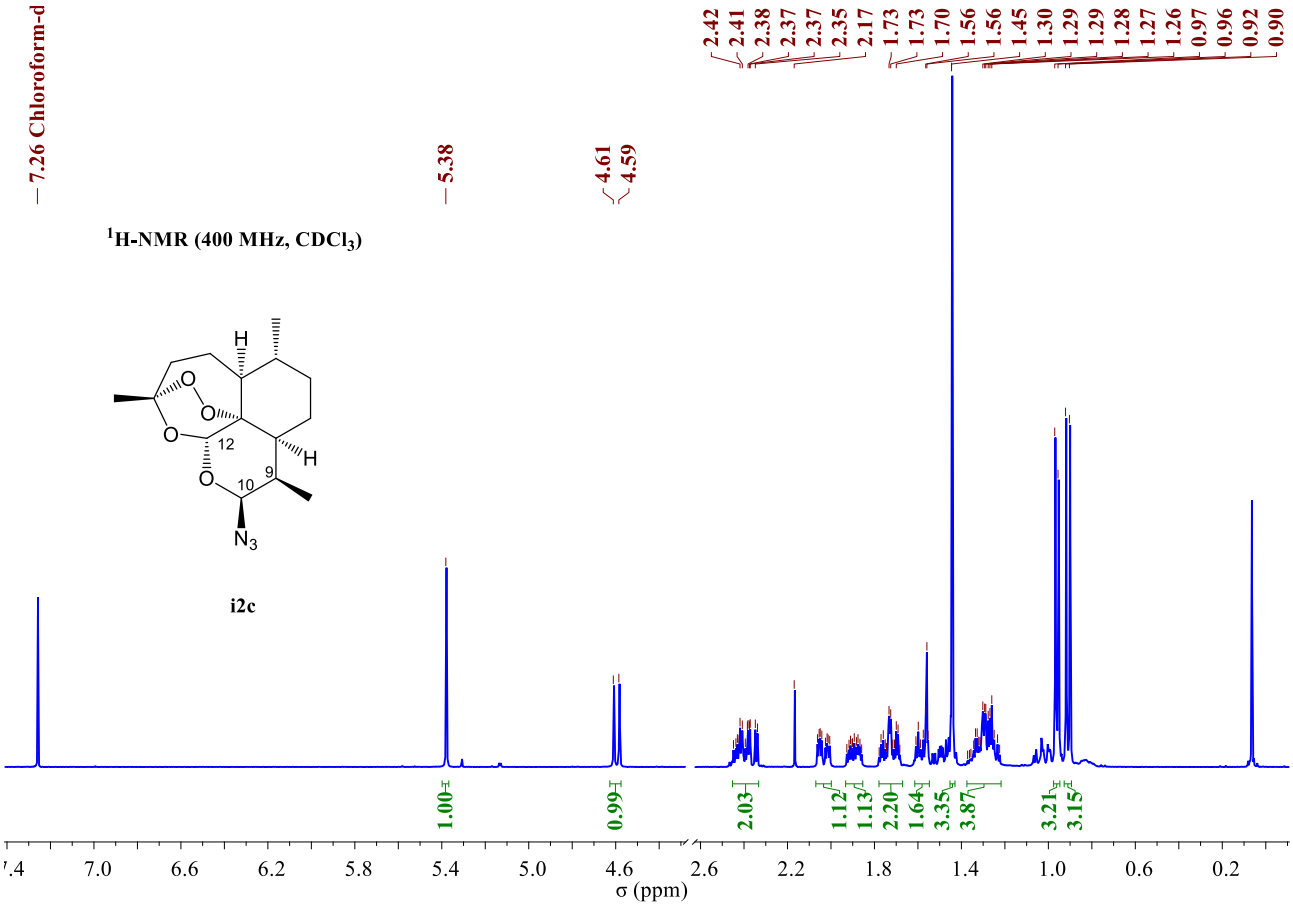

3. Intermediate 3:

IR

ATR-KBr window

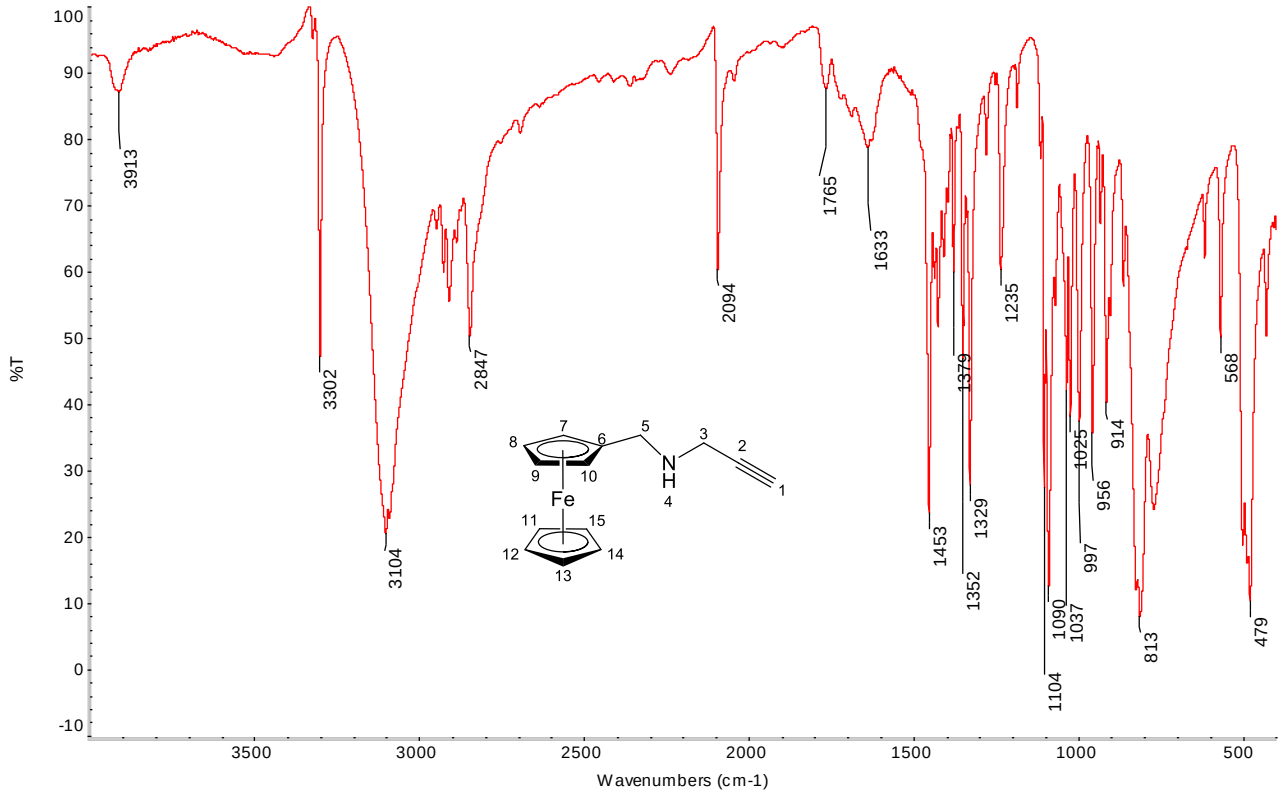

^{1}H-NMR:

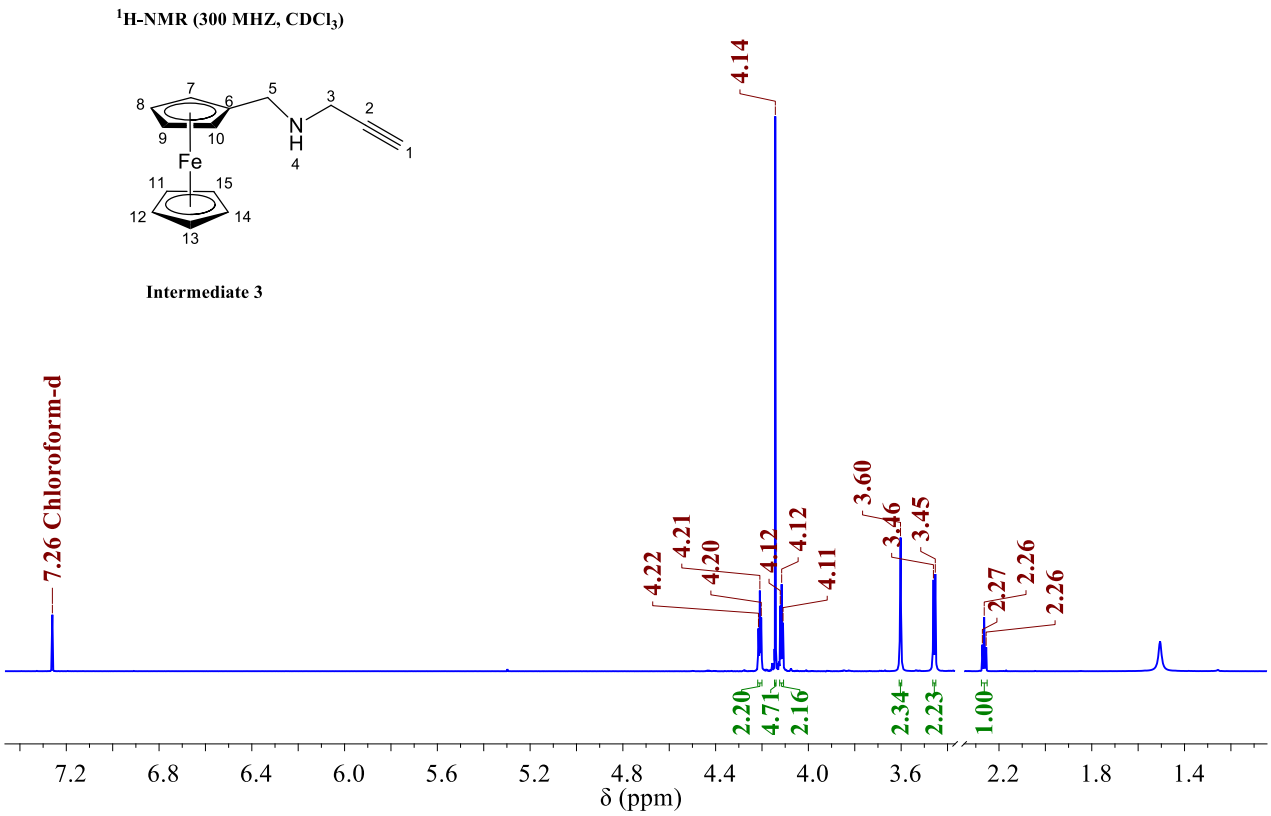

$^{13}C\{^1H\}$-NMR

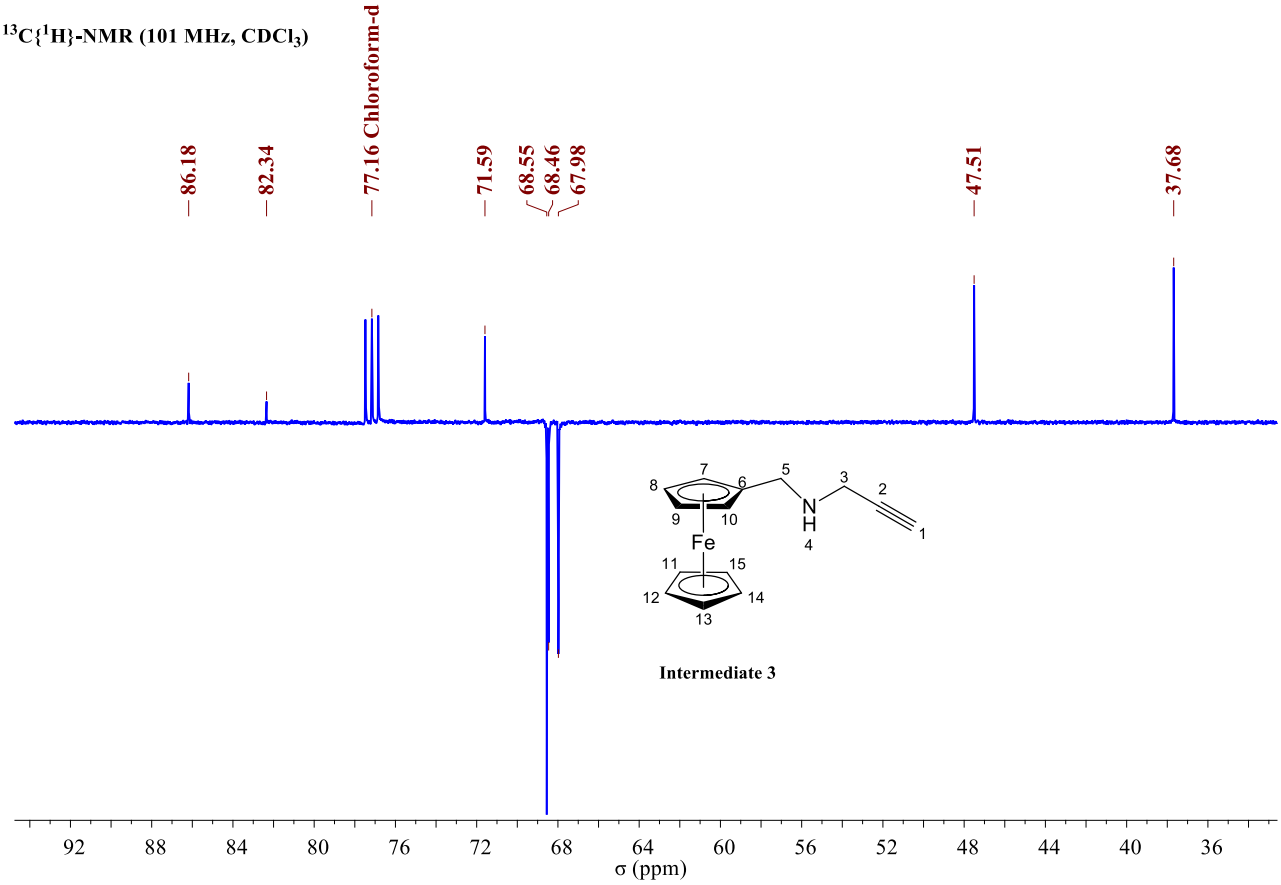

4. Intermediate 4 (ARS):

IR

ATR-KBr window

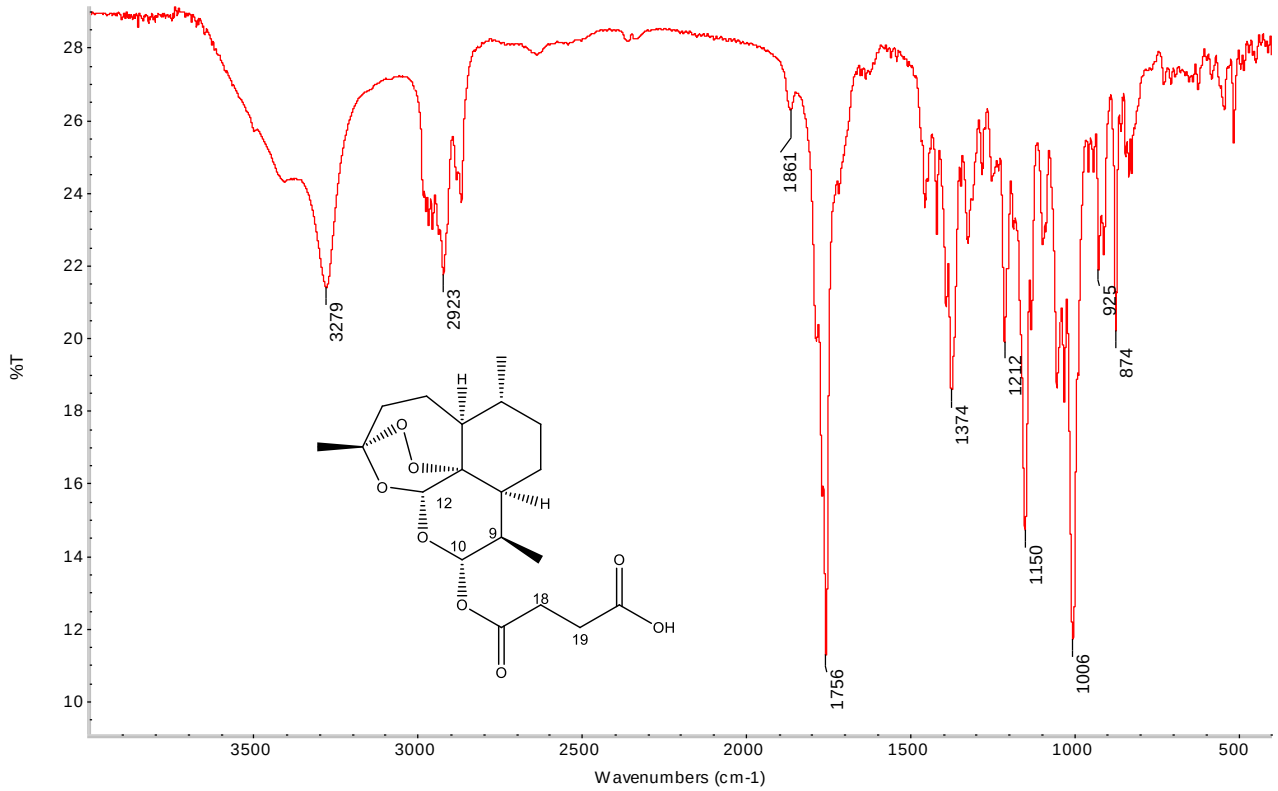

^{1}H-NMR:

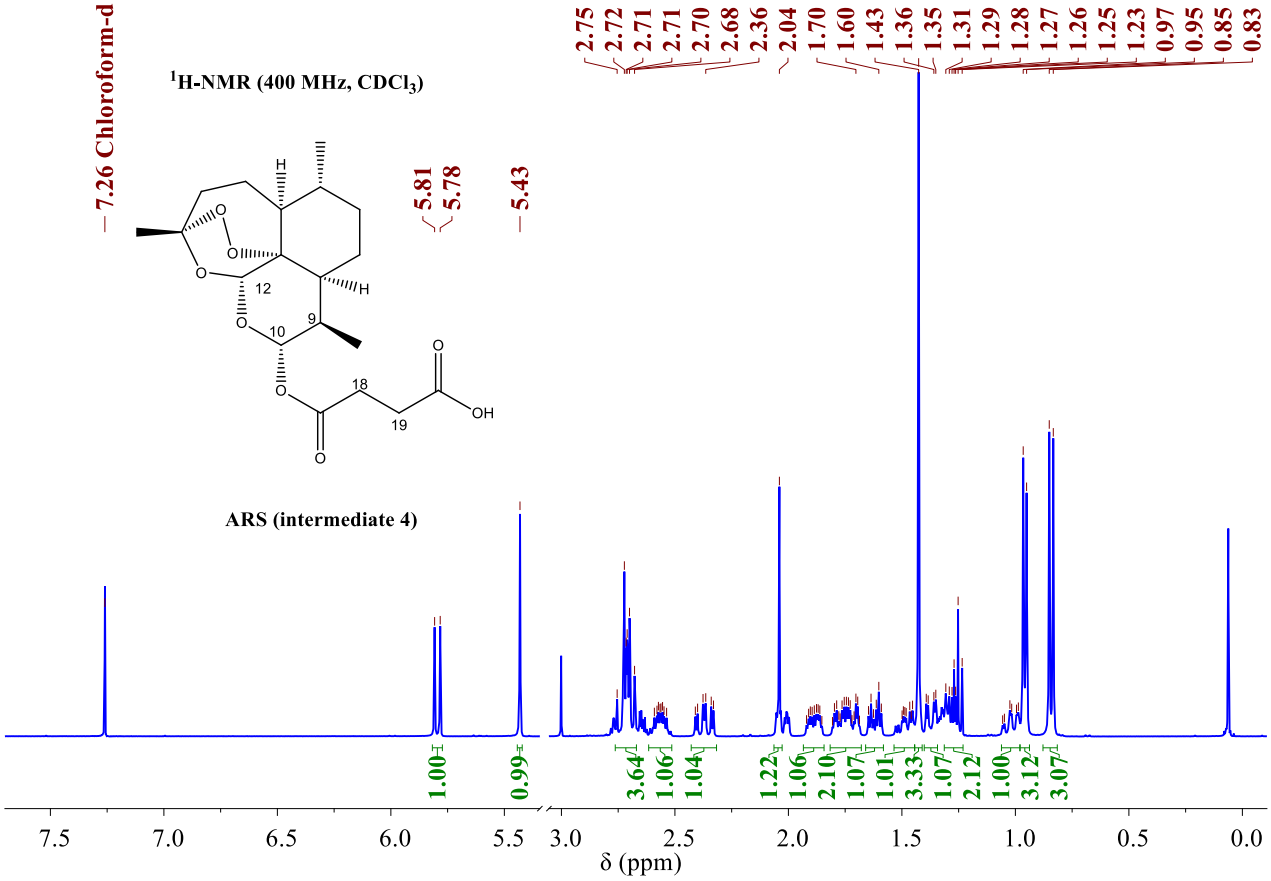

5. Intermediate 5:

IR

ATR-KBr window oxime:

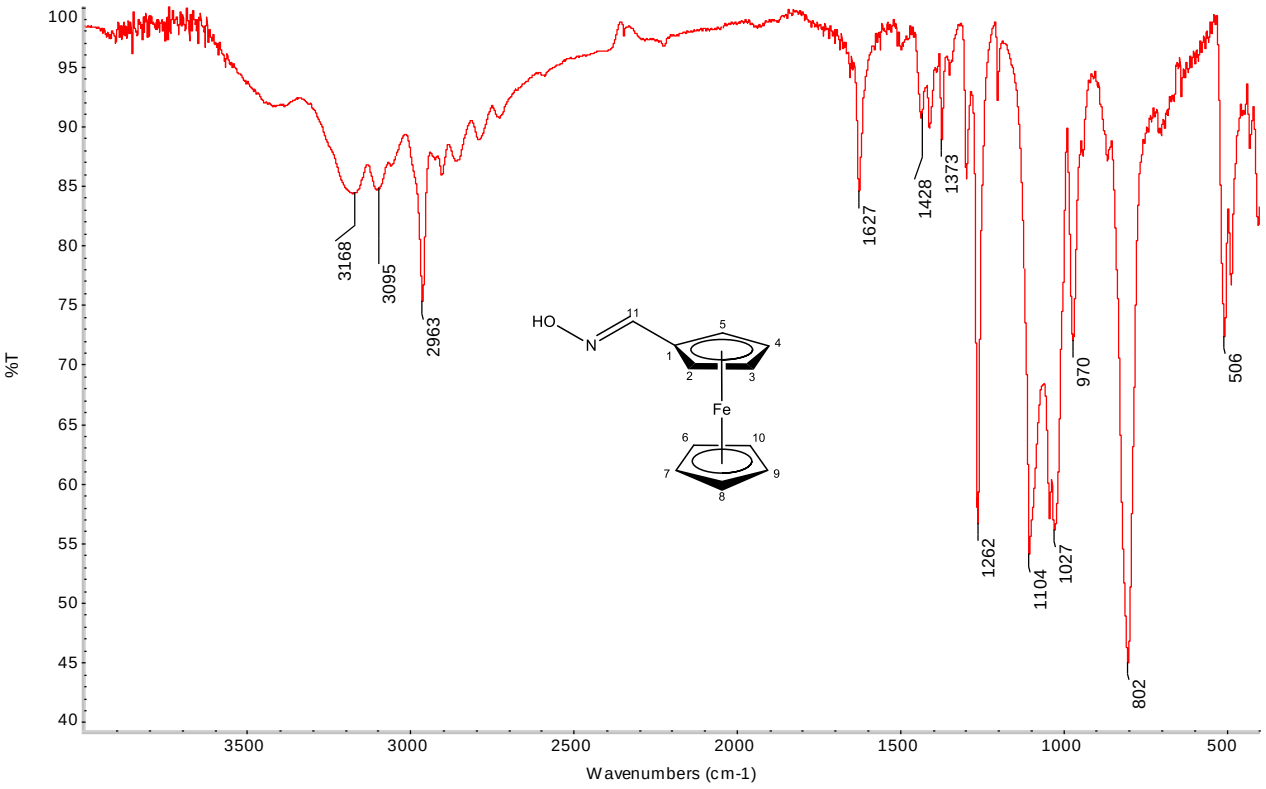

ATR-ATR window of amine:

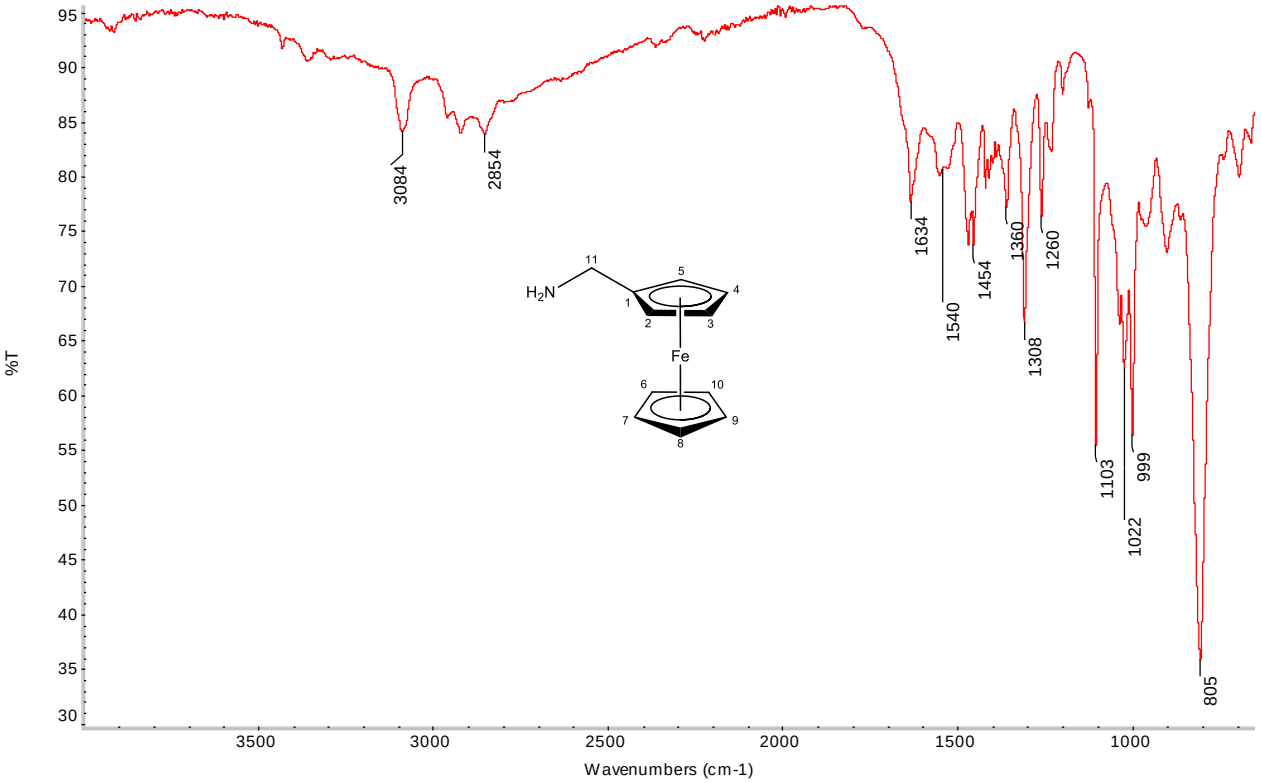

^{1}H-NMR:

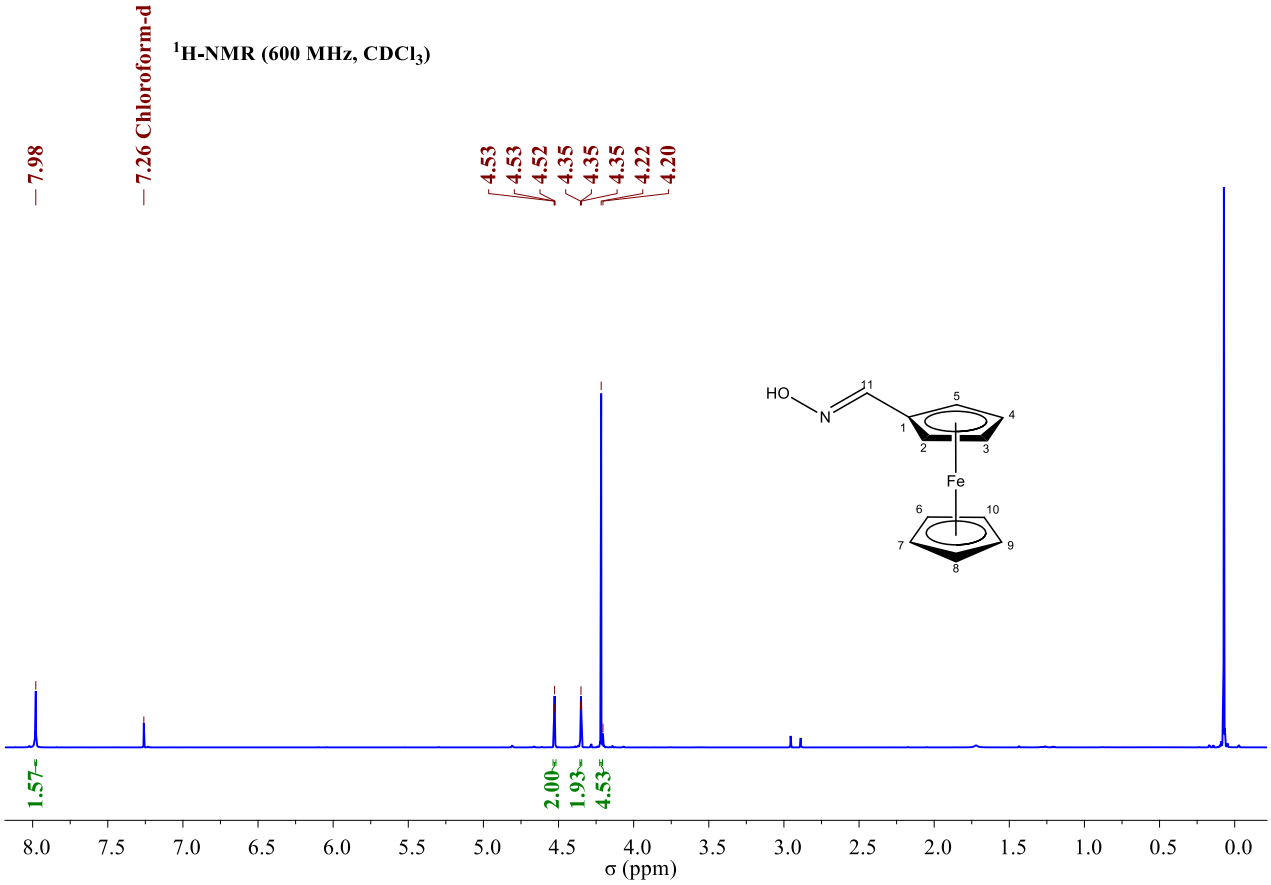

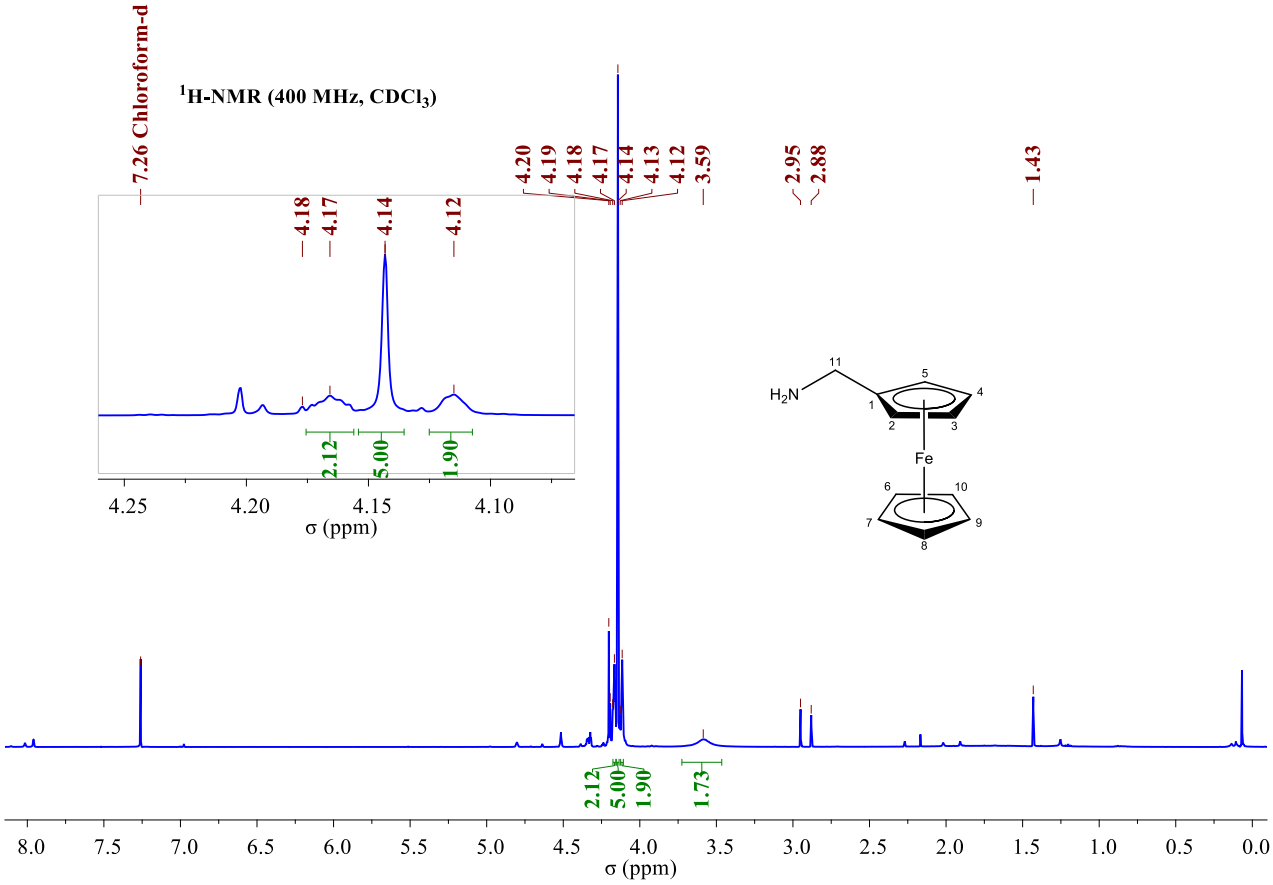

6. Compound 1:

IR

ATR-KBr window

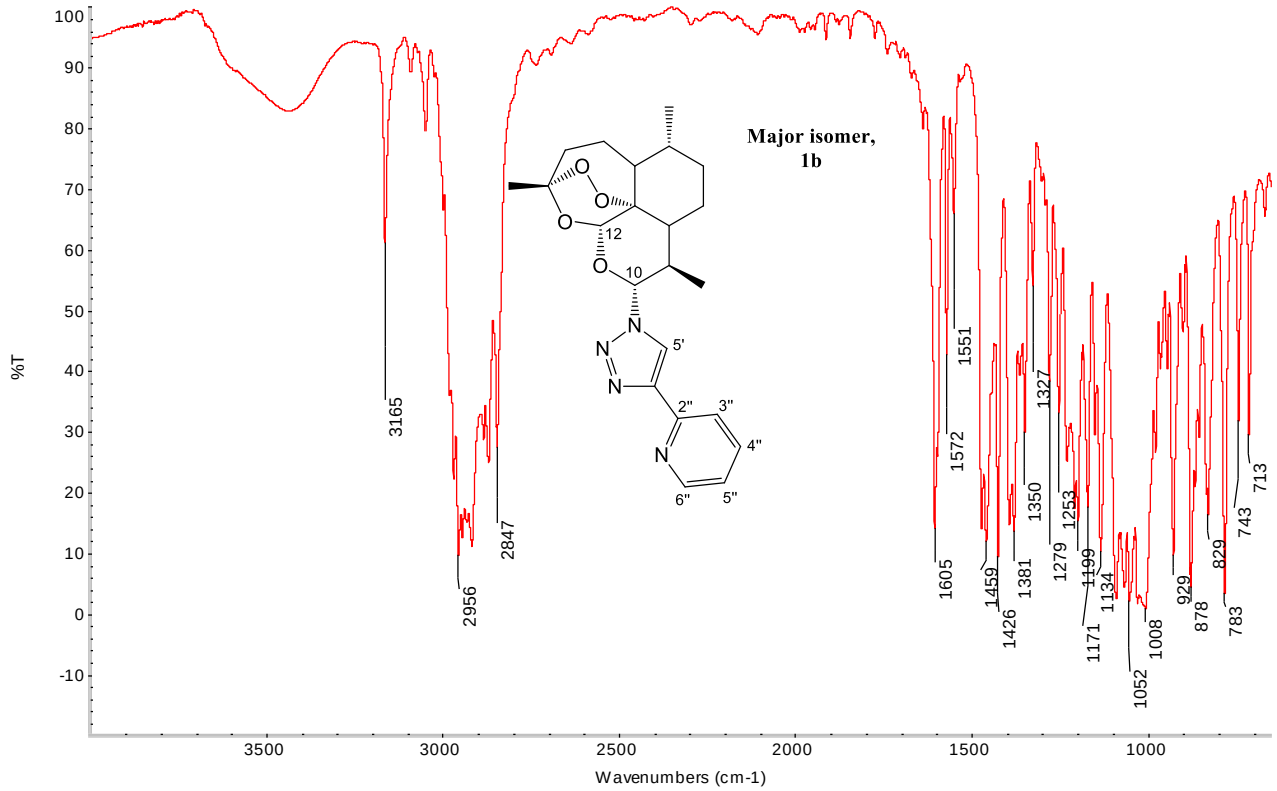

[1]H-NMR:

[1]H-NMR (400 MHz, $CDCl_3$)

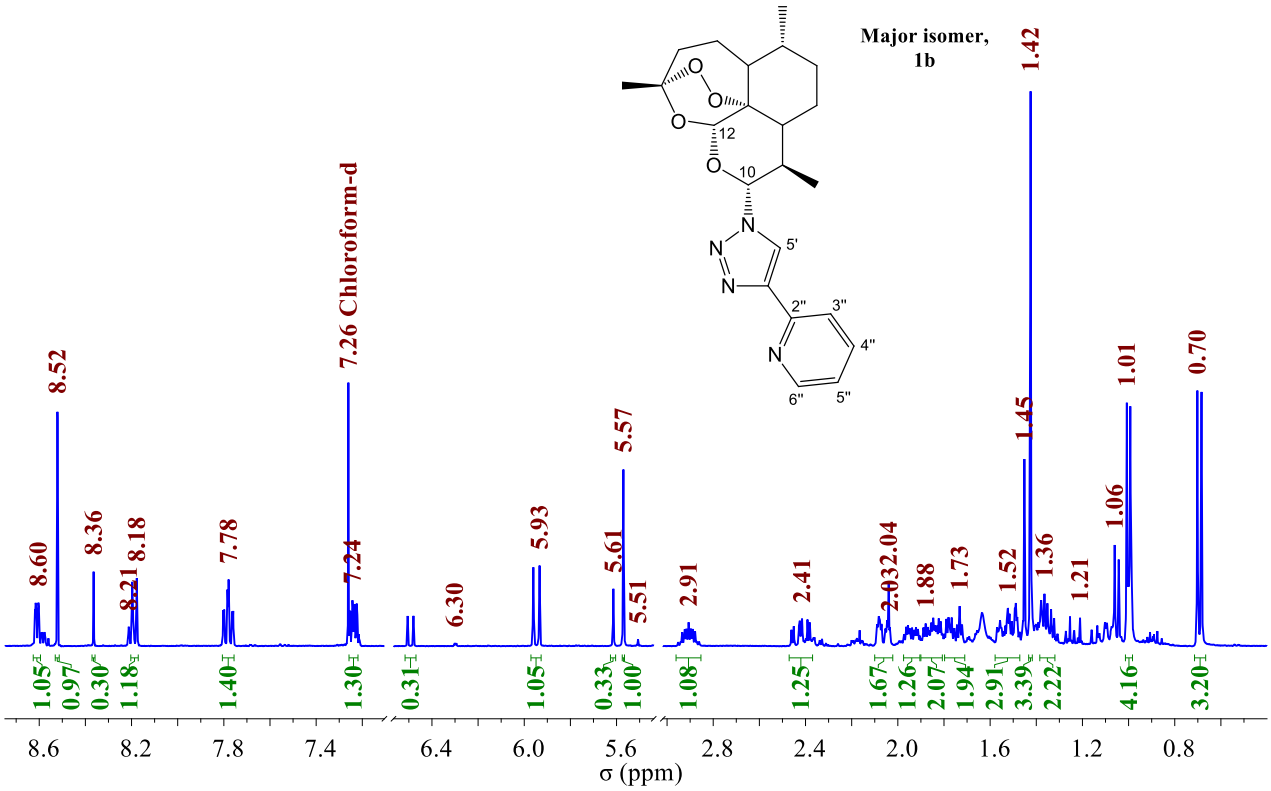

$^{13}C\{^{1}H\}$-NMR

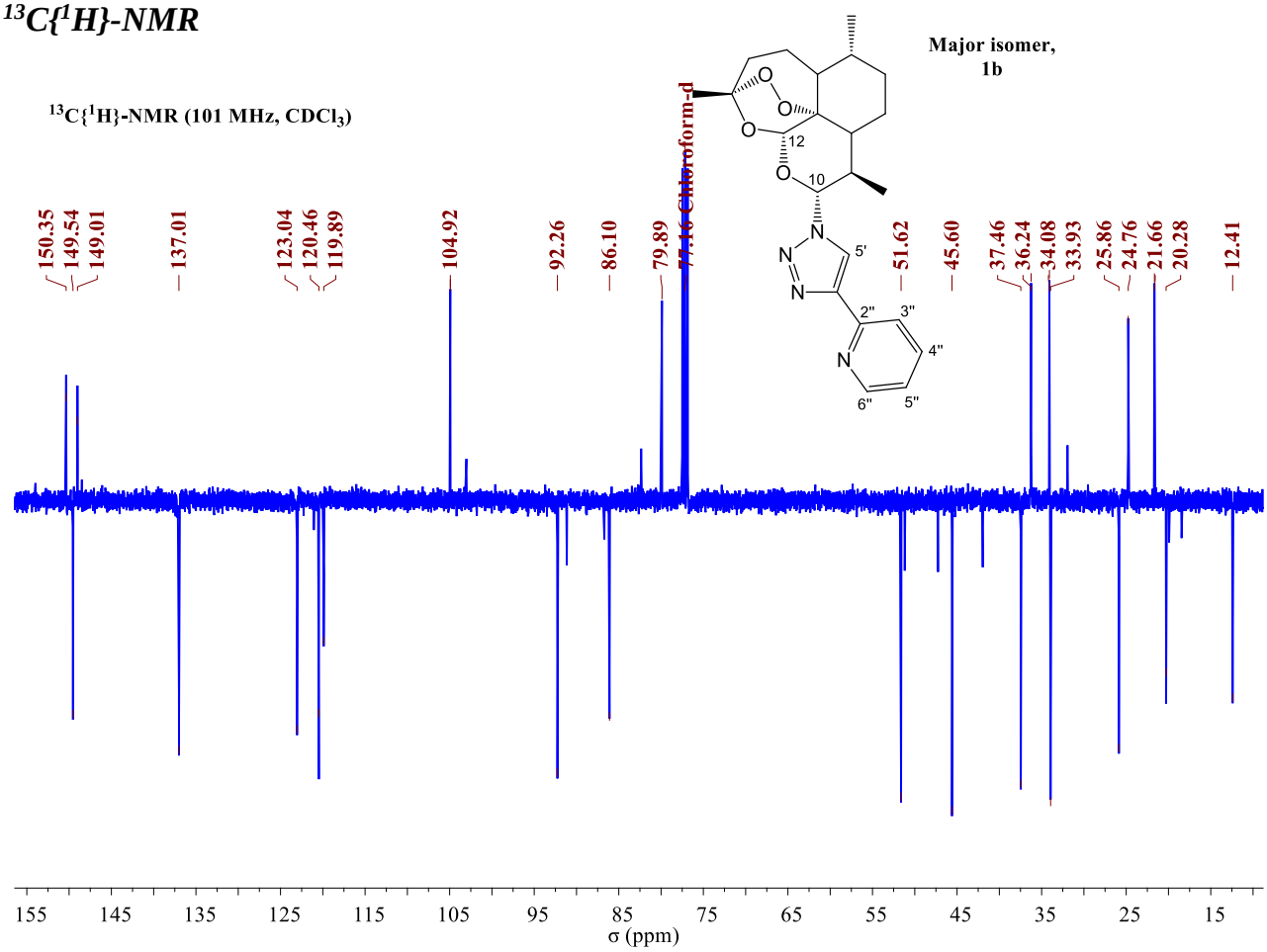

7. Compound 2a:

IR

ATR-ZnSe

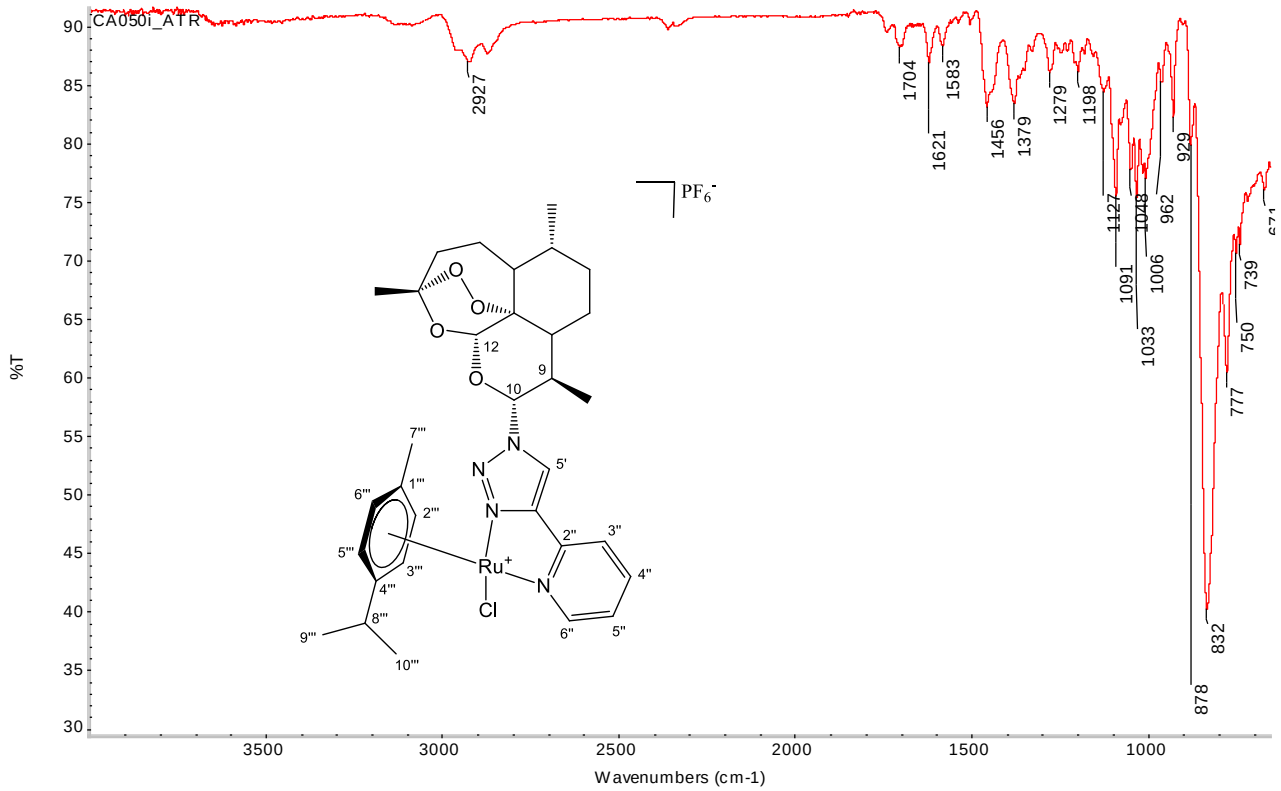

^{1}H-NMR:

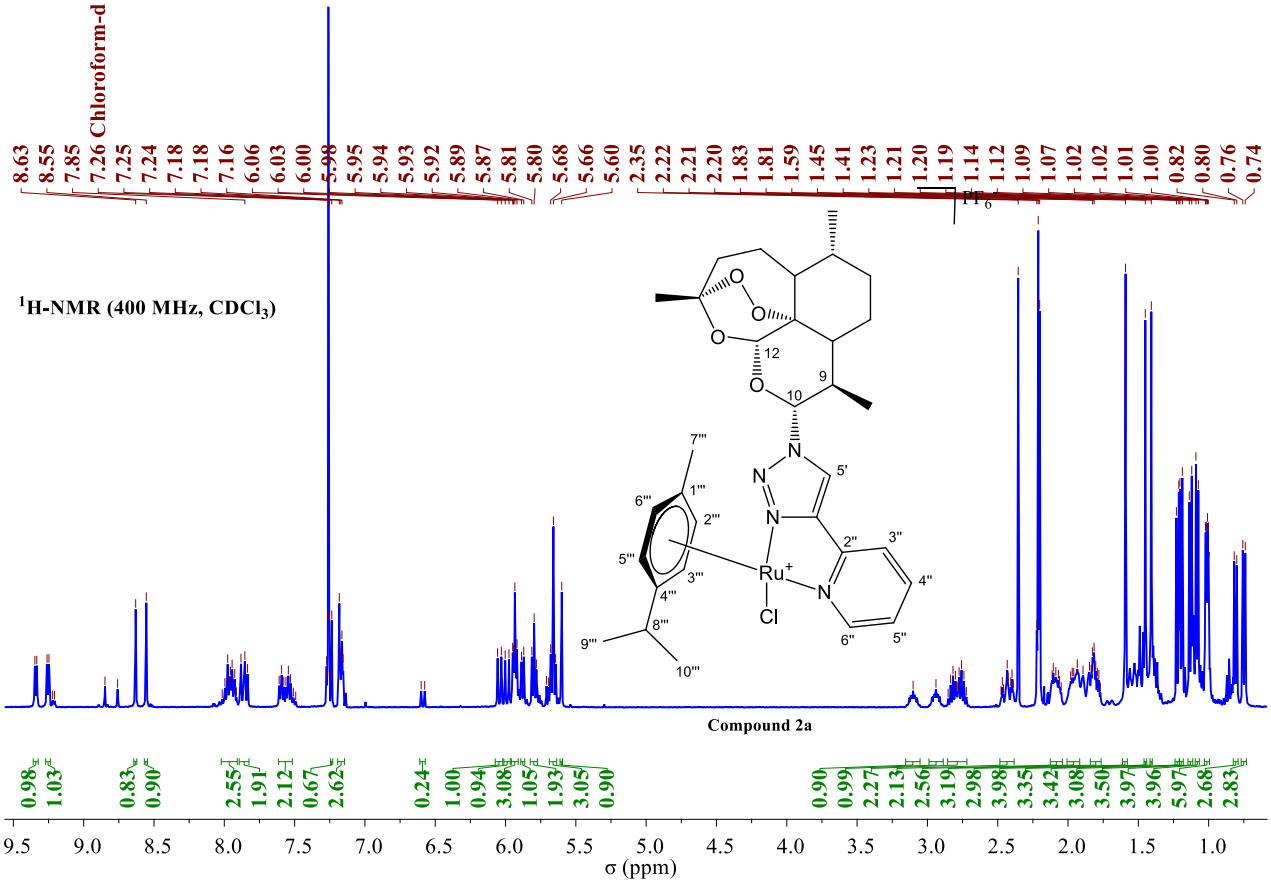

13C{1H}-NMR

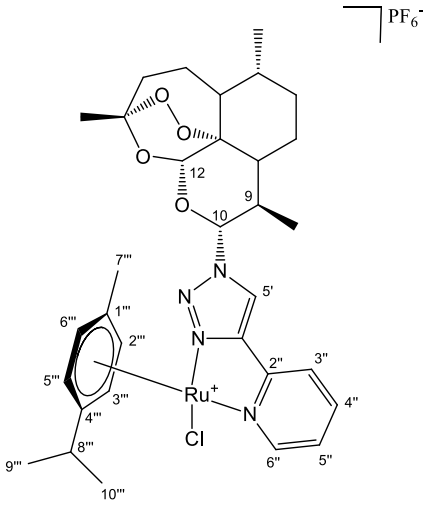

Compound 2a

$^{13}C\{^{1}H\}$-NMR (101 MHz, $CDCl_3$)

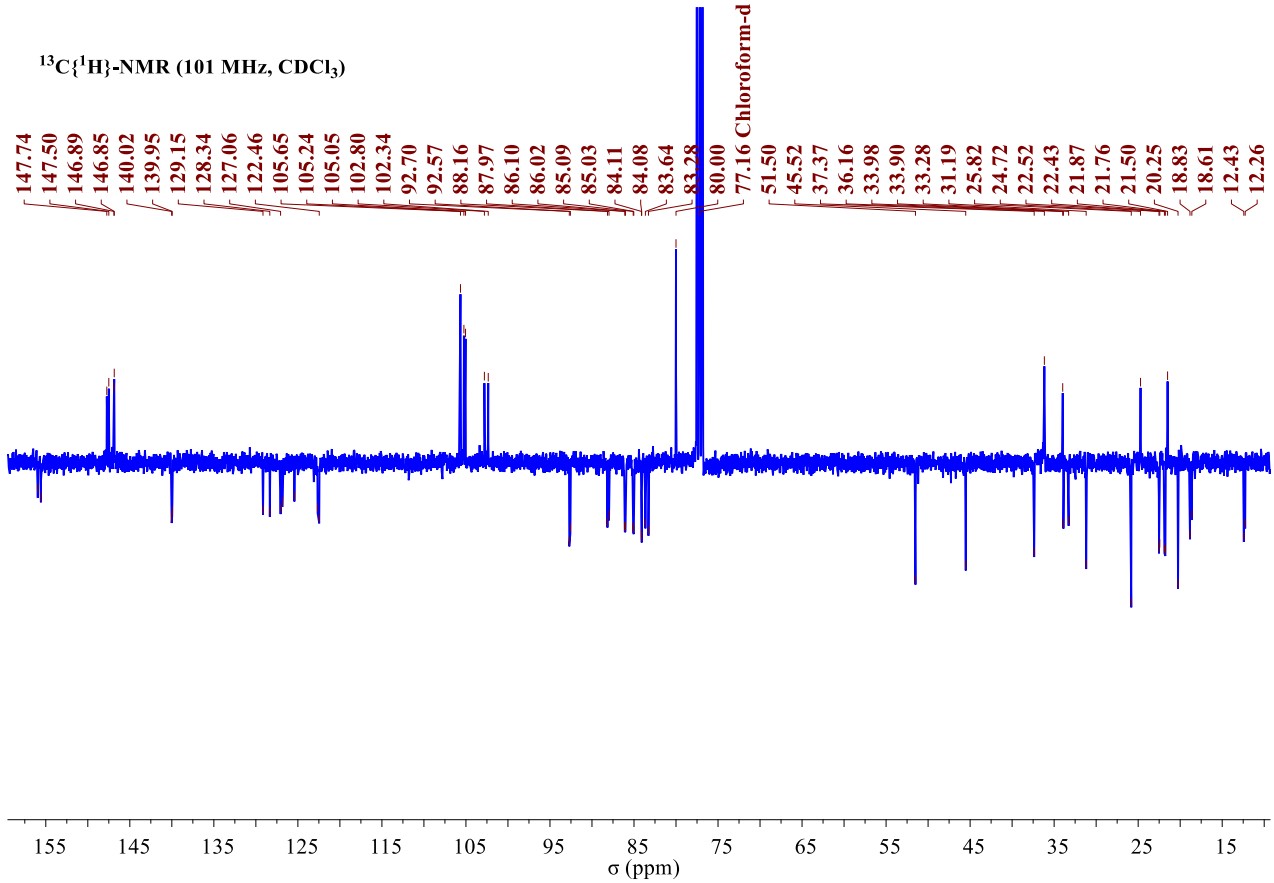

8. Compound 2b:

IR

ATR-ZnSe

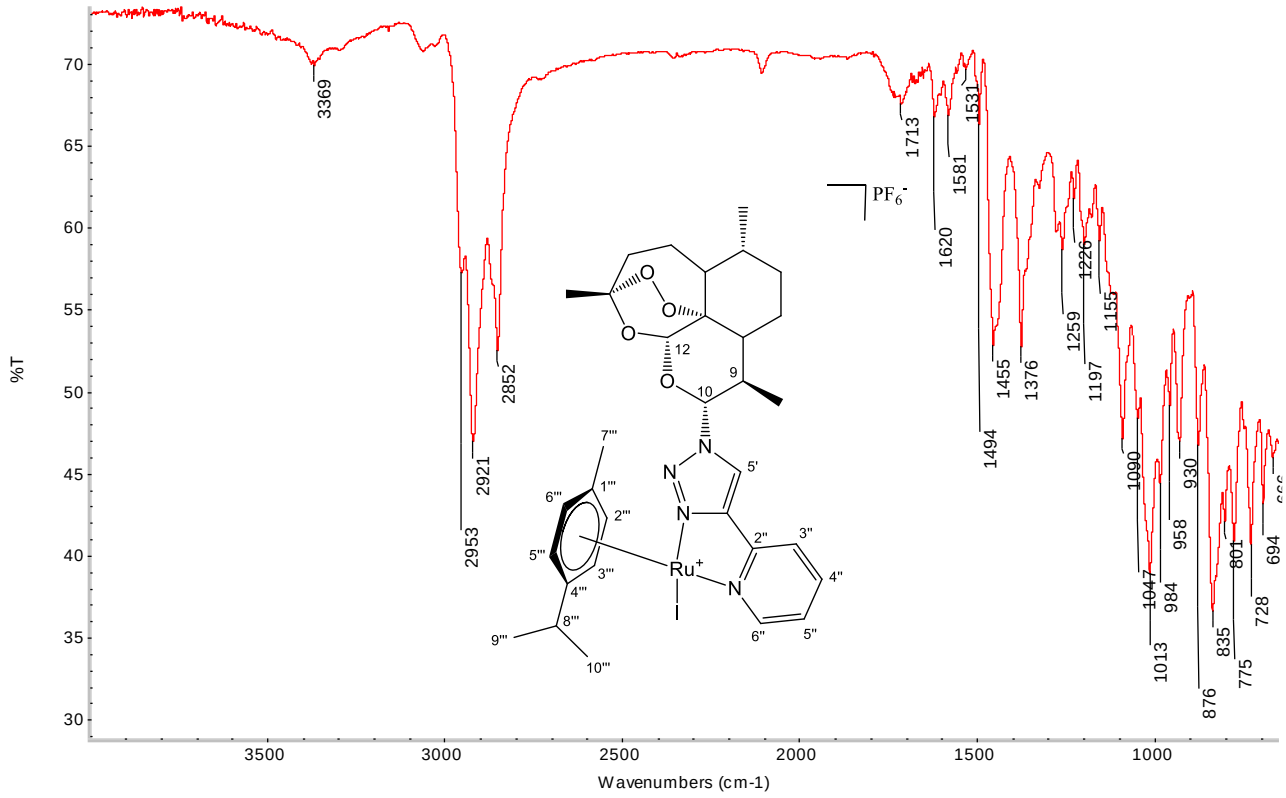

^{1}H-NMR:

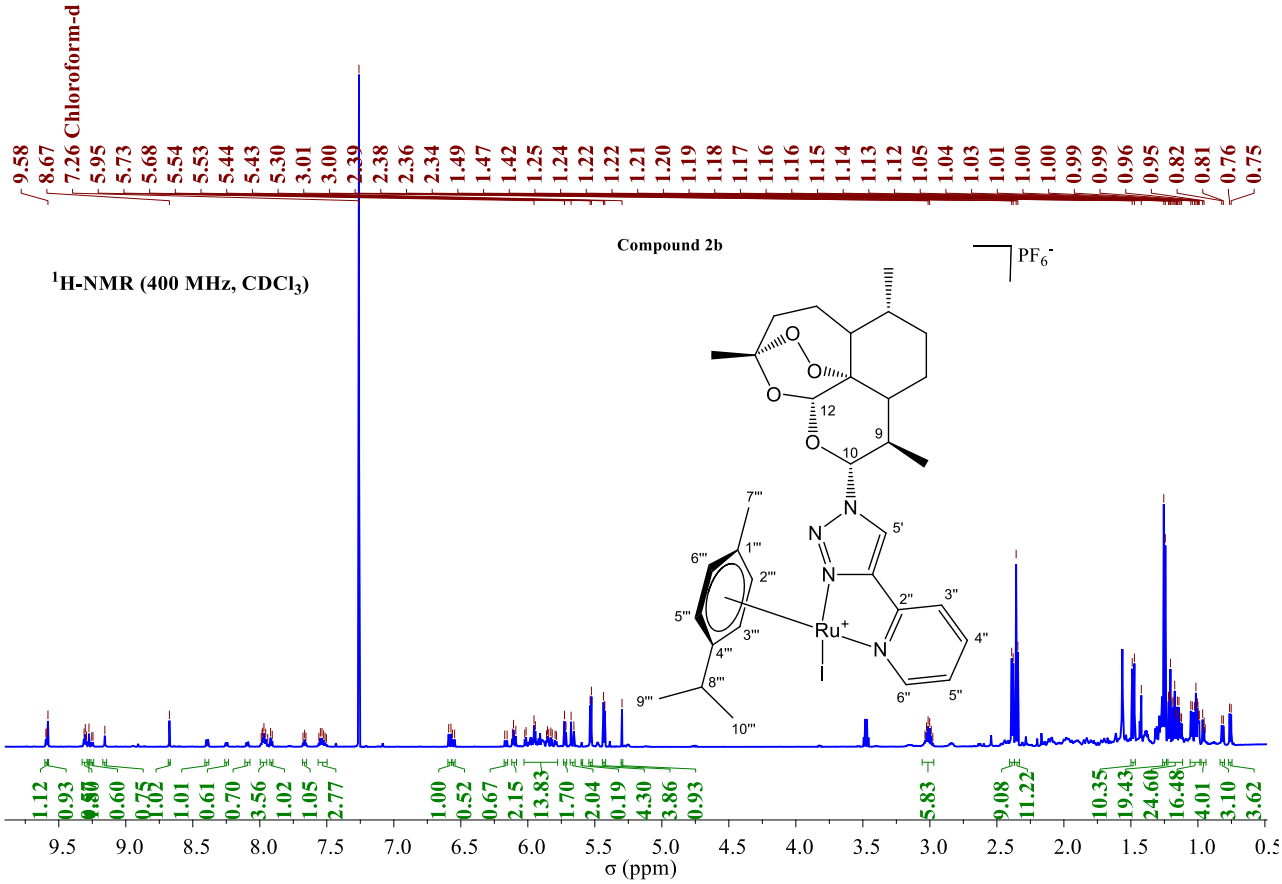

9. Compound 3:

IR

ATR-KBr window

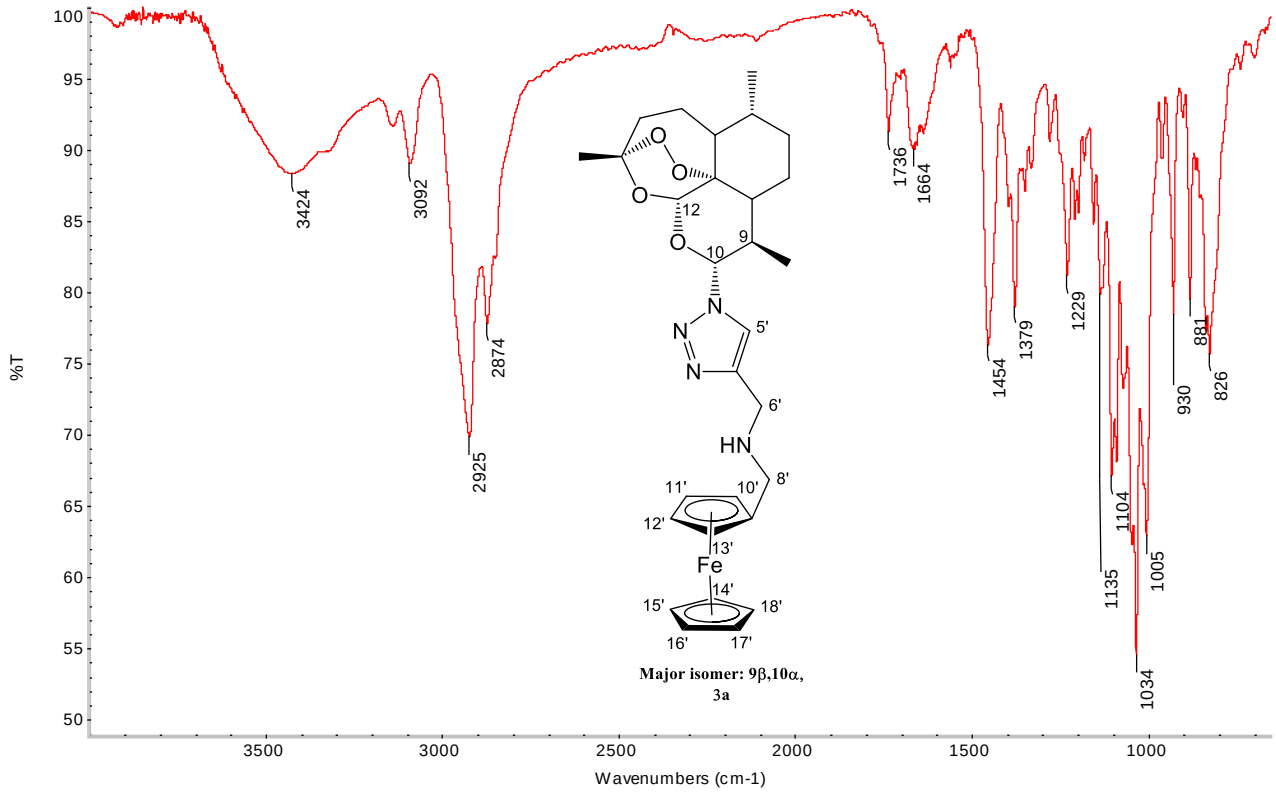

^{1}H-NMR:

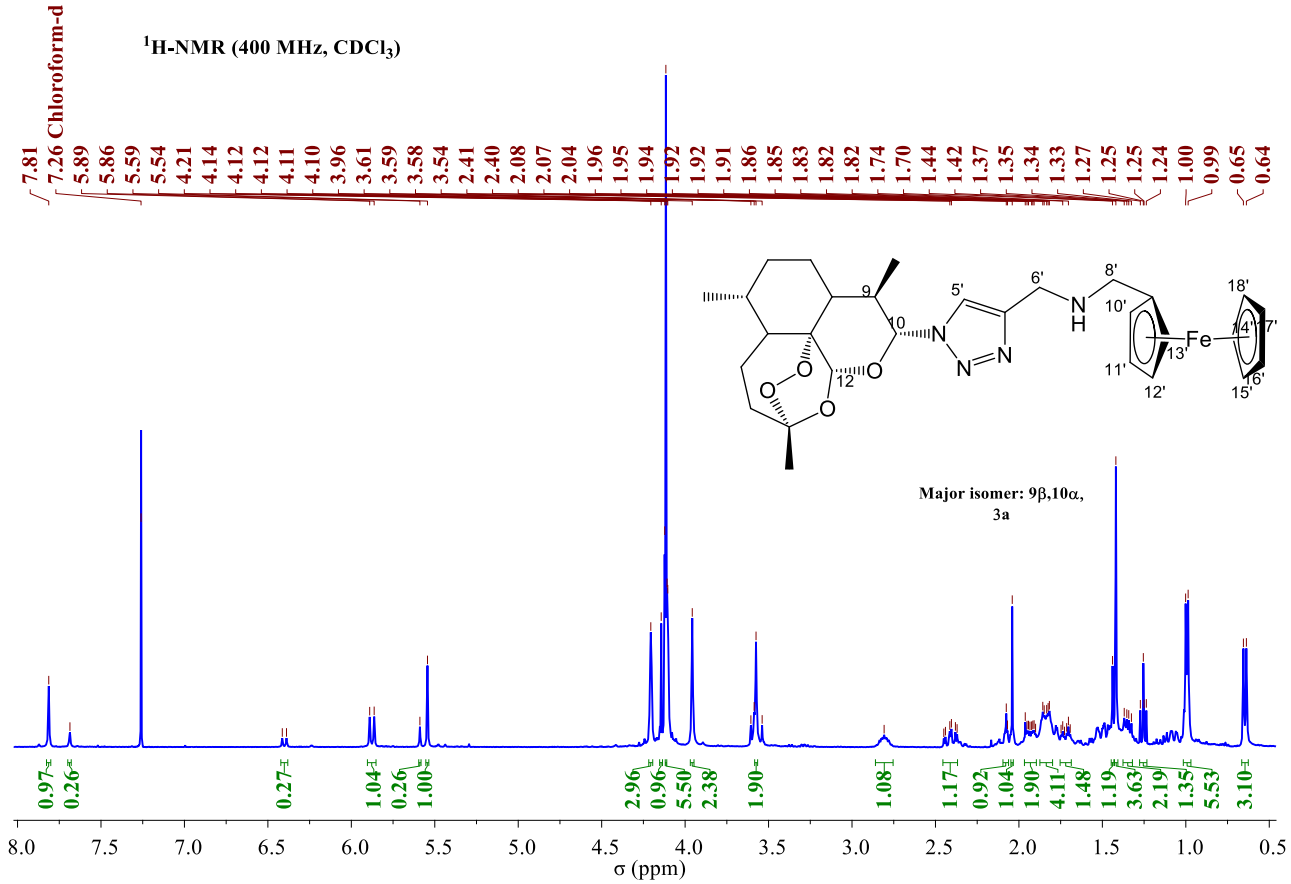

$^{13}C\{^{1}H\}$-NMR

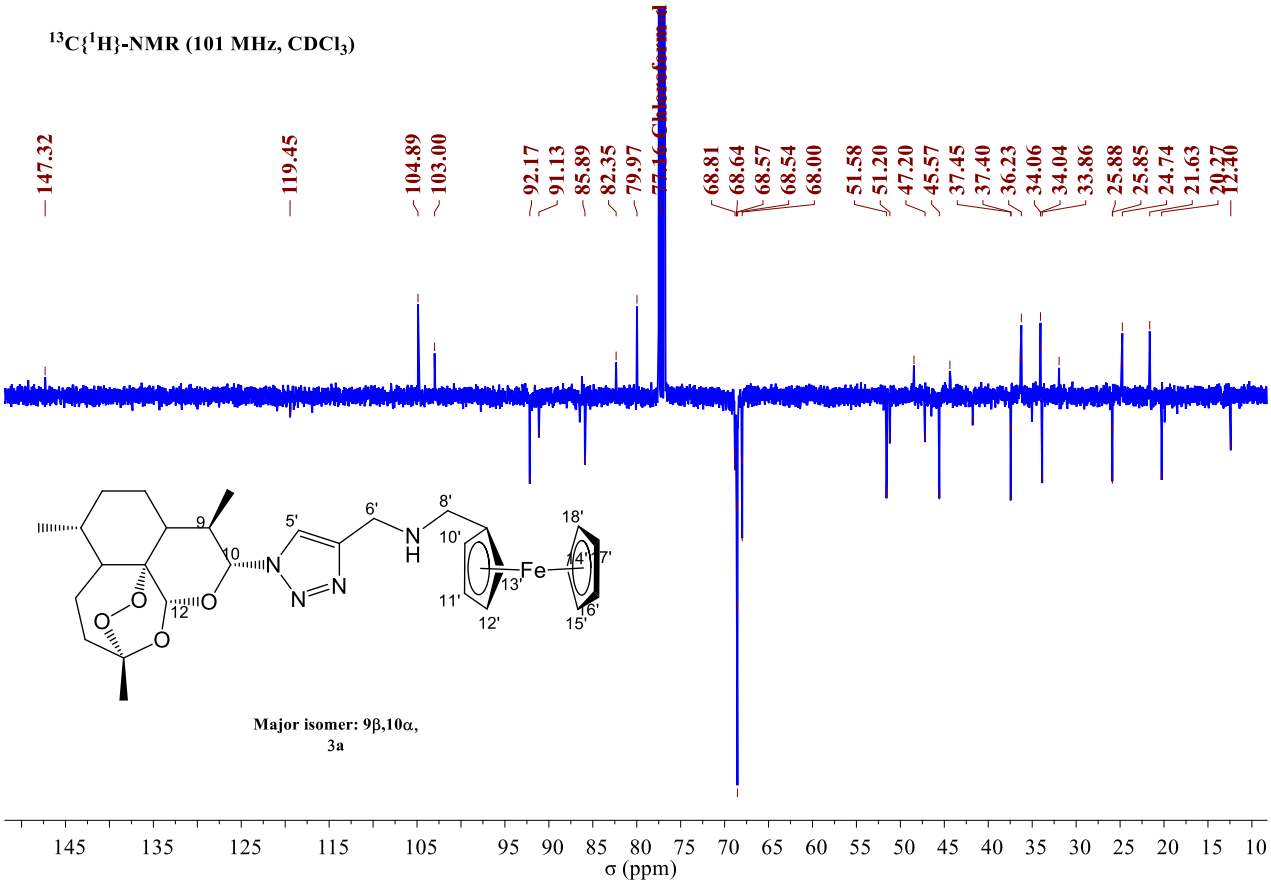

10. Compound 4:

IR

ATR-KBr window

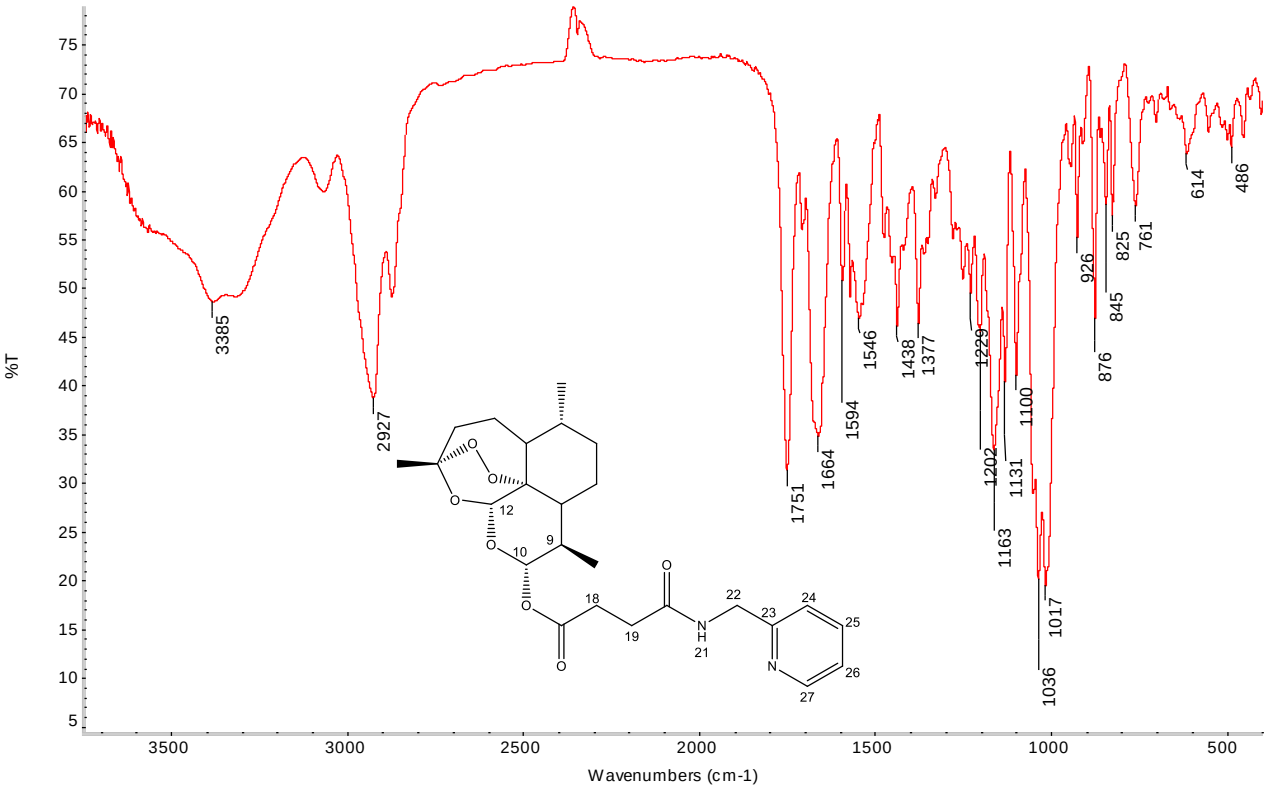

^{1}H-NMR:

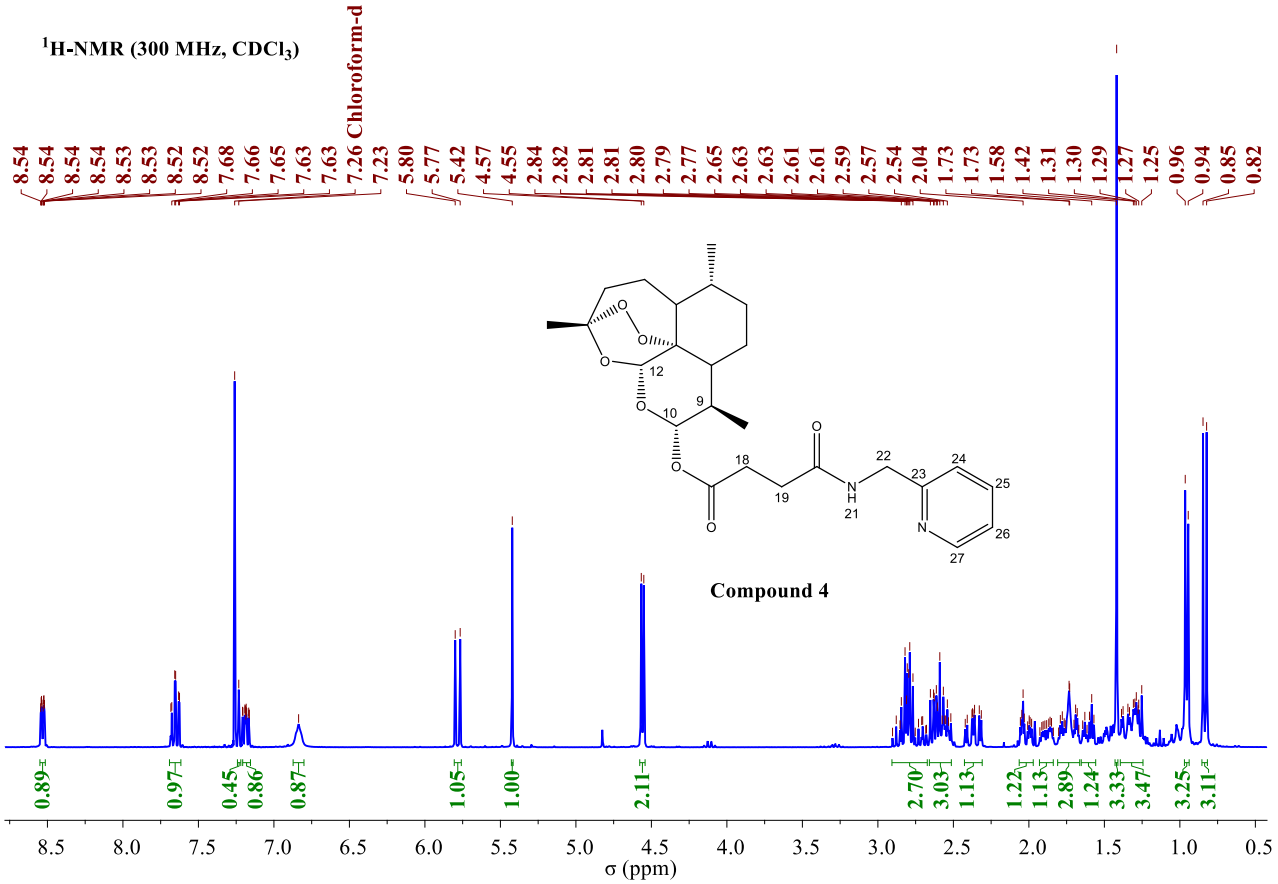

$^{13}C\{^{1}H\}$-NMR

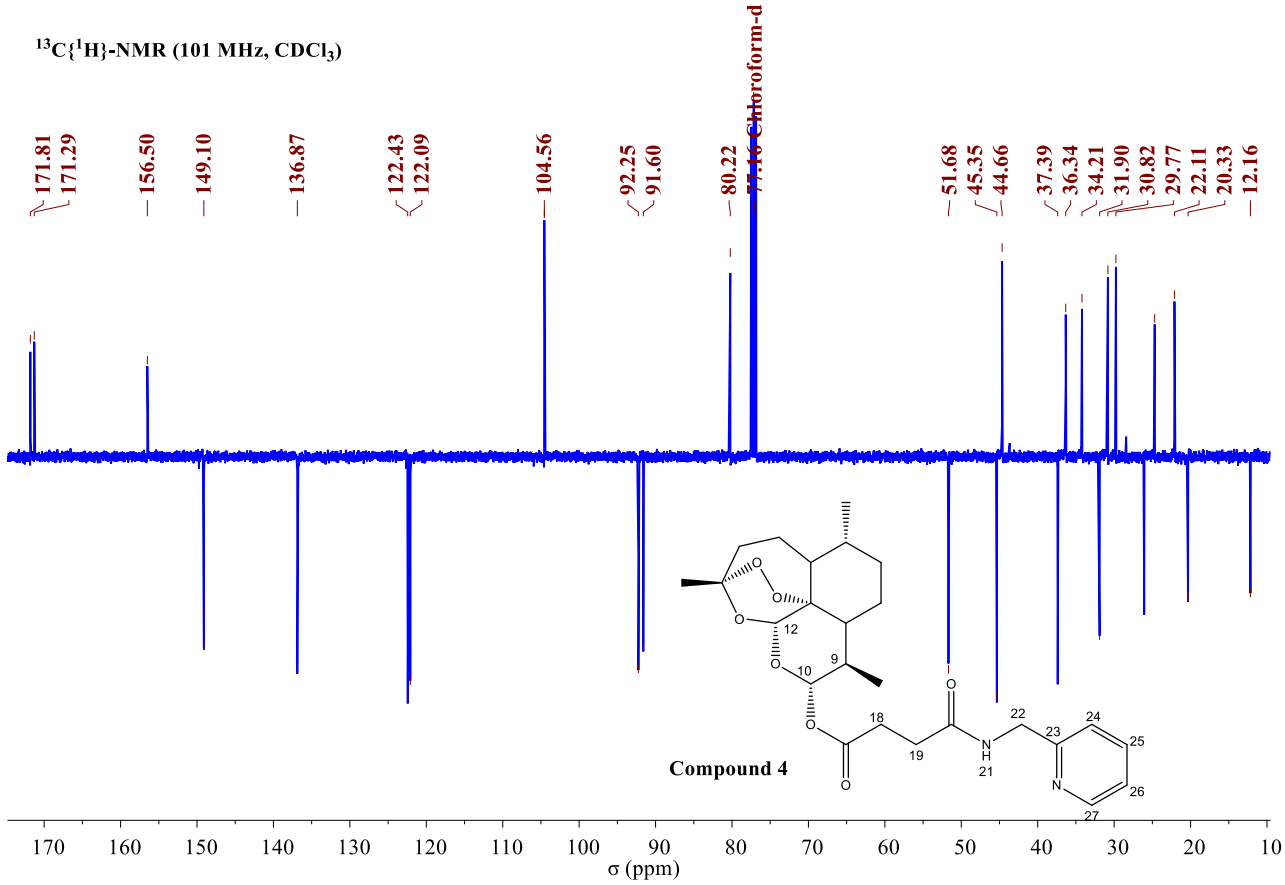

11. Compound 5a:

IR

ATR-ZnSe

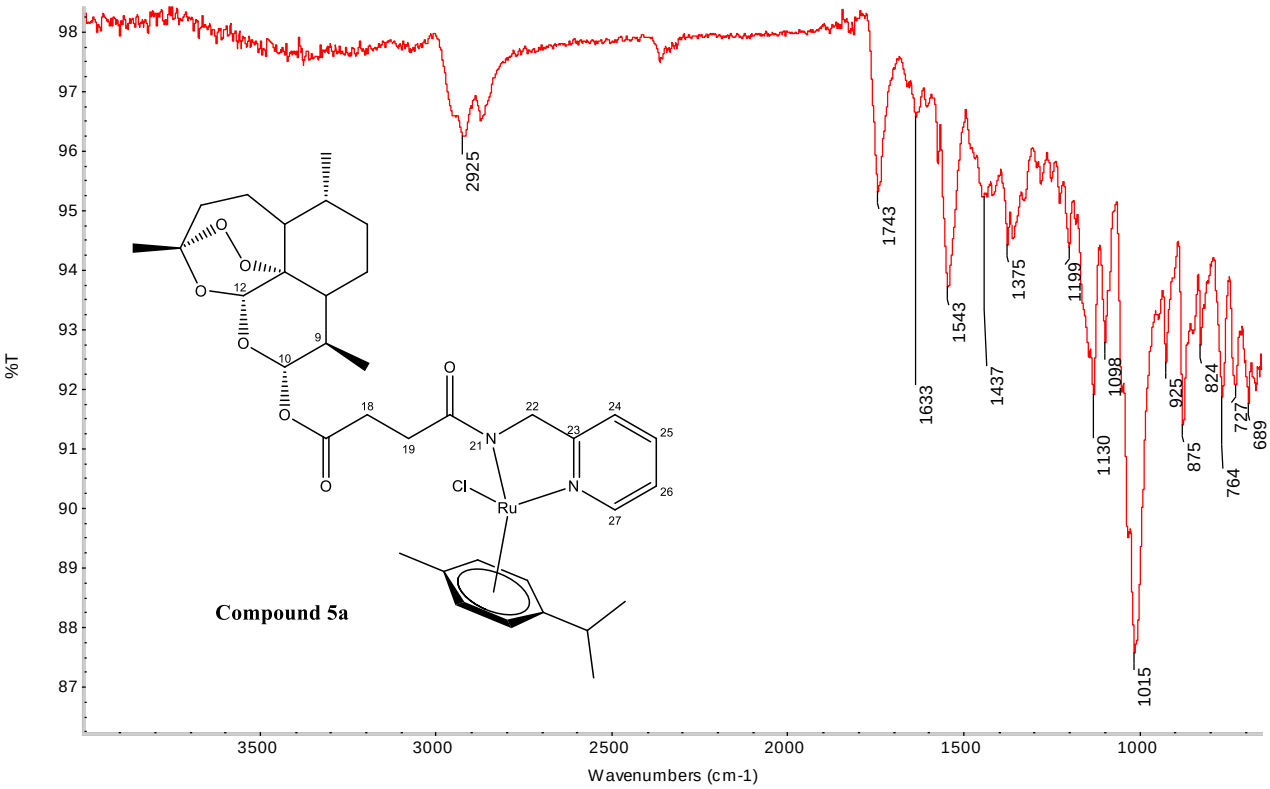

1H-NMR:

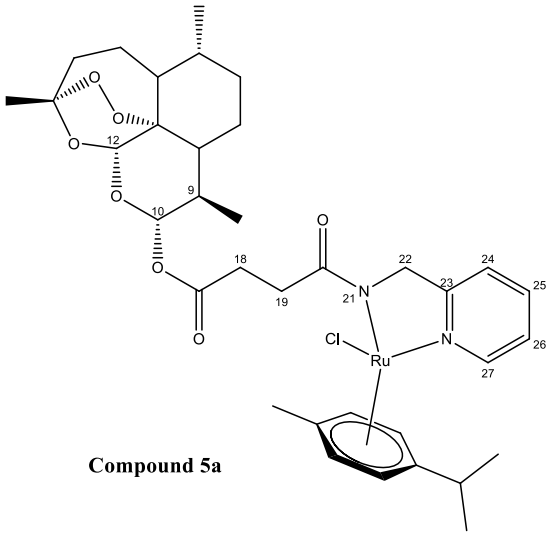

Compound 5a

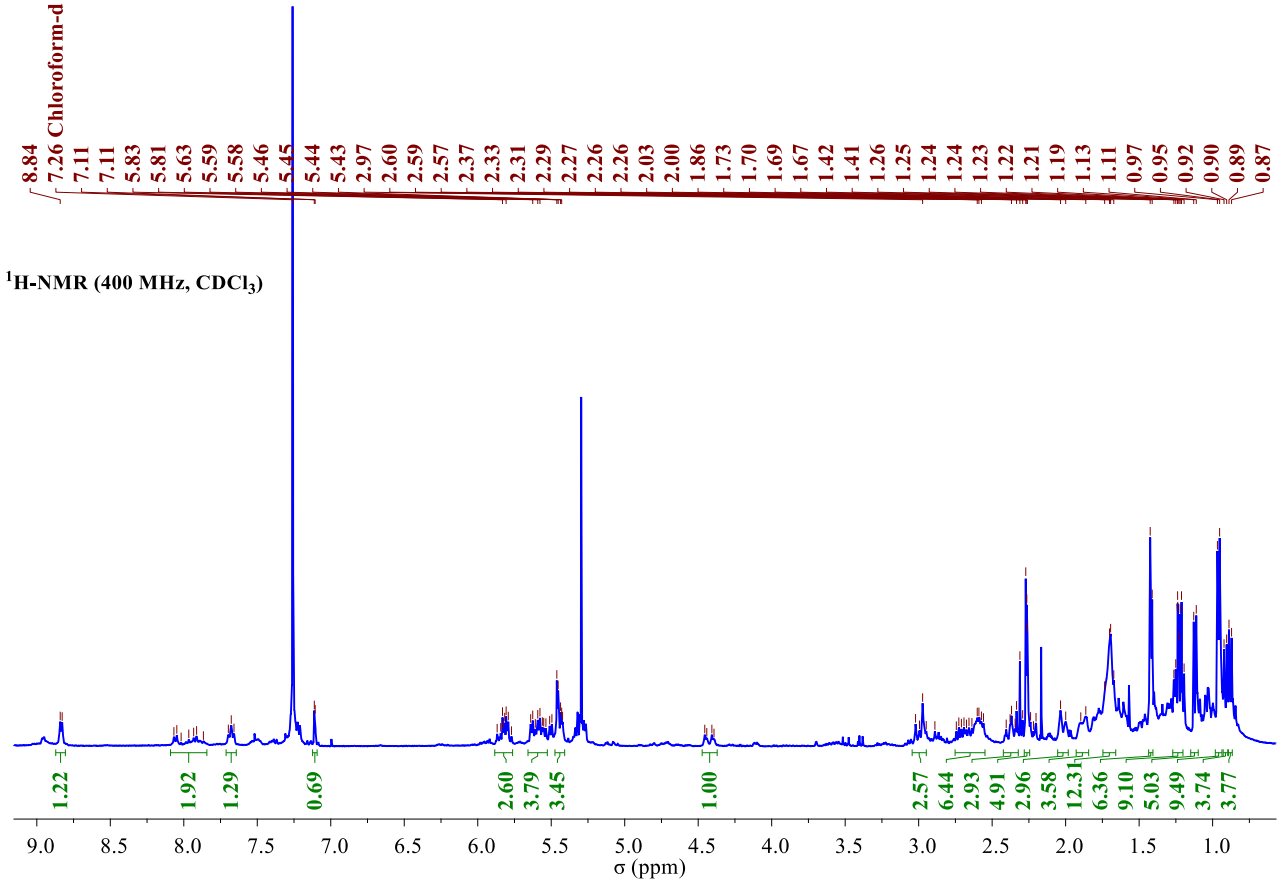

^{1}H-NMR (400 MHz, $CDCl_3$)

12. Compound 5b:

IR

ATR-ZnSe

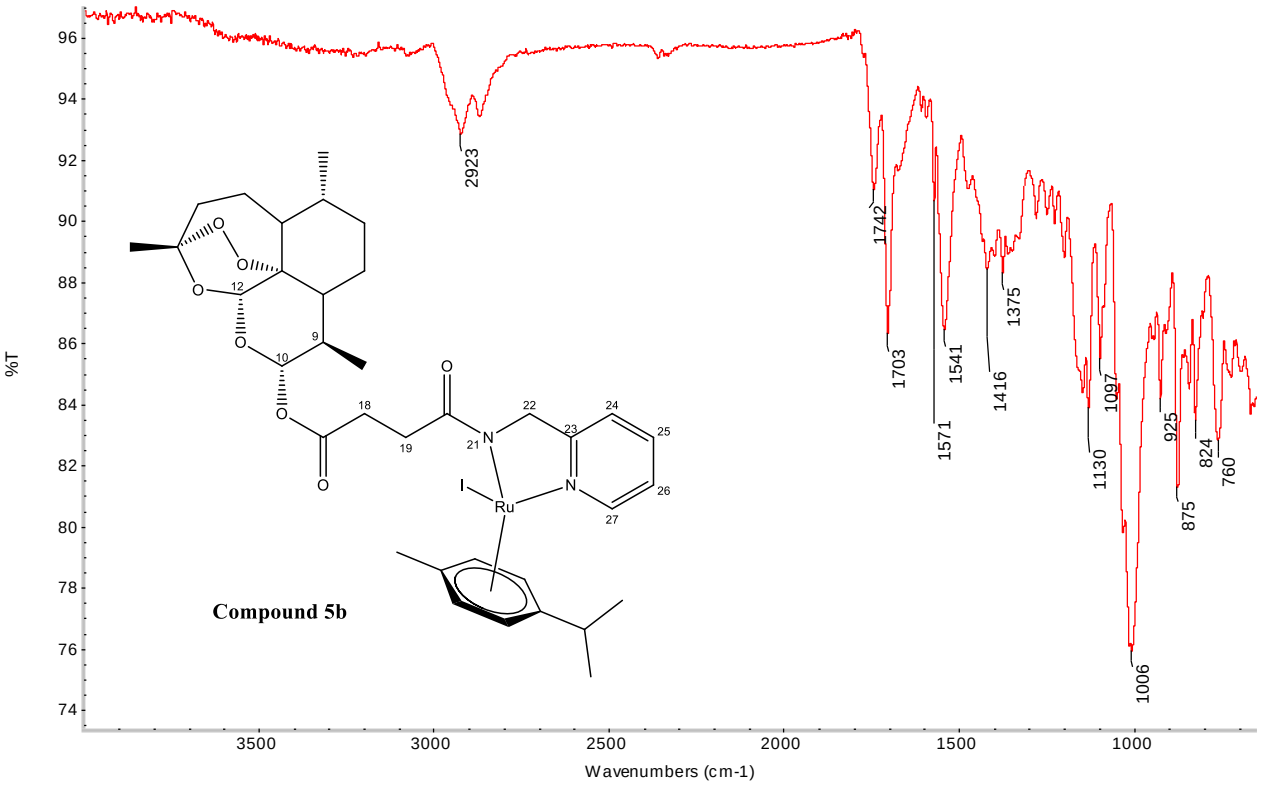

^{1}H-NMR:

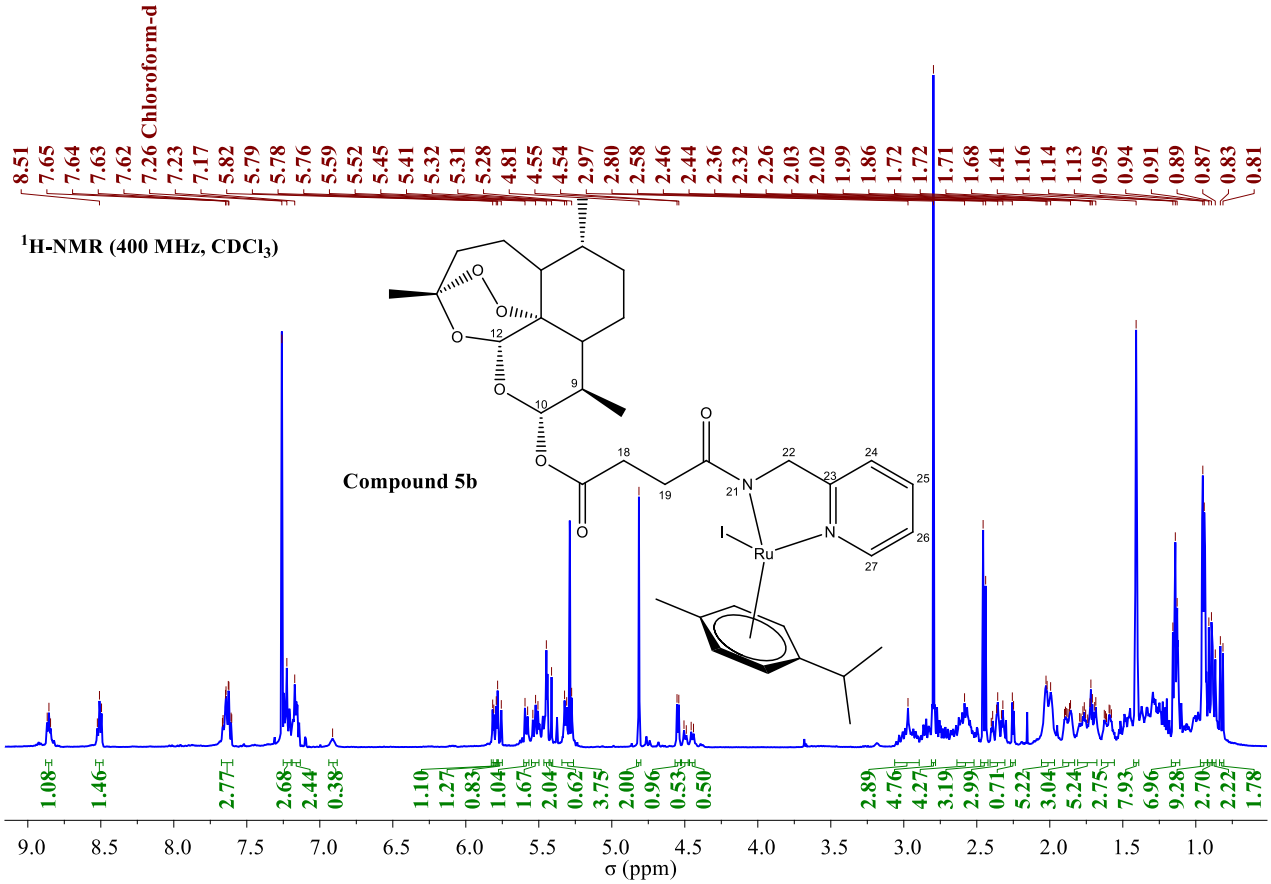

$^{13}C\{^{1}H\}$-NMR

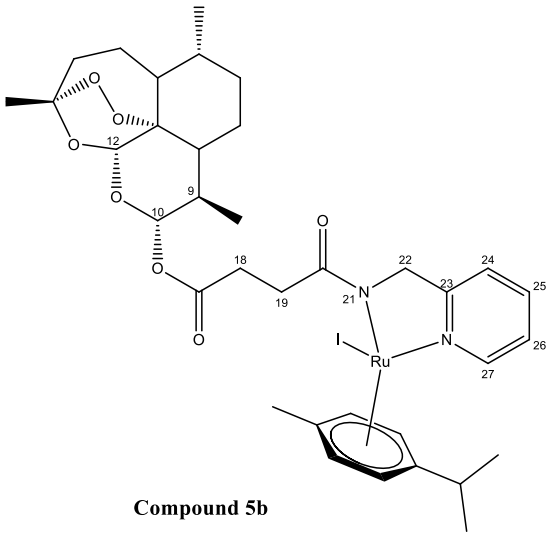

Compound 5b

$^{13}C\{^{1}H\}$-NMR (101 MHz, $CDCl_3$)

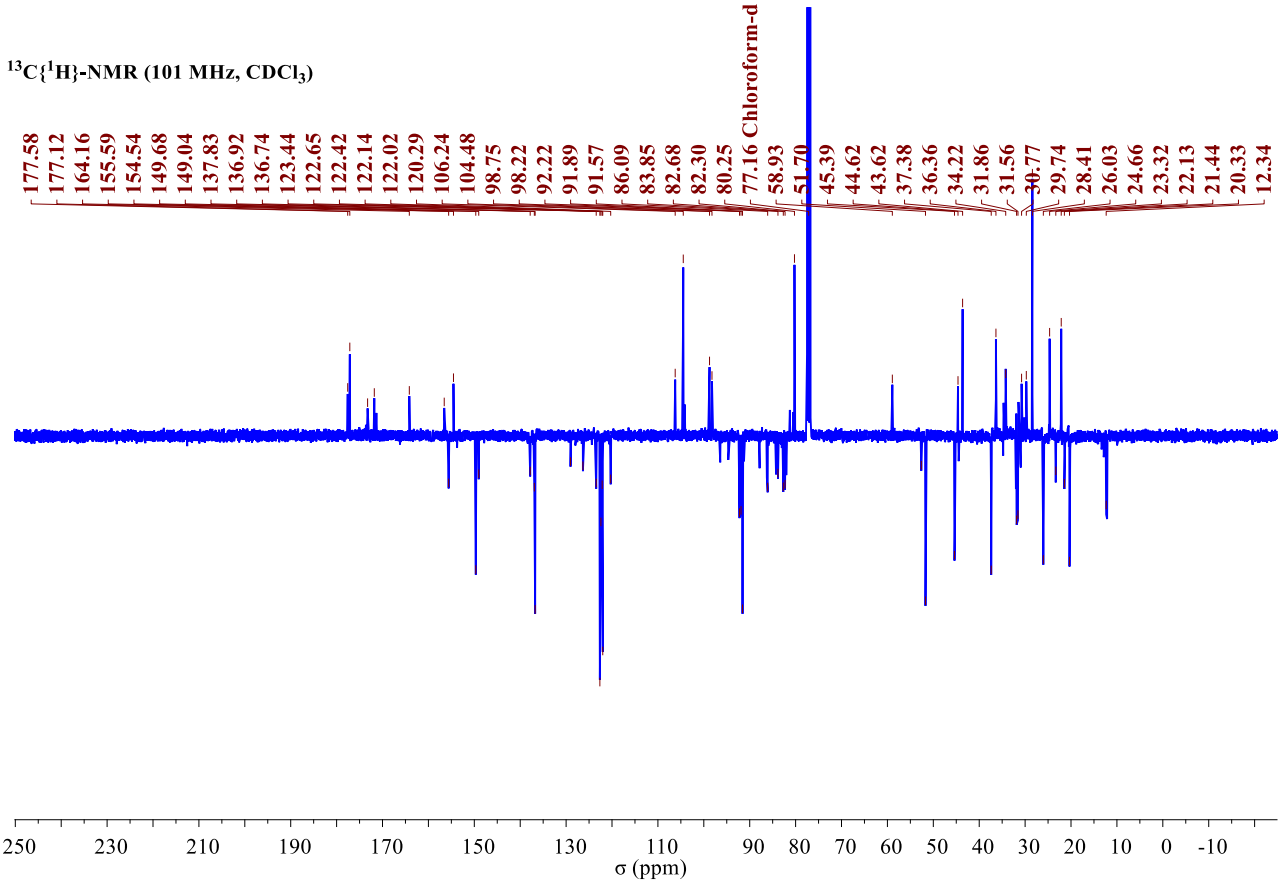

13. Compound 6:

IR

ATR-ZnSe

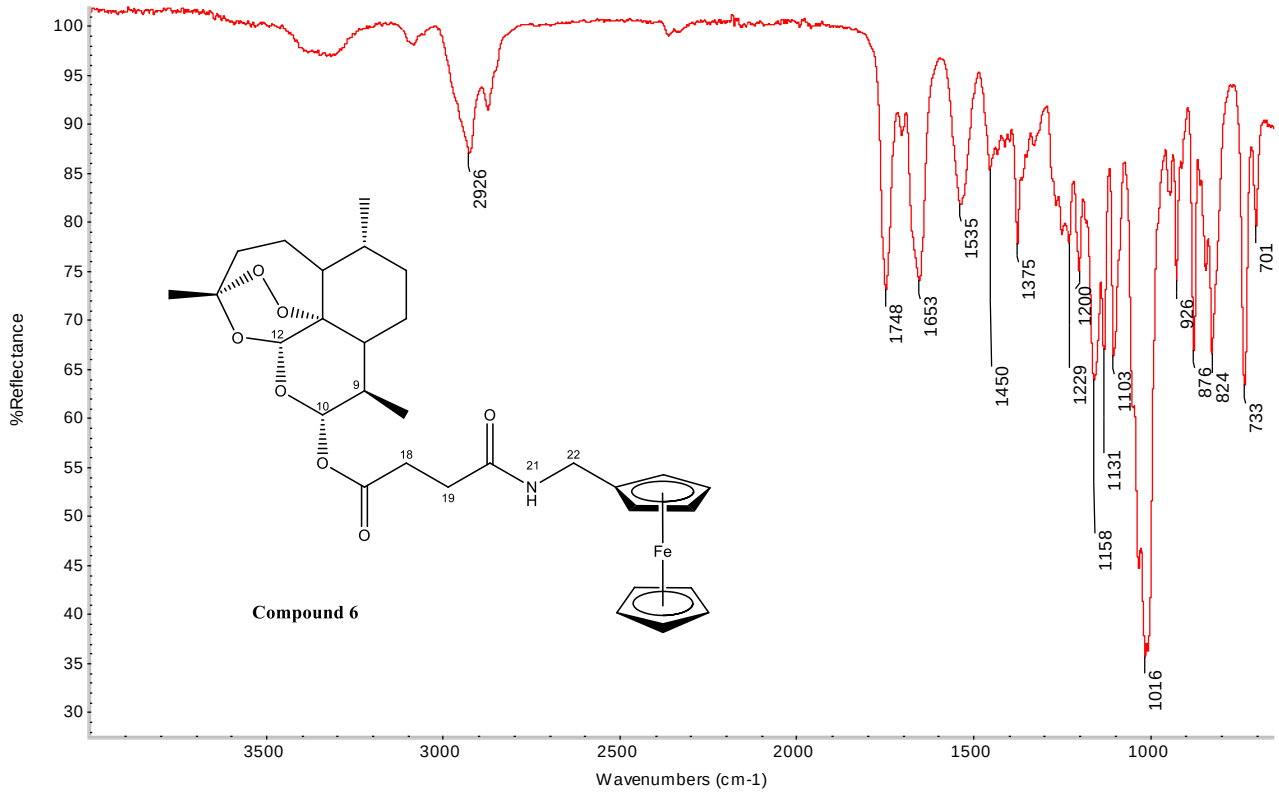

^{1}H-NMR:

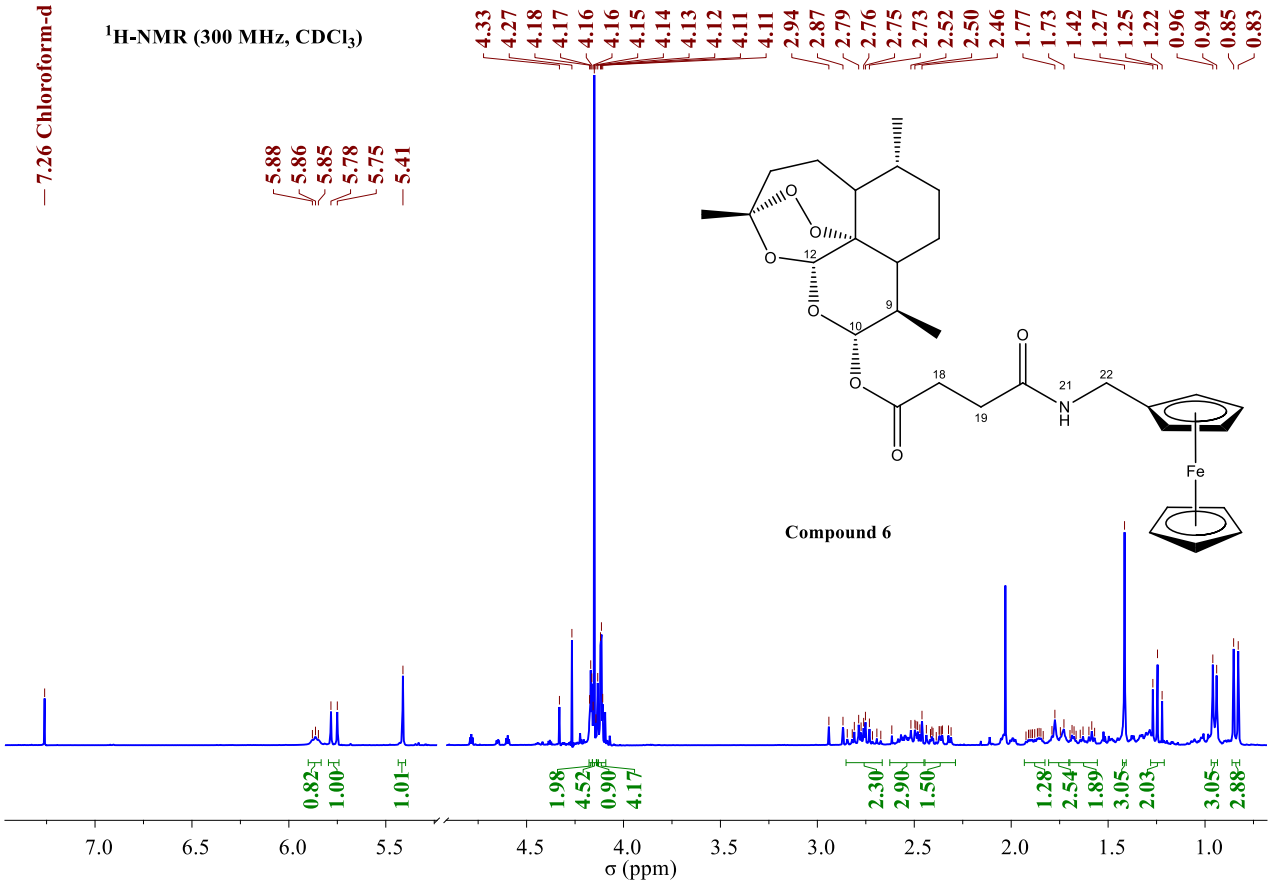

$^{13}C\{^{1}H\}$-NMR